

25 JUNE 1967

LMSC-A847882, Vol. II

p. 183

HANDBOOK OF THERMAL DESIGN DATA FOR MULTILAYER INSULATION SYSTEMS

FINAL REPORT, VOLUME II

CF

HIGH-PERFORMANCE INSULATION THERMAL DESIGN CRITERIA

NAS 8-20353

CRYOGENIC STAGE PROGRAMS



Prepared For
GEORGE C. MARSHALL SPACE FLIGHT CENTER
HUNTSVILLE, ALABAMA

Prepared By
R. M. COSTON, PROJECT MANAGER,
CRYOGENIC STAGE PROGRAMS

67-34910
(ACCESSION NUMBER)
180
(PAGES)
CR-87485
(NASA CR OR TMX OR AD NUMBER)

(THRU)
by
(CODE)
(CATEGORY)

Lockheed

MISSILES & SPACE COMPANY

A GROUP DIVISION OF LOCKHEED AIRCRAFT CORPORATION

SUNNYVALE, CALIFORNIA

CONTENTS

Section		Page
	ILLUSTRATIONS	v
	TABLES	ix
	INTRODUCTION	xi
1	GASES	1-1
2	METALS	2-1
3	FIBERGLASS LAMINATES	3-1
4	MULTILAYER INSULATIONS	4-1
	4.0 Introduction	4.0-1
	4.1 Substrates	4.1-1
	4.2 Multilayer-Insulation-System Materials	4.2-1
	4.3 Multilayer Composites	4.3-1
	4.4 Attachment Methods	4.4-1
	4.5 Experimental Methods	4.5-1
5	REFERENCES	5-1
Appendix		
I	CALCULATION OF SHINGLE PERFORMANCE	I-1
II	CONVERSION FACTORS	II-1

PRECEDING PAGE BLANK NOT FILMED.

ILLUSTRATIONS

Figure		Page
1-1	Density of Gases as a Function of Temperature	1-5
1-2	Thermal Conductivity of Gases as a Function of Temperature	1-7
1-3	Specific heat of Gases as a Function of Temperature	1-9
1-4	Viscosity of Gases as a Function of Temperature	1-11
1-5	Viscosity of Fluornine as a Function of Temperature	1-13
2-1	Linear Thermal Expansion of Metals as a Function of Temperature	2-5
2-2	Thermal Conductivity of Metals as a Function of Temperature	2-7
2-3	Thermal Conductivity of Titanium Alloys as a Function of Temperature	2-9
2-4	Thermal Conductivity Integrals of Pure Aluminum as a Function of Temperature	2-13
2-5	Thermal Conductivity Integrals of Various Aluminum Alloys as a Function of Temperature	2-21
2-6	Thermal Conductivity Integrals of Titanium as a Function of Temperature	2-29
2-7	Thermal Conductivity Integrals of Several Commercial Titanium Alloys	2-35
2-8	Thermal Conductivity Integrals of Ferrous Alloys as a Function of Temperature	2-41
2-9	Specific Heat of Metals as a Function of Temperature	2-47
2-10	Emittance of Metals as a Function of Temperature	2-49
2-11	Emissivity of Chemically Cleaned Copper and 1/4-Mil Thick Aluminum Foil as a Function of Temperature	2-51
3-1	Linear Thermal Expansion of Fiberglass Laminates as a Function of Temperature	3-3
3-2	Thermal Conductivity of Fiberglass Laminates as a Function of Temperature	3-5
3-3	Thermal Conductivity Integrals of Glass and Plastic as a Function of Temperature	3-7

Figure		Page
3-4	Specific Heat of Fiberglass Laminates as a Function of Temperature	3-9
4.1-1	Thermal Conductivity of Substrate Material as a Function of Temperature	4.1-3
4.1-2	Thermal Conductivity of Fiberglass Batting as a Function of Nitrogen Gas Pressure and Batting Density	4.1-5
4.1-3	Specific Heat of Substrate Materials as a Function of Temperature	4.1-7
4.2-1	Linear Thermal Expansion of Multilayer-Insulation-System Materials as a Function of Temperature	4.2-5
4.2-2	Thermal Conductivity of Multilayer-Insulation-System Materials as a Function of Temperature	4.2-7
4.2-3	Effective Thermal Conductivity of Dexiglas Spacer Material as a Function of Hot-Boundary Temperature and Bulk Density	4.2-9
4.2-4	Effect of Thermal Conductivity of Tissuglas Spacer Material vs Hot-Boundary Temperature and Bulk Density	4.2-11
4.2-5	Scattering Cross Sections of Tissuglas and Dexiglas Spacer Material as a Function of Wavelength	4.2-13
4.2-6	Specific Heat of Multilayer-Insulation-System Materials as a Function of Temperature	4.2-15
4.2-7	Emissivity of Radiation Shields as a Function of Temperature	4.2-17
4.2-8	Aluminum Mylar Surface Emittance vs Coating Thickness	4.2-19
4.2-9	Emittance of Gold Deposited on Mylar vs Deposition Thickness	4.2-21
4.2-10	Emittance of Silver Deposited on Mylar vs Deposition Thickness	4.2-23
4.2-11	Total Hemispherical Emittance of Several Aluminum Surface as a Function of Temperature	4.2-25
4.2-12	Total Hemispherical Emittance of Vacuum Deposited Gold on Kapton	4.2-27
4.2-13	Total Hemispherical Emittance of Vacuum Deposited Silver on Kapton	4.2-29
4.2-14	Thickness of Aluminum, Gold, and Silver Films as a Function of Film Electrical Resistance	4.2-31
4.3-1	Unit Weight of Multilayer Composites as a Function of Number of Radiation Shields	4.3-3
4.3-2	Nominal Density of Multilayer Composites as a Function of Layer Packing Density	4.3-5
4.3-3	Effect of Layer Density on Thermal Conductivity	4.3-7

Figure		Page
4.3-4	Effect of Layer Density on Thermal Conductivity for Singly-Aluminized Crinkled Mylar	4.3-9
4.3-5	Effect of Layer Density on Dimplar Thermal Conductivity	4.3-11
4.3-6	Effect of Layer Density on Thermal Conductivity of Mylar Plus Foam	4.3-13
4.3-7	Nominal-Density/Thermal Conductivity Product of Multilayer Composites as a Function of Layer Packing Density	4.3-15
4.3-8	Effective Thermal Conductivities of Several Combinations of Shield and Spacer Materials	4.3-17
4.3-9	Influence of Hot-Boundary Temperature on Effective Thermal Conductivity	4.3-19
4.3-10	Effective Thermal Conductivity of Multilayer Insulation System Measured Parallel to the Layers	4.3-21
4.3-11	Effective Thermal Conductivity Parallel to Layer of Aluminum Foil as a Function of Temperature	4.3-23
4.3-12	Thermal Conductivity of Multilayer Composites as a Function of Gas Pressure	4.3-25
4.3-13	Normalized Thermal Conductivity of Multilayer Composites as a Function of Gas Pressure	4.3-27
4.3-14	Permeability of Multilayer Composites as a Function of Layer Packing Density	4.3-29
4.3-15	Effective of Gas Molecular Weight on Diffusion Coefficients	4.3-33
4.3-16	Heat Flux of Multilayer Composites as a Function of Compressive Load	4.3-35
4.3-17	Heat Flux Ratio of Multilayer Composites as a Function of Compressive Load	4.3-37
4.3-18	Specific Heat of Multilayer Composites as a Function of Temperature	4.3-39
4.4-1	Effective Thermal Conductivity of Multilayer Shingle Insulation as a Function of Shingle Length	4.4-3
4.4-2	Thermal Conductivity of Shingle Multilayer Insulation as a Function of Warm-Side Temperature	4.4-5
4.4-3	Thermal Conductivity of Button Multilayer Insulation as a Function of Outer Boundary Temperature	4.4-7
4.4-4	Normalized Heat Flow Through Multilayer Systems as a Function of Point-Source Leakage Rate	4.4-9
4.4-5	Probable Vent Paths Through Multilayer Insulation for Point-Source Leakage Test	4.4-11

Figure		Page
4.5-1	Flat-Plate Calorimeter	4.5-2
4.5-2	Flat-Plate Calorimeter Schematic Diagram	4.5-3
4.5-3	Ratio of Heat Flux to Calorimeter to Heat Flux for One-Dimensional Case	4.5-7
4.5-4	Ratio of Heat Fluxes as a Function of Edge Temperature and Thermal Conductivities	4.5-8
4.5-5	Ratio of Heat Fluxes as a Function of Intermediary Insulation Width at Outer Radius	4.5-8
4.5-6	Photograph of Cryostat Components	4.5-12
4.5-7	Cryostat Cross Section	4.5-13
4.5-8	Schematic of Cryostat and Associated Instrumentation	4.5-14
I-1	Shingle Nomenclature	I-2
I-2	Radiant Energy Transport Through Shingle Gap at 139°R -- 532°R	I-4
I-3	Radiant Engery Transport Through Shingle Gap at 37°R -- 400°R	I-5

TABLES

Table		Page
1-1	Physical Properties of Cryogenic Liquids	1-3
2-1	Density of Metals	2-3
3-1	Characteristics of Fiberglass Laminates	3-1
4.2-1	Properties of Multilayer-Insulation-System Materials	4.2-3
4.3-1	Diffusion Coefficient Data	4.3-31

INTRODUCTION

The Handbook of Thermal Design Data for Multilayer Insulation Systems was originally prepared under Contract NAS 8-11347 for the Marshall Space Flight Center by R. T. Parmley of the Lockheed Missiles & Space Company. Revision and updating of this handbook has been accomplished as a part of Contract NAS 8-20353 for MSFC. The technical managers of the latter contract at MSFC were Mr. G. Comer and Mr. J. Vaniman. The prime intent in assembling the data presented in this volume is to provide a sourcebook of consistent data on thermal and physical properties of multilayer insulations so that the data can be applied in mathematical thermal models of cryogenic propellant tankage.

Multilayer insulations by nature have highly anisotropic thermal transport characteristics which are in general severely changed by small perturbations in layer density, interstitial gas pressure, basic material physical and optical properties, and the temperature environment to which they are subjected. It is upon these highly unpredictable thermal transport properties that the thermal performance of cryogenic vehicles must be predicted. Additional uncertainty is brought about by the lack of standard data acquisition and reporting methods. Further confusion is added to the multilayer insulation picture with the large variations possible in the basic insulation materials properties. Recent studies completed by Lockheed and Arthur D. Little, Inc. have shown that the emittance of ostensibly similar radiation shield materials from various manufacturers can vary by 50 percent. Factors affecting the shield emittance are aluminized layer thickness, rate of film deposition, pressure in vacuum chamber during deposition, and the purity of the base metal being deposited.

Keeping in mind the previously mentioned factors affecting the performance of multilayer insulation, it must also be recognized that in the manufacture of multilayer insulations and their application to actual storage vessels the insulation will suffer in thermal performance. In the case of presently available multilayer insulation thermal

performance data to predict propellant storage times in space, the thermal analyst must constantly keep in mind the shortcomings of this data and use caution in interpreting predictions.

The data collected for this handbook have been presented in a manner which will obviate the uncertainties and data dispersions found in the literature. Where they are available, actual data points have been plotted and compared with data from various sources.

In reviewing the literature an obvious gap has appeared in available multilayer insulation thermal design data. This gap is due to the lack of information on the reliability and reproducibility of thermal design data. A literature survey has shown that there have been no serious attempts at generating this much needed information. Before accurate predictions of cryogenic space vehicle lifetimes can be made this information will be required.

The second intent of this report is to provide readily available design data for general usage by designers and thermal analysts of cryogenic space vehicles who will not necessarily employ the mathematical models. A variety of design data is presented, including thermal conductivity, specific heat, density, linear thermal expansion, weight per unit area, and maximum material operating temperatures.

Only the most promising materials under investigation were included in this compilation. If data on a specific material were not available, a similar material was chosen to represent the properties in that material class.

The data presented in this report are divided into four major categories, as follows:

1. Gases
2. Metals
3. Fiberglass Laminates
4. Multilayer Insulations
 - 4.1 Substrates
 - 4.2 Multilayer-Insulation-System Materials
 - 4.3 Multilayer Composites

Appendix I CALCULATION OF SHINGLE PERFORMANCE

The effective thermal conductivity, k_{eff} , of NRC-2 shingle insulation can be calculated by the following equation:

$$k_{\text{eff}} = \frac{I}{\Delta T} q_{\text{TOTAL}} = \frac{I}{\Delta T} (q_r + q_c + q_{\perp}) \quad (1)$$

where

- I = nominal multilayer thickness
- ΔT = temperature drop across multilayers
- q_r = equivalent heat flux, normal to the tank wall, due to radiation tunneling between shingles
- q_c = equivalent heat flux, normal to the tank wall, due to solid conduction along shingles
- q_{\perp} = heat flux for an equivalent number of parallel shields, normal to the tank wall (experimental value)

In order to calculate q_r , the radiant heat rate per foot of shingle width, Q_G , is determined first:

$$Q_G = \frac{A_1 \sigma (T_1^4 - T_2^4) [2 \ln (2 L/b) - 1]}{(2 L/b)} \quad (2)$$

where:

- A_1 = effective gap spacing area normal to layers
- σ = Stefan-Boltzmann constant
- T_1 = warm-side temperature

T_2 = cold-side temperature
 L = shingle length
 b = shingle gap width = $\frac{I}{N \cos \theta} \cong \frac{I}{N}$ (when θ is small)
 $\sin \theta = \frac{I}{L}$
 N = number of effective layers

Shingle nomenclature is illustrated in Fig. I-1.

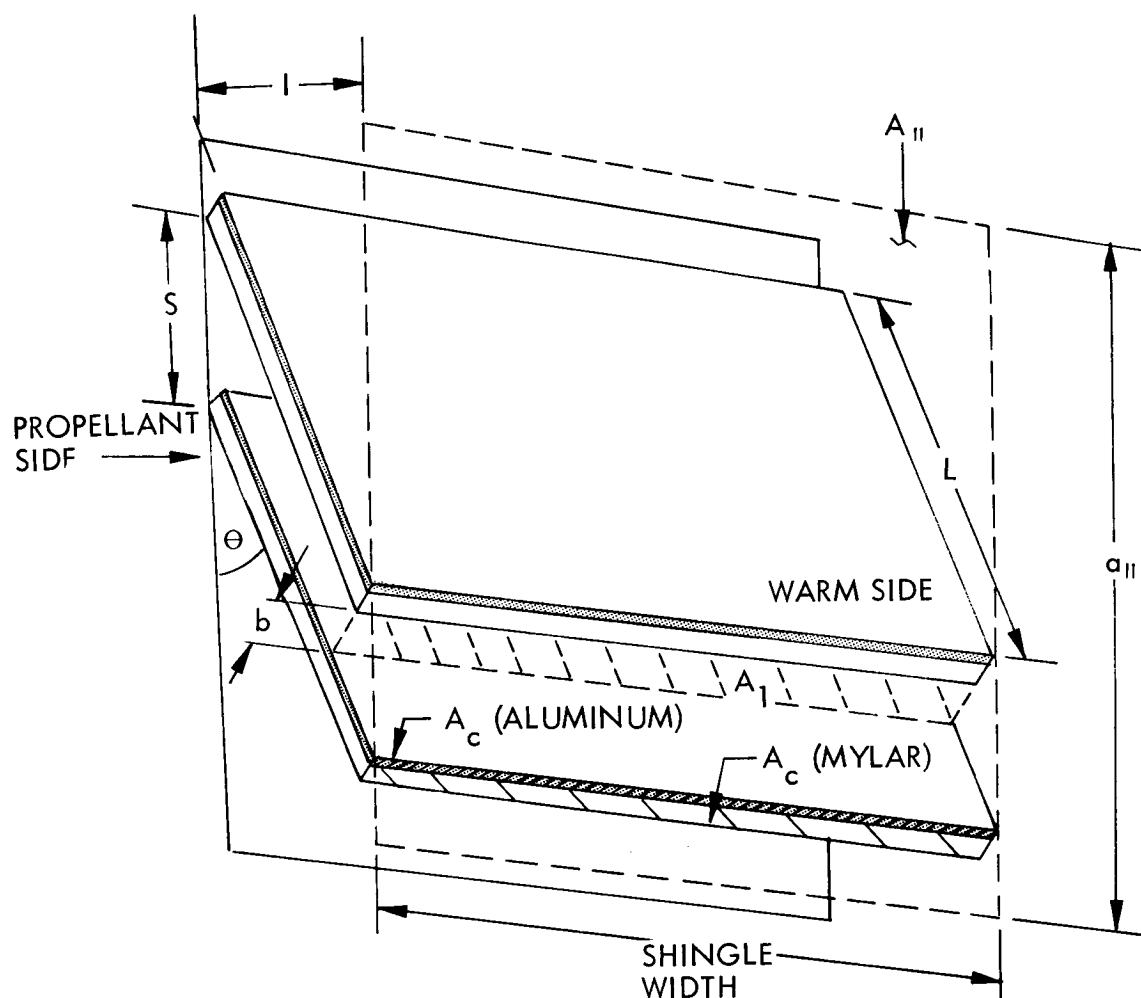


Fig. I-1 Shingle Nomenclature

For convenience, Q_G , the heat rate per foot of shingle width, has been computed and graphed as a function of the shingle gap spacing, b , and shingle length, L . Figures I-2 and I-3 show Q_G for different boundary temperatures. Values of Q_G obtained from these figures would be divided by the shingle spacing parallel to the cold surface in order to obtain q_r .

$$q_r = \frac{Q_G}{S} \quad (3)$$

where

$$S = \frac{L \cos \Theta}{N} \cong \frac{L}{N} \text{ (when } \Theta \text{ is small)}$$

To calculate q_c , solid conduction along the shield, the following equation is used:

$$q_c = \frac{\Delta T a_{\parallel} N}{L^2 \cos \Theta} \left[\left(\frac{A_{cAl}}{A_{\parallel}} k_{Al_2} \right) + \left(\frac{A_{cMY}}{A_{\parallel}} k_{MY_2} \right) \right] \quad (4)$$

where

- A_{cAl} = solid conduction area of one shingle for aluminized film
- A_{cMY} = solid conduction area of one shingle for Mylar substrate
- A_{\parallel} = surface area parallel to tank wall
- a_{\parallel} = unit length parallel to tank wall and normal to bond line
- k_{Al_2} = thermal conductivity of aluminum at the cold temperature
- k_{MY} = thermal conductivity of Mylar at the cold temperature

NOTE

$\cos \Theta$ approaches 1 when Θ is small.

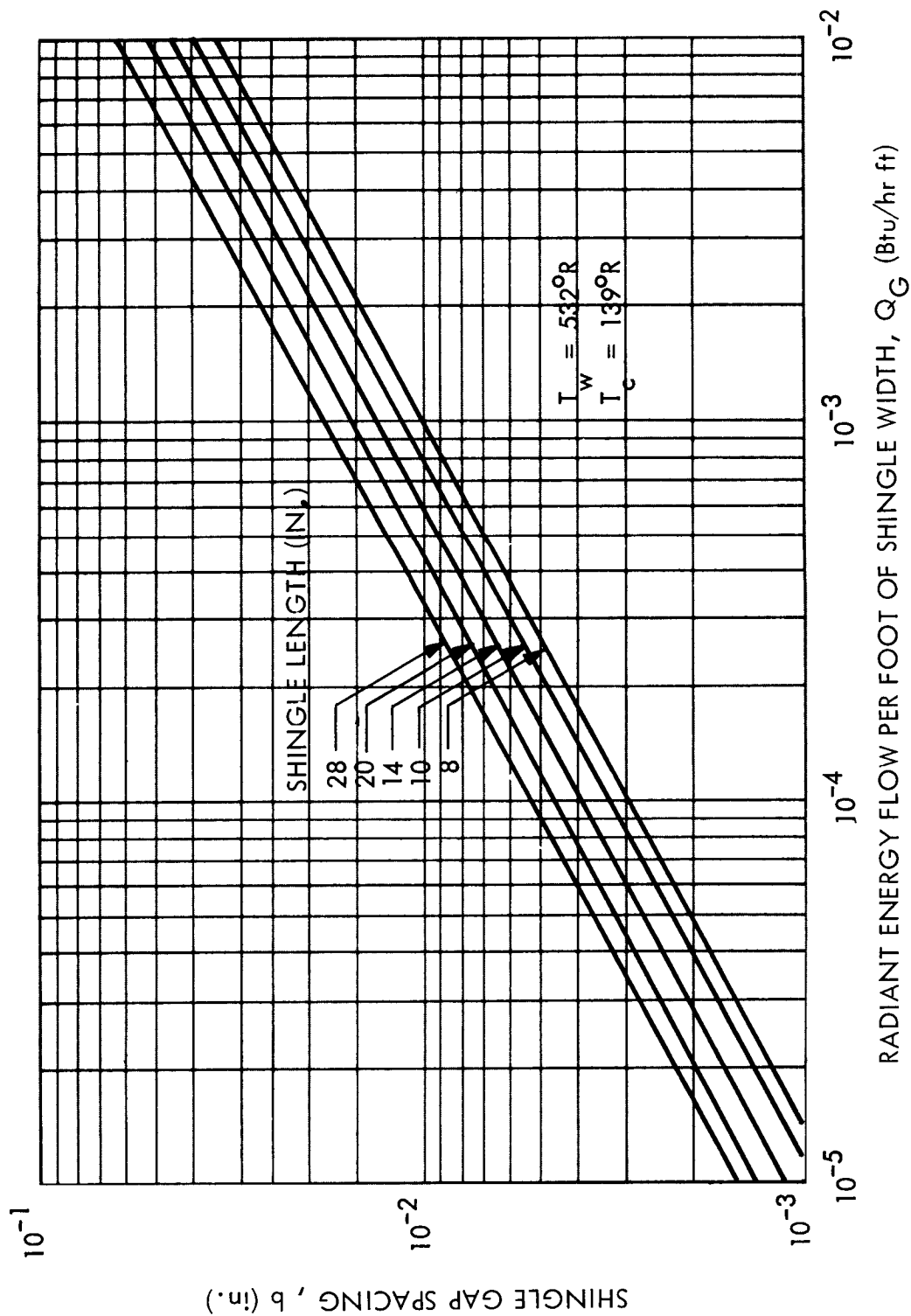


Fig. I-2 Radiant Energy Transport Through Shingle Gap at $139^\circ R - 532^\circ R$

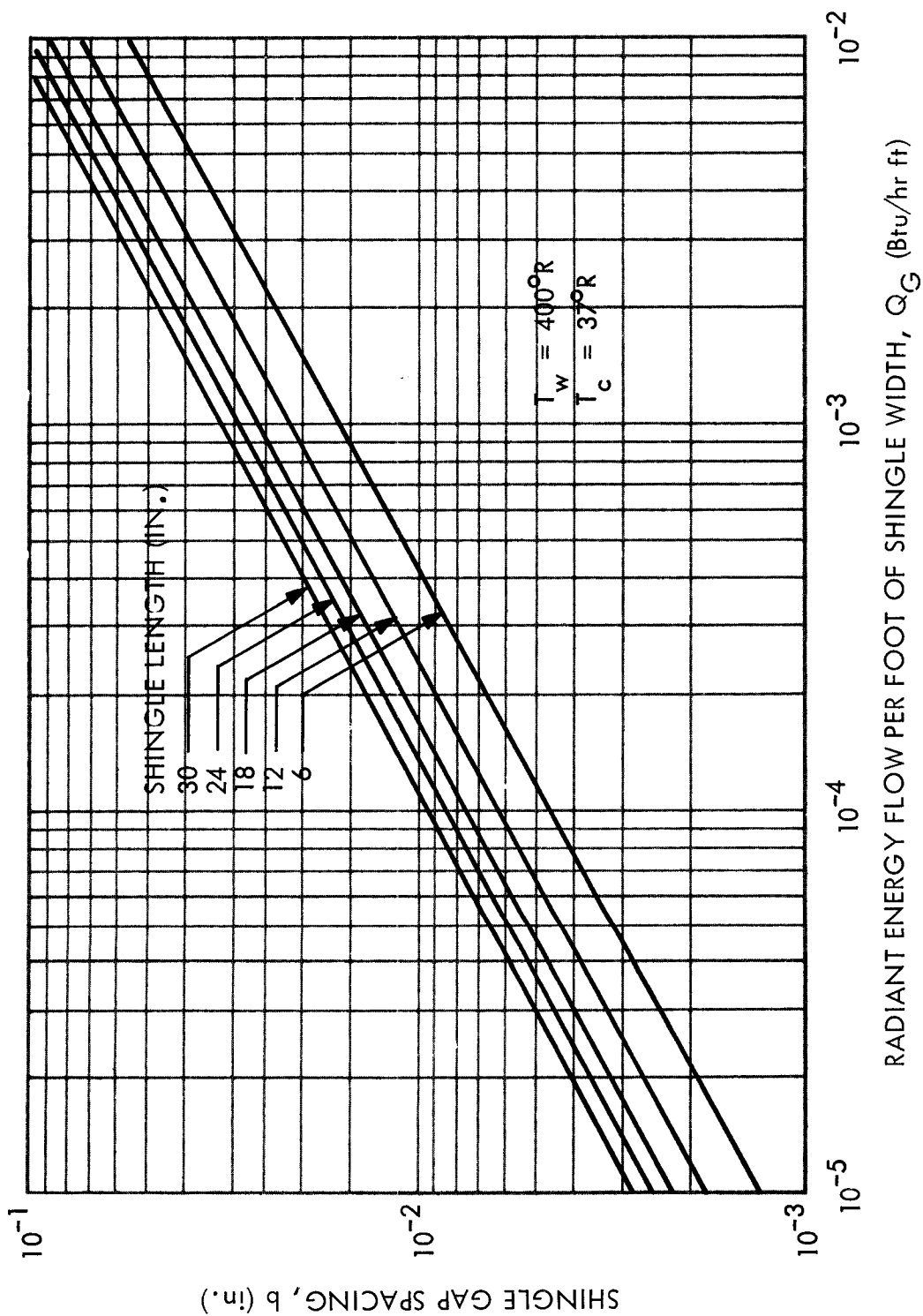


Fig. I-3 Radiant Energy Transport Through Shingle Gap at $37^\circ R - 400^\circ R$

1. GASES

Multilayer insulation systems may be purged on the launch pad and vented during ascent flight, and must be designed to provide a near-vacuum within the multilayers when in space. In space applications, the equilibrium values of effective conductivity are desired. These values are achieved essentially when the gas pressures within the multilayer system are less than 10^{-5} torr. Factors which influence the attainment of this pressure include efficiency of the venting process, extent of outgassing, and permeability of seals, welds, and tank penetrations to gaseous propellants.

This section summarizes pertinent data about purge gases, residual trace gas, and potential leakage of gaseous propellants. The specific gases considered in each category are as follows:

<u>Purge Gases</u>	<u>Residual Trace Gas</u>	<u>Gaseous Propellants</u>
Helium	Air	Hydrogen
Neon		Oxygen
Nitrogen		Fluorine

The data presented for each gas include boiling point, triple points, critical constants, heat of vaporization, heat of fusion, density, conductivity, specific heat, and viscosity.

Physical Properties of Cryogenic Liquids

At room temperature, normal hydrogen ($n\text{-H}_2$) is 75 percent ortho-hydrogen. 25 percent para-hydrogen. At the boiling point, equilibrium hydrogen ($e\text{-H}_2$) is 99.79 percent para-hydrogen.

Table 1-1
PHYSICAL PROPERTIES OF CRYOGENIC LIQUIDS

Cryogenic Liquid	Boiling Pt. at 1 Atm (°R)	Triple Points		Critical Constants		Latent Heat of Vaporization at 1 Atm (Btu/lb)	Latent Heat of Fusion at Triple Point (Btu/lb)	Density at B.P. ₃ (lb/ft ³)	Molecular Weight
		Temp. (°R)	Press. (psia)	Temp. (°R)	Press. (psia)				
Fluorine	153.1 (1)*	96.4 (95)	0.032 (99)***	259.5 (94)	808.5 (94)	74.1 (94)	5.78 (96)	—	38.0
Helium	7.59 (93)	λ 3.92 (93)**	λ 0.73 (93)**	9.36 (93)	33.2 (93)	8.8 (94)	—	1.061 (95)	4.0
Hydrogen								0.083 (95)	
n-H ₂	36.70 (93)	25.12 (93)	1.044 (93)	59.74 (93)	190.8 (93)	192.6 (93)	25.0 (97)		2.016
e-H ₂	36.49 (93)	24.86 (93)	1.021 (93)	59.39 (93)	187.7 (93)	190.4 (93)	25.1 (97)		
Neon	49.1 (1)	44.3 (95)	6.27 (95)	80.6 (94)	400.0 (94)	37.1 (94)	2.7 (98)	0.593 (95)	20.18
Nitrogen	139.3 (93)	113.7 (93)	1.82 (93)	227.0 (93)	492.0 (93)	85.2 (94)	11.0 (1)	0.276 (95)	28.02
Oxygen	162.3 (93)	97.8 (93)	0.022 (93)	278.6 (93)	737.0 (93)	91.7 (94)	5.94 (1)	0.296 (95)	32.00

*Reference numbers shown in parentheses.

**Lambda point.

***Calculated from vapor pressure equations for solid and liquid fluorine.

Density of Gases as a Function of Temperature

The density curves for neon and fluorine below 492° R were calculated by means of the perfect gas law.

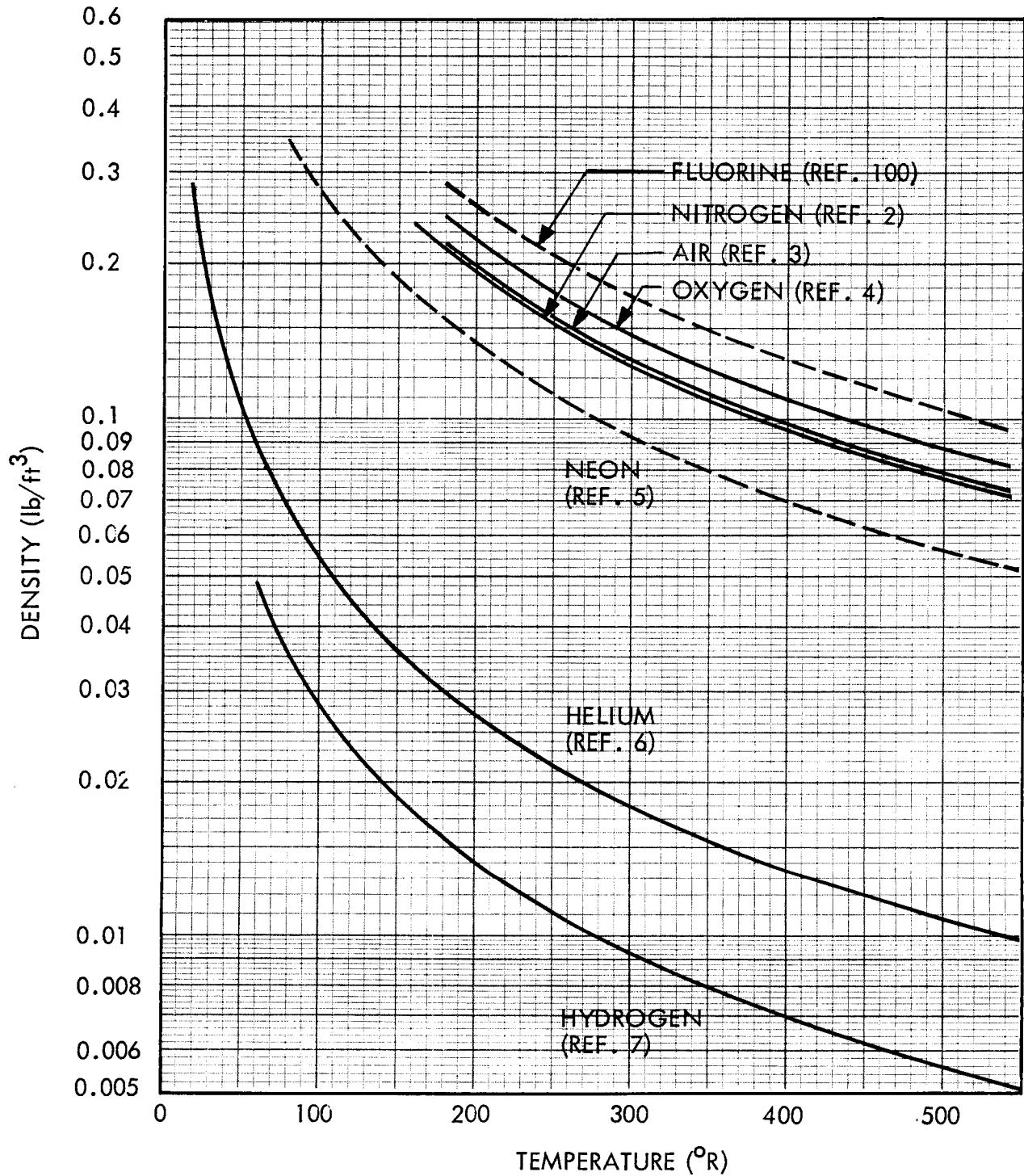


Fig. 1-1 Density of Gases as a Function of Temperature

Thermal Conductivity of Gases as a Function of Temperature

At room temperature, normal hydrogen is 75 percent ortho-hydrogen and 25 percent para-hydrogen. At 37° R, hydrogen is 99.79 percent para-hydrogen.

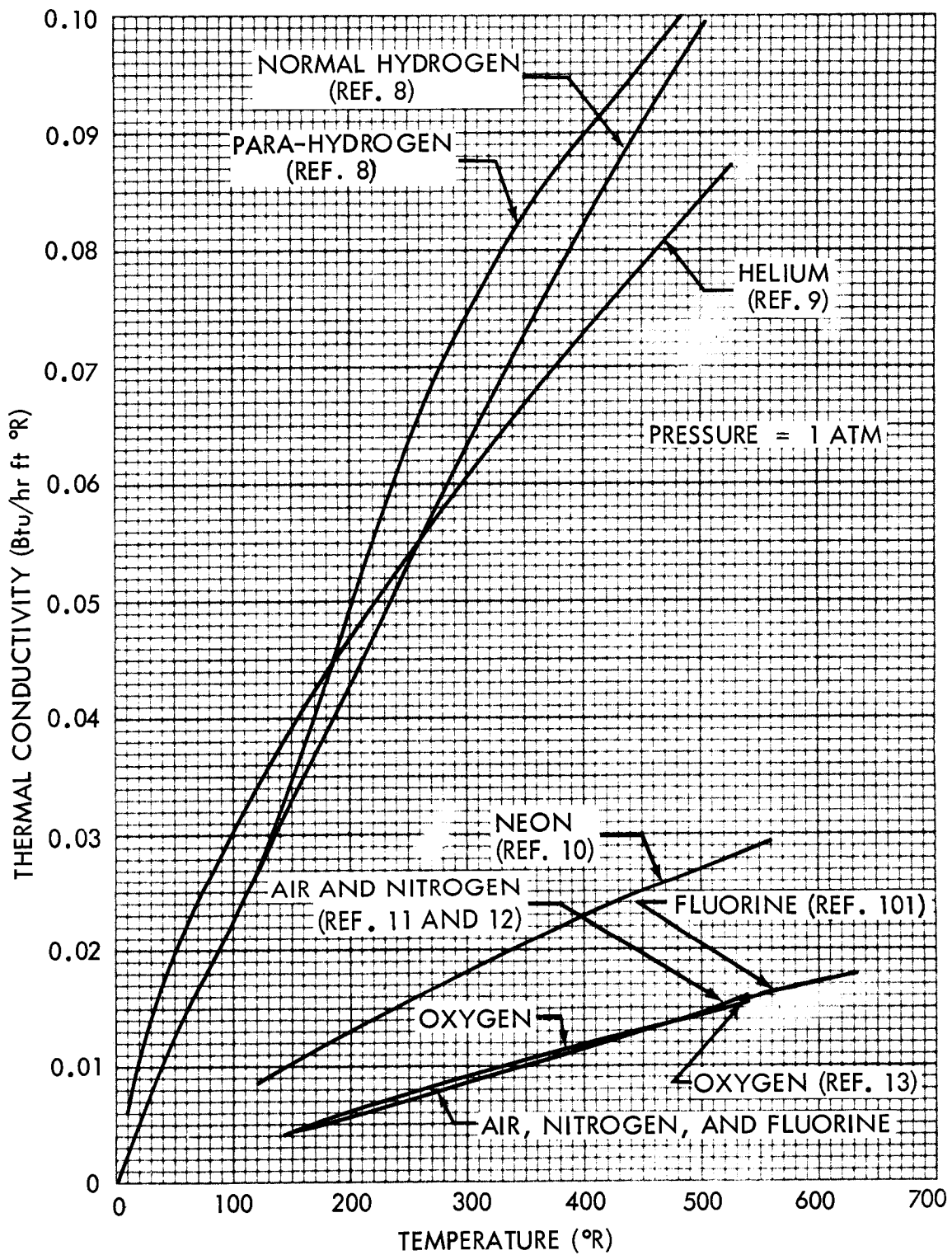


Fig. 1-2 Thermal Conductivity of Gases as a Function of Temperature

Specific Heat of Gases at Constant Pressure as a Function of Temperature at 1 Atm.

The helium curve was extrapolated between 90° and 450° R.

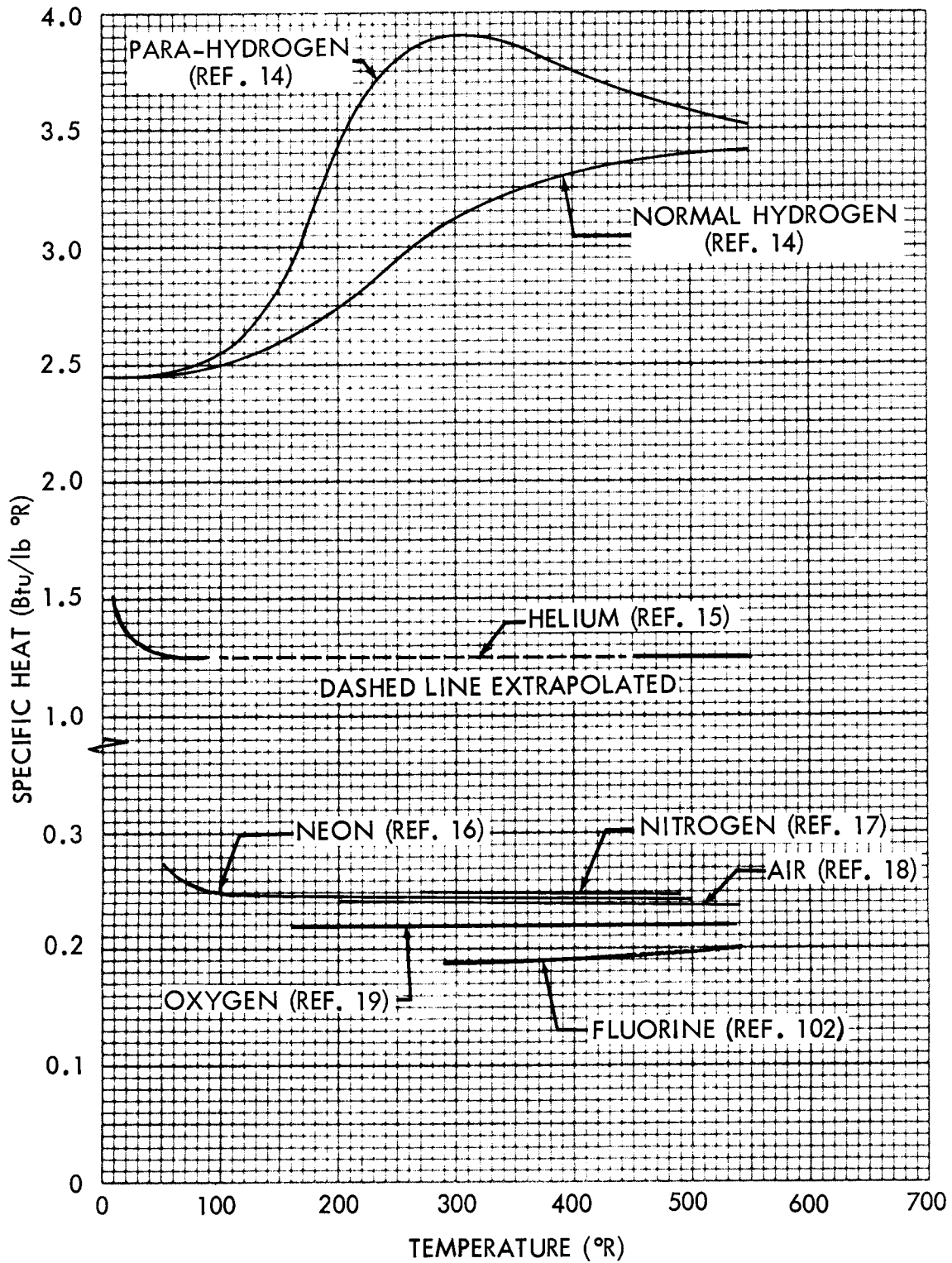


Fig. 1-3 Specific Heat of Gases at Constant Pressure as a Function of Temperature at 1 Atm.

Viscosity of Gases as a Function of Temperature

The viscosity of purge gas influences its rate of venting from the multilayer insulation during early times in the ascent flight (in the continuum flow regime). High viscosity gas resists flow through the multilayer insulation.

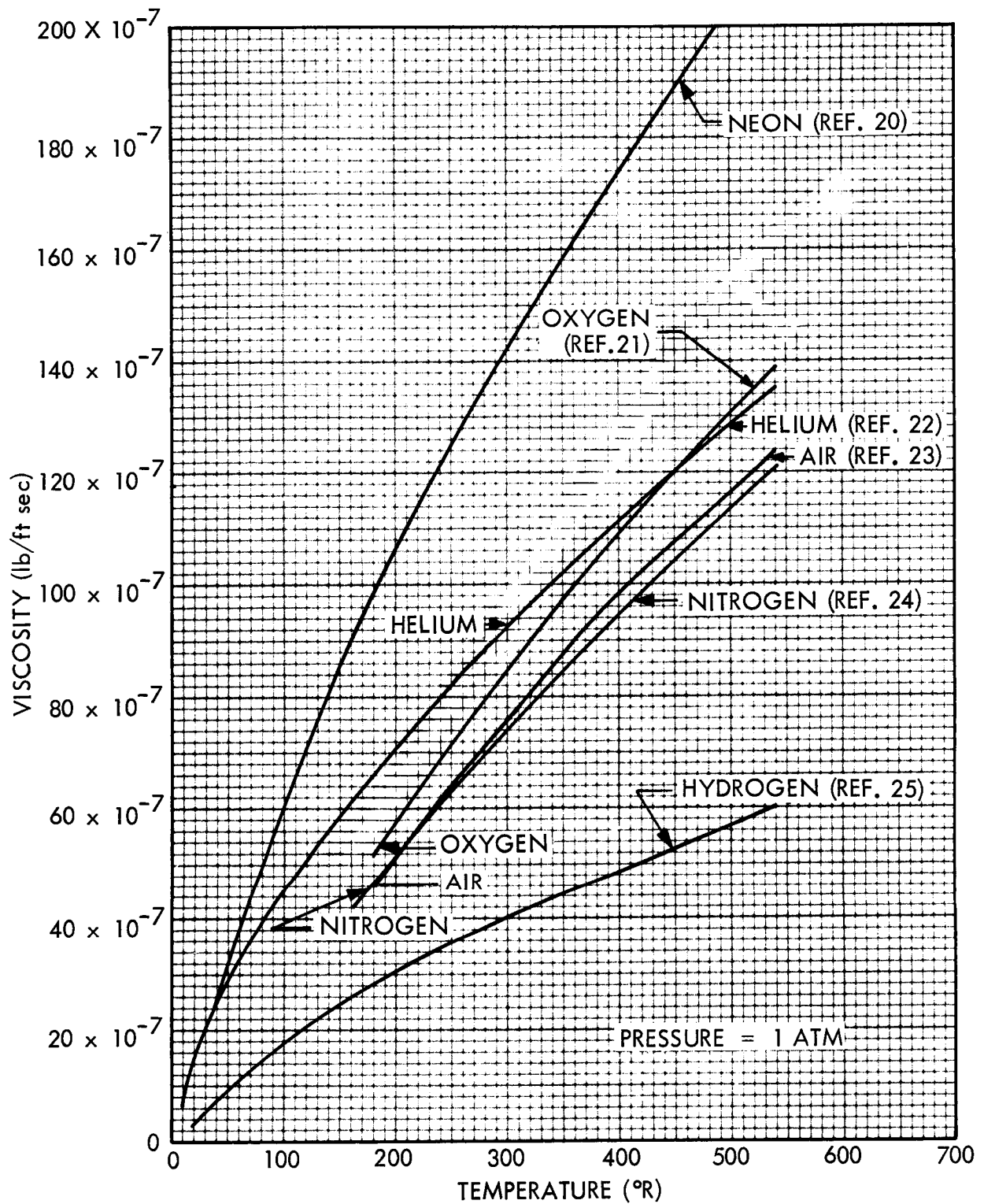


Fig. 1-4 Viscosity of Gases as a Function of Temperature

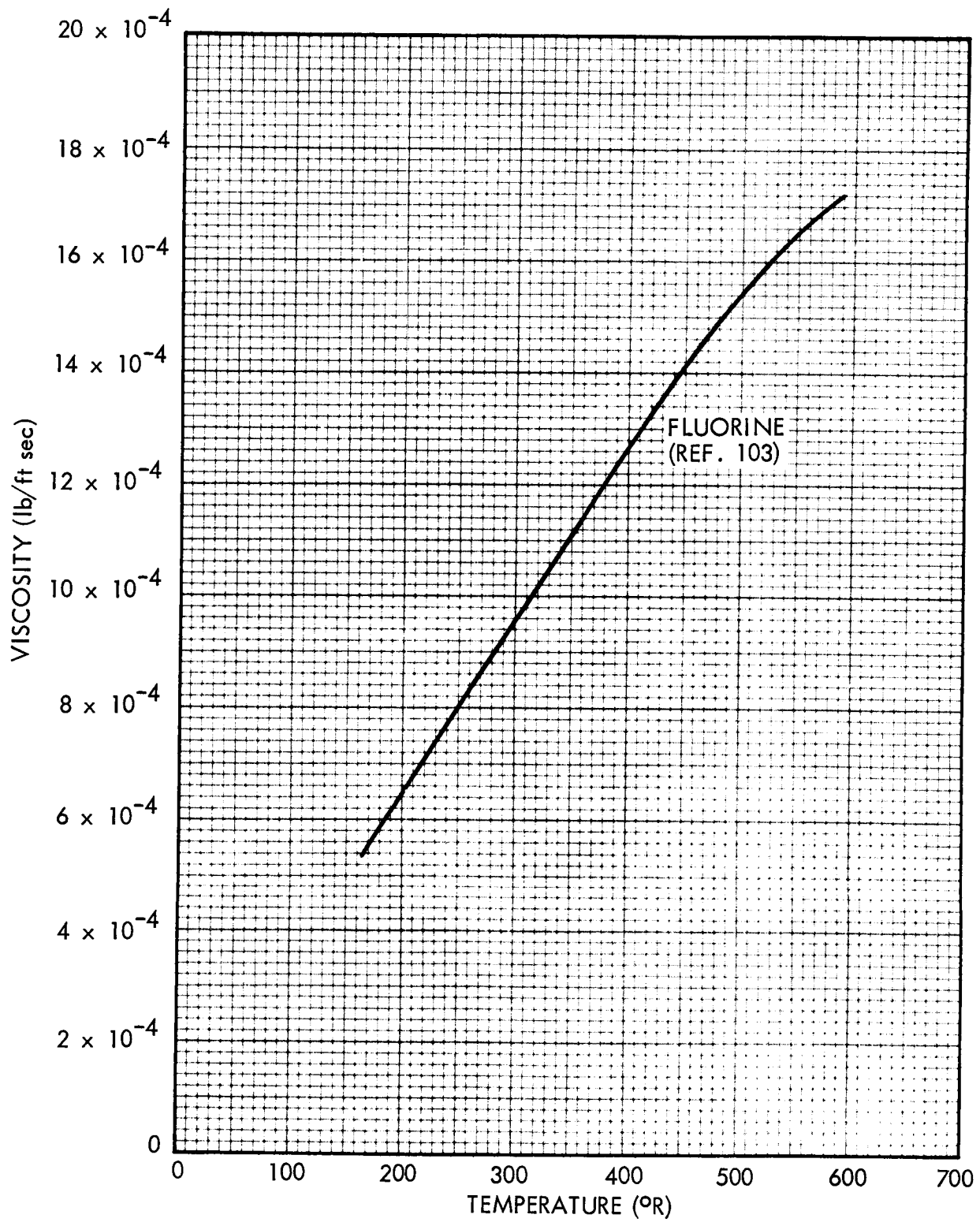


Fig. 1-5 Viscosity of Fluorine as a Function of Temperature

2. METALS

The thermal effectiveness of a multilayer insulation system is influenced by the type and quantity of structural, plumbing, and electrical line penetrations through the insulation to the propellant tank. The selection of materials for fabricating these penetrations depends on structural properties, thermal properties, cost, and ease of fabrication. This section of the Handbook provides pertinent design data for metals used in most of the insulation penetrations.

The metals selected for reporting are those which exhibit good low-temperature structural properties. Where data for a specific metal are not available, data for similar metals are provided. Data for high-purity metals are presented, also, for reference purposes. The data presented include density, linear thermal expansion, thermal conductivity, specific heat, and emissivity.

Density of Metals

The aluminum alloys shown are normally used for propellant tanks, the stainless steels for plumbing lines, and the titanium alloys for tank support structures.

Table 2-1

DENSITY OF METALS

Metals	Density at 75° F	
	lb/in. ³	lb/ft ³
ALUMINUM	0.097	168
2024	0.100	173
2219	0.102	176
6061	0.098	169
7039	0.099	171
7075	0.101	175
STAINLESS STEELS		
301	0.286	494
304	0.29	—
316	0.29	—
347	0.29	—
TITANIUM	0.163	281
5A1 2.5Sn	0.162	280
6A1 4V	0.161	278

Linear Thermal Expansion of Metals as a Function of Temperature

Certain curves were adjusted slightly so that zero percent expansion falls at 538° R. This shift does not affect the relative value of thermal expansion between two temperatures.

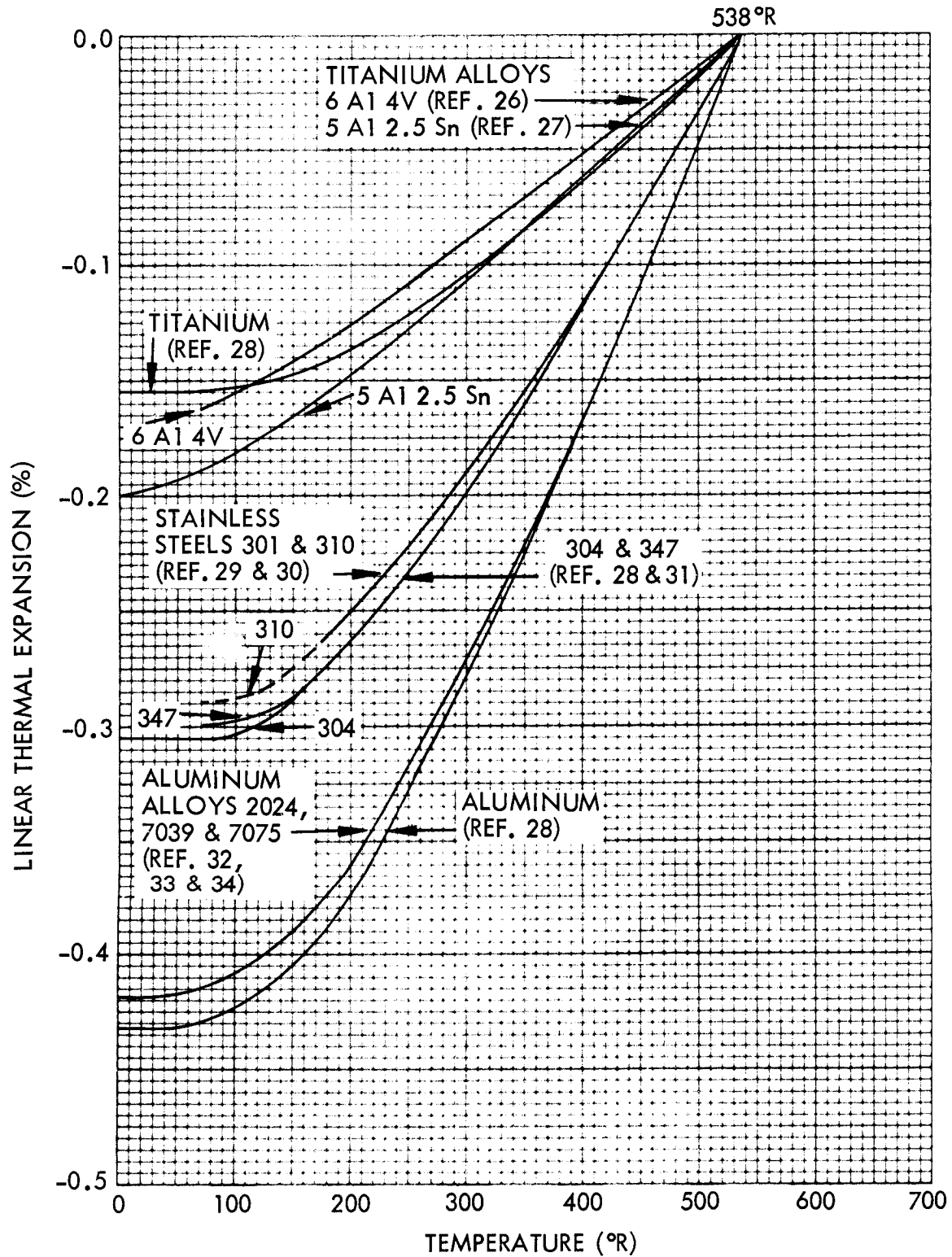


Fig. 2-1 Linear Thermal Expansion of Metals as a Function of Temperature

Thermal Conductivity of Metals as a Function of Temperature

The thermal conductivity of 7075-T6 aluminum in the annealed condition is higher than for the same material in the tempered condition. This characteristic is typical of an alloy after annealing.

The thermal conductivity of four commercial titanium alloys and several stainless alloys have been included in a separate figure for clarity. The titanium alloys are alloyed as follows:

4A1-3Mo-1V - 4.4% Al, 1.0% V, 3.0% Mo, 0.1% Fe, 0.03% C, 0.011% N

2.5A1-16V - 2.75% Al, 14.95% V, 0.21% Fe, 0.03% C, 0.015% N

6A1-4V - 5.89% Al, 3.87% V, 0.15% Fe, 0.02% C, 0.015% N

13V-11Cr-3A1 - 3.5% Al, 13.9% V, 10.4% Cr, 0.25% Fe, 0.04% C, 0.025% N

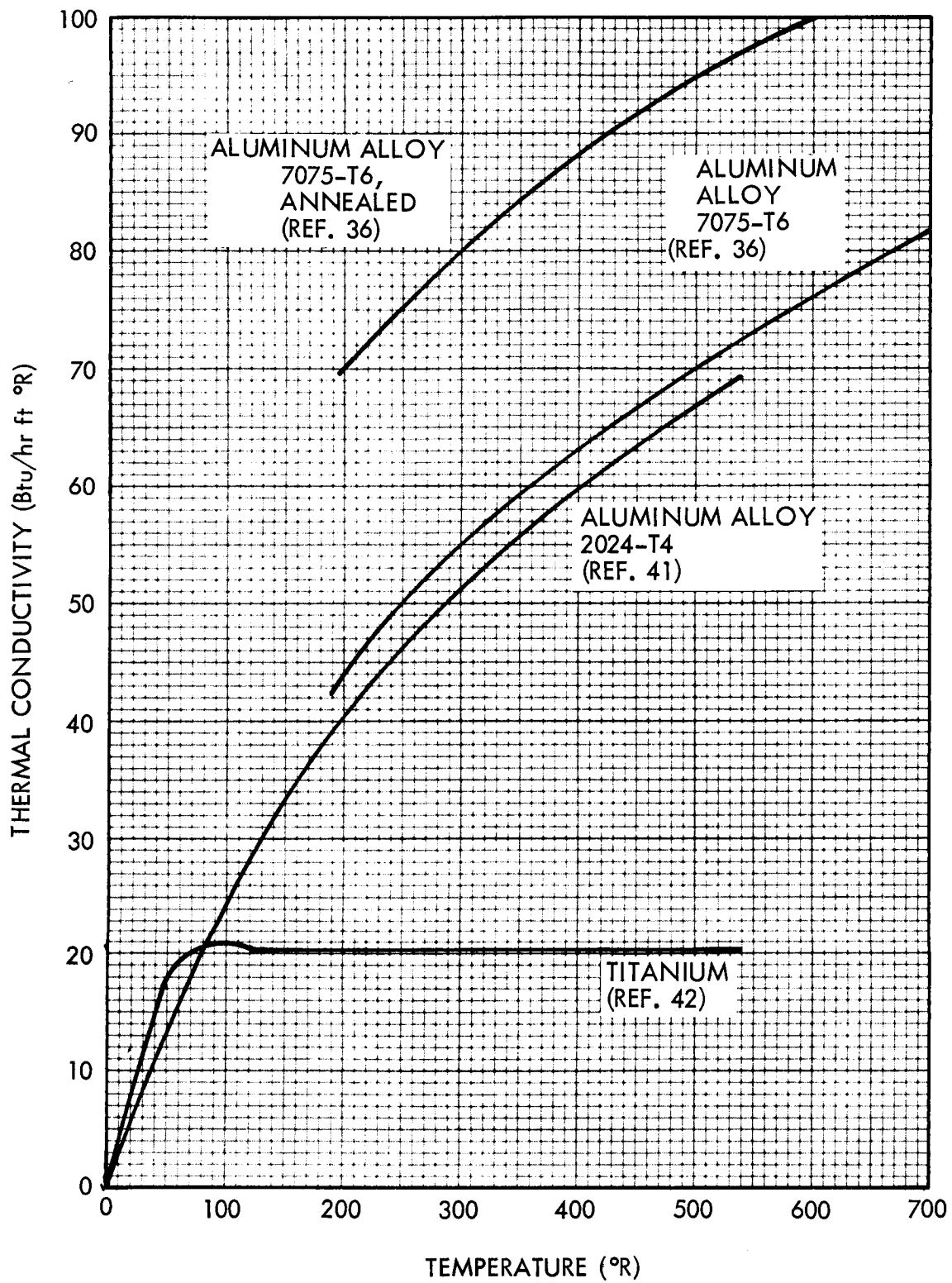


Fig. 2-2 Thermal Conductivity of Metals as a Function of Temperature

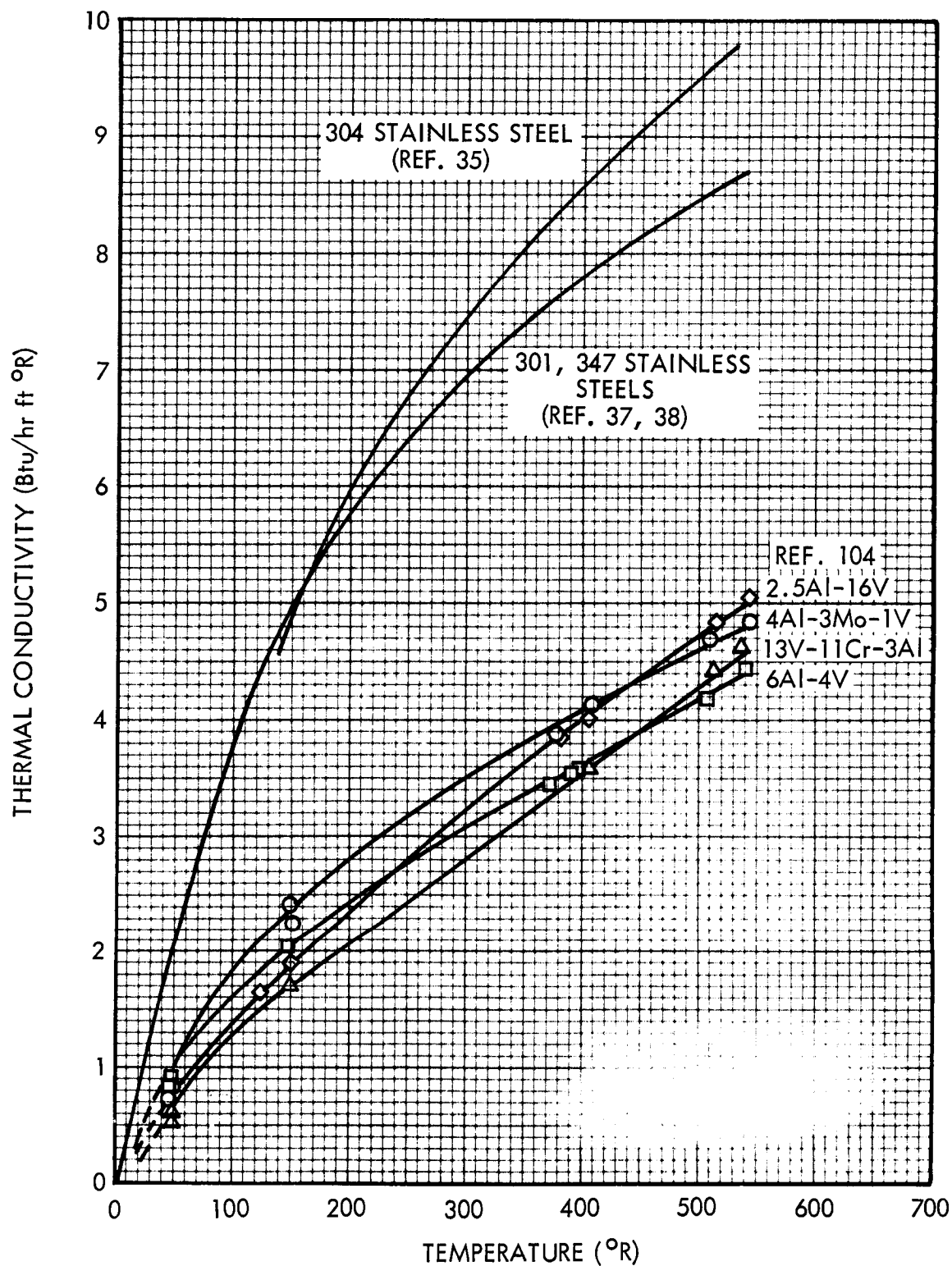


Fig. 2-3 Thermal Conductivity of Titanium Alloys as a Function of Temperature

Thermal Conductivity Integrals of Metals

The thermal conductivity integrals for metallic solids are presented in this section as a function of temperature. The thermal conductivity integral is defined from the Fourier Equation for steady unidirectional heat conduction as follows:

$$Q = kA \frac{dT}{dx}$$

where

Q = Rate of heat conduction, negative in the direction of increasing length

k = Thermal conductivity

A = Cross-sectional area of the heat conduction path, normal to the direction of heat flow

$\frac{dT}{dx}$ = Temperature gradient along the path at the section under consideration

T = Temperature

x = Length

For a constant cross-sectional area the Fourier Equation becomes

$$Q \frac{L}{A} = \int_{T_1}^{T_2} k dT$$

where T_1 and T_2 are the temperatures at any two points along the path of heat flow, and L is the distance between these two points.

The thermal conductivity integrals plotted in this section as function of temperature are values of

$$\int_{T_o}^{T_L} k dT$$

where T_O and T_L are temperatures along a heat flow path communicating between heat reservoirs at $T_O = 7.2^\circ\text{R}$ and T_L at length L for T_O . The heat flow along a conductor of constant cross-section A , through length L , may then be determined from the difference of the thermal conductivity integrals

$$Q \frac{L}{A} = \int_{T_1}^{T_2} k \, dT = \int_{T_O}^{T_2} k \, dT - \int_{T_O}^{T_1} k \, dT$$

In order to extend the usefulness and accuracy of the data presented, temperature scales have been expanded and data have been plotted on a series of graphs to cover the entire temperature range of interest.

Thermal Conductivity Integrals of Pure Aluminum
as a Function of Temperature

Aluminum I - 99.996% pure, single crystal (ALCOA)
99.99% pure, cold drawn (ALCOA)

Aluminum II - 99% commercial pure (ALCOA) drawn

All data were obtained from Ref. 104.

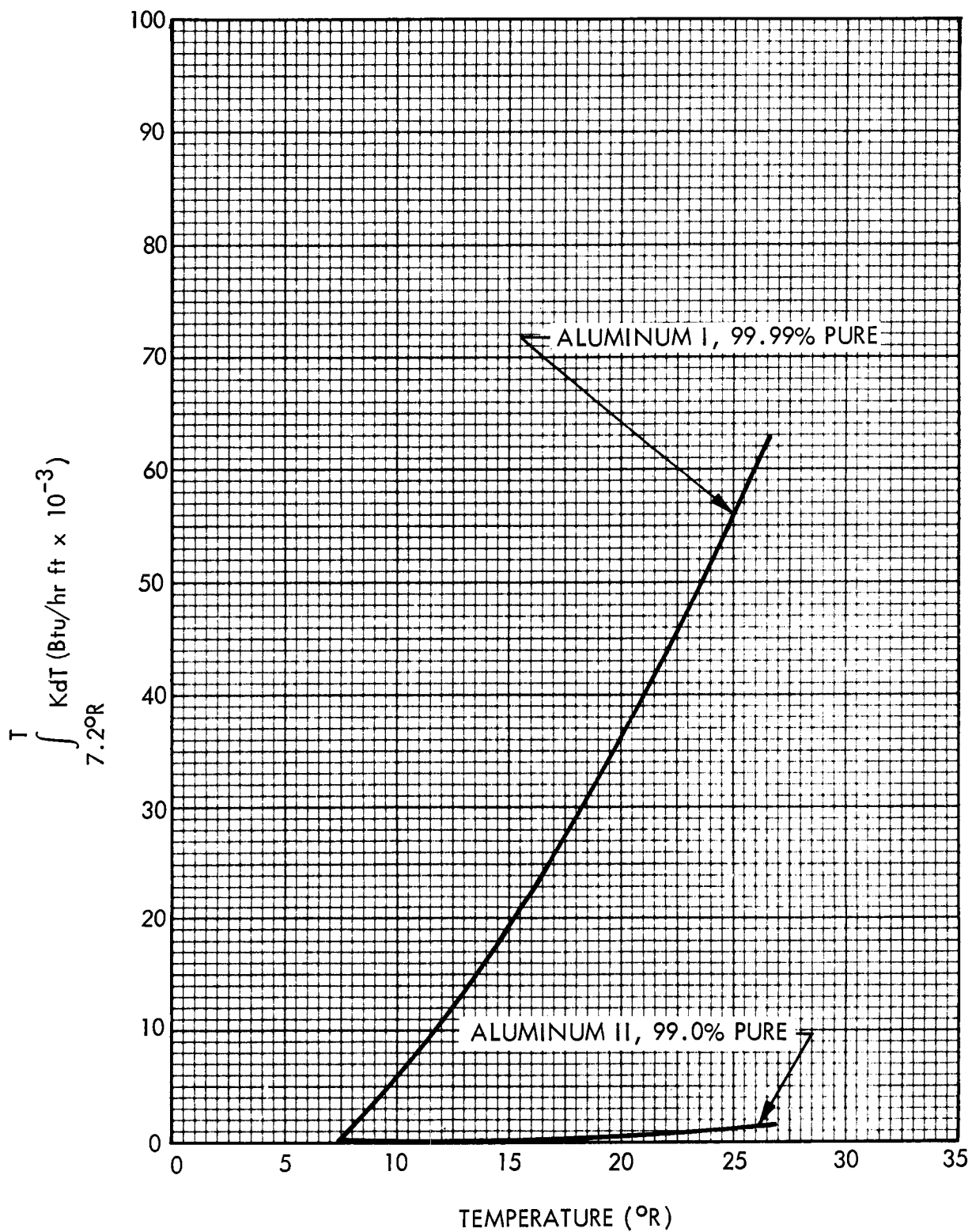


Fig. 2-4(a) Thermal Conductivity Integrals of Pure Aluminum as a Function of Temperature

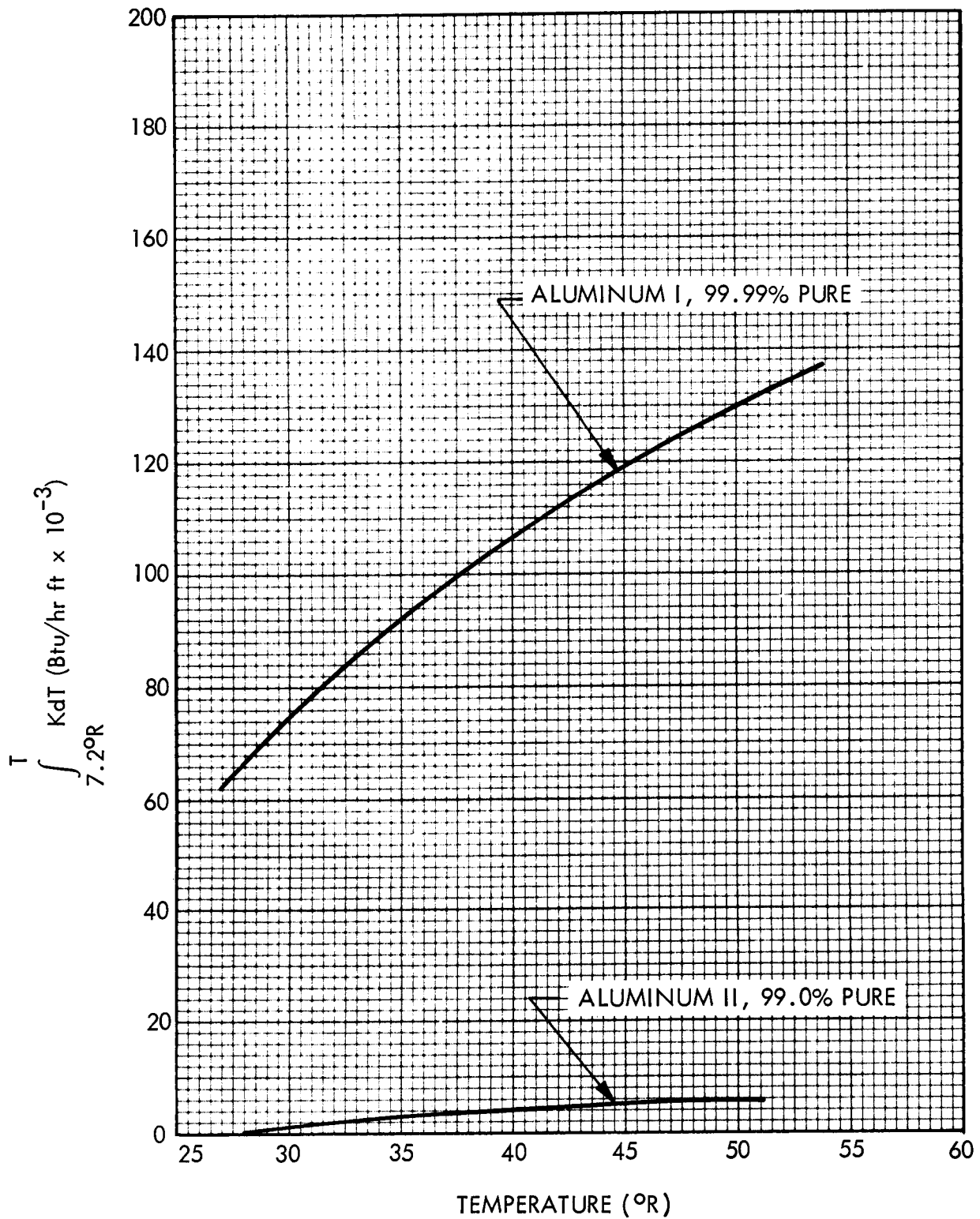


Fig. 2-4(b) Thermal Conductivity Integrals of Pure Aluminum as a Function of Temperature

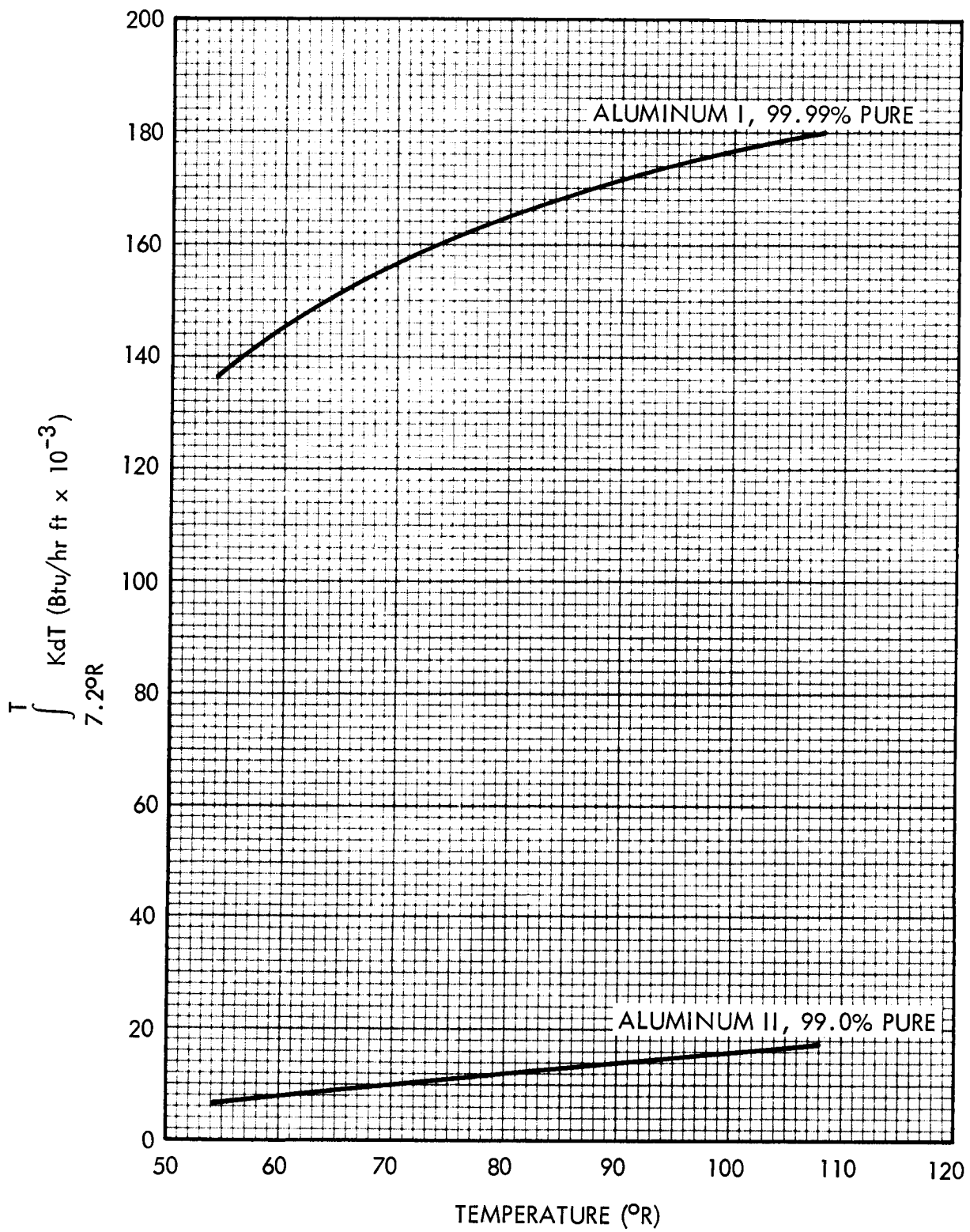


Fig. 2-4(c) Thermal Conductivity Integrals of Pure Aluminum as a Function of Temperature

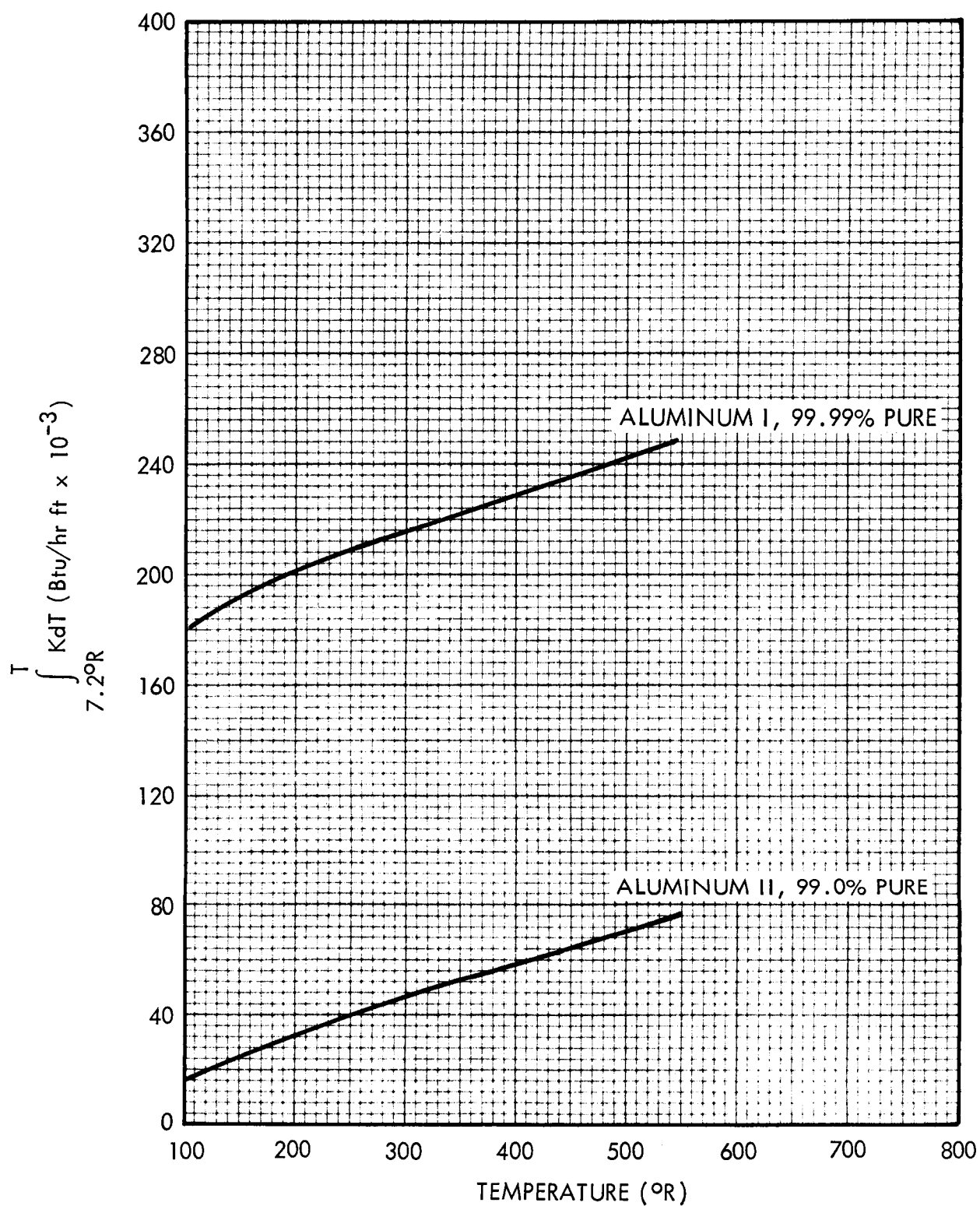


Fig. 2-4(d) Thermal Conductivity Integrals of Pure Aluminum as a Function of Temperature

Thermal Conductivity Integrals of Various Aluminum Alloys
as a Function of Temperature

The alloys cited in the graphs are composed of the various elements as follows:

1100-F - ALCOA, 99% pure aluminum as fabricated

6063-T5 - ALCOA, 0.4% Si, 0.7% Mg, 98.5% Al, as fabricated

3003-F - ALCOA, 1.2% Mn, 98.5% Al, as fabricated

4S - 0.16% Cu, 1.02% Mg, 1.20% Mn, 0.52% Fe, 0.13% Si, 0.02% Cr, 0.02% Ti

5052-O - 0.25% Cr, 2.5% Mg, 97% Al, annealed

5154-O - 0.25% Cr, 3.5% Mg, 96% Al, annealed

75-S - 1.5% Cu, 5.5% Zn, 2.5% Mg, 0.2% Mn, 0.3% Cr

2024-T4 - 0.6% Mn, 1.5% Mg, 4.5% Cu, 93% Al, solution heat treated

All data were obtained from Ref. 104

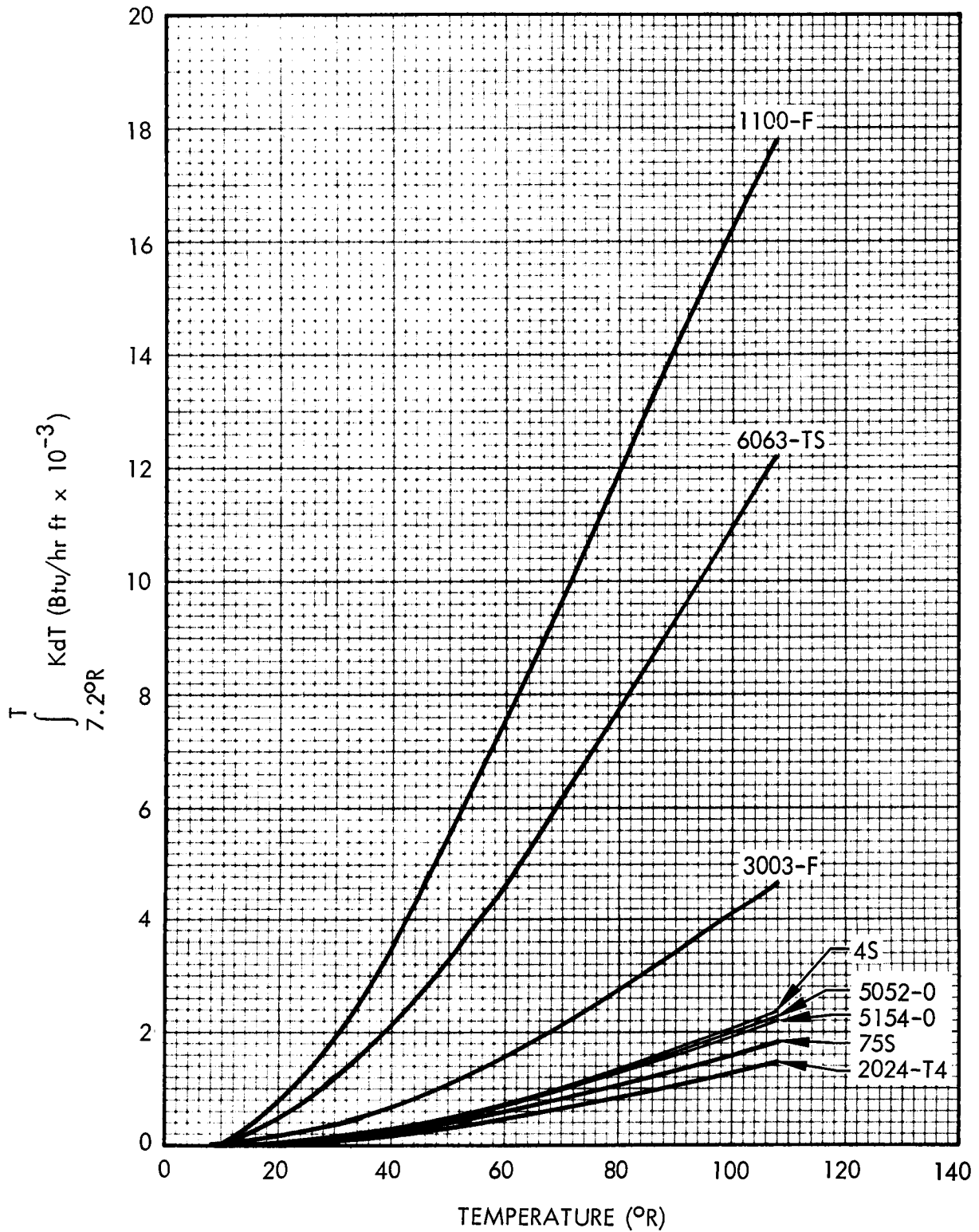


Fig. 2-5(a) Thermal Conductivity Integrals of Various Aluminum Alloys as a Function of Temperature

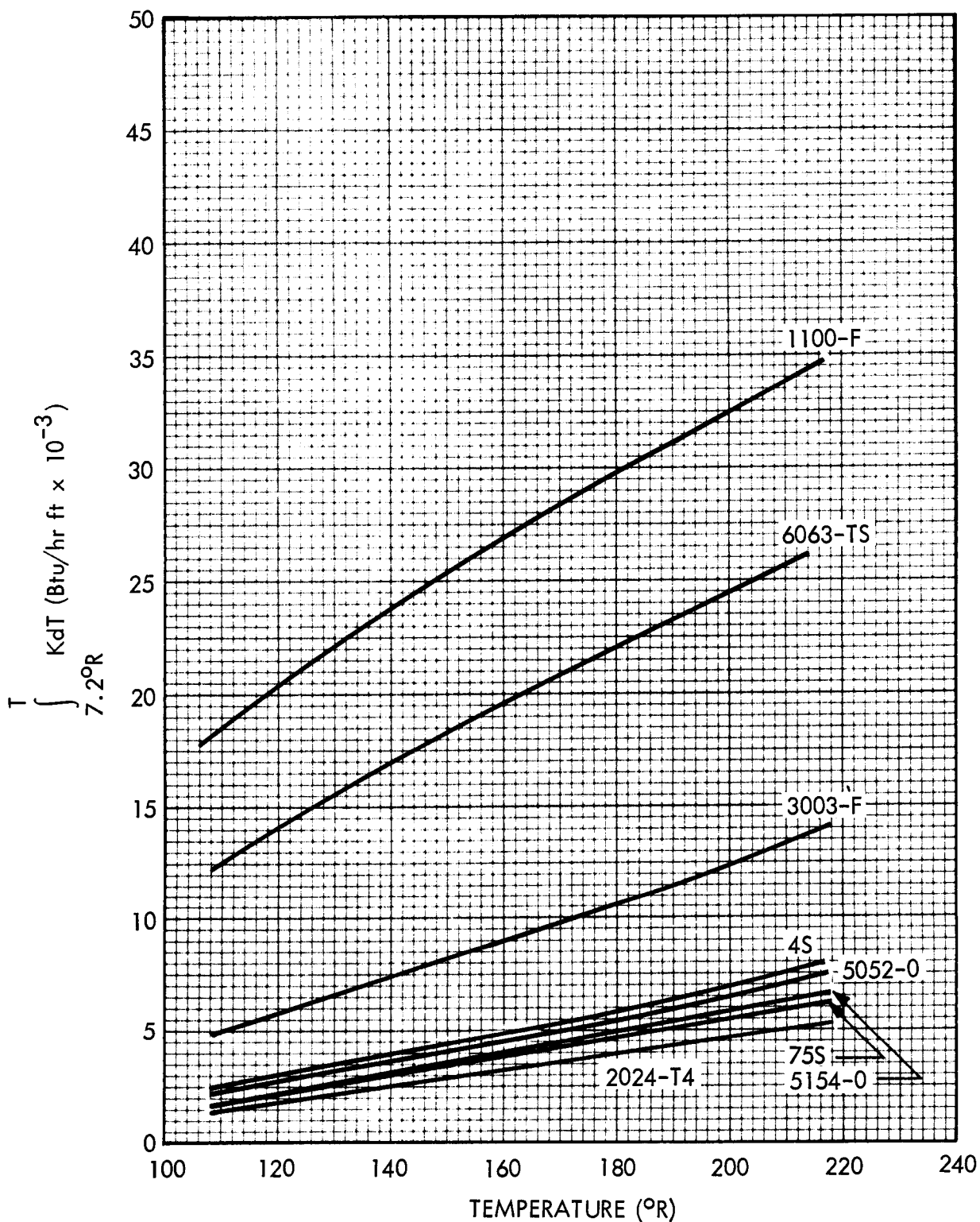


Fig. 2-5(b) Thermal Conductivity Integrals of Various Aluminum Alloys as a Function of Temperature

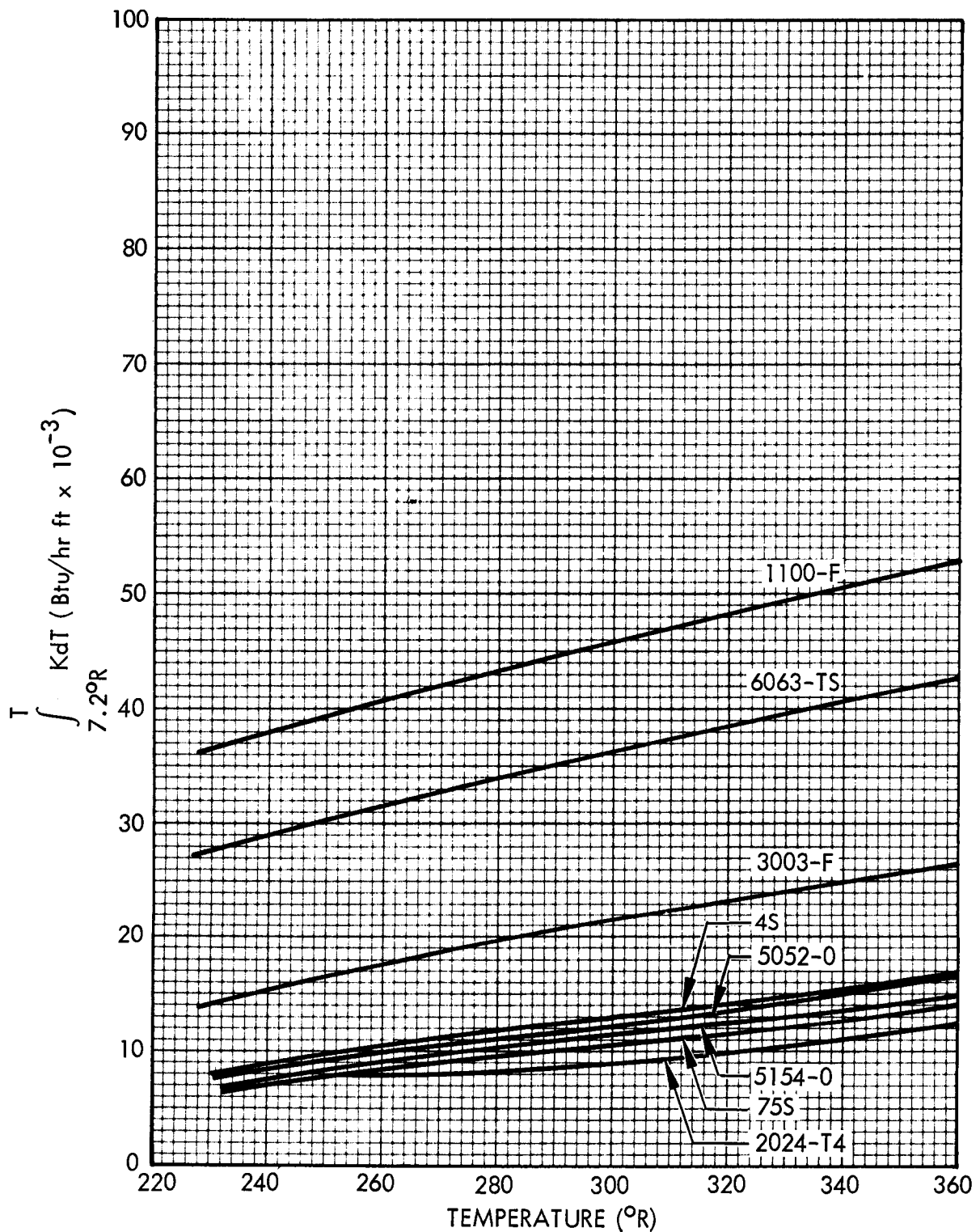


Fig. 2-5(c) Thermal Conductivity Integrals of Various Aluminum Alloys as a Function of Temperature

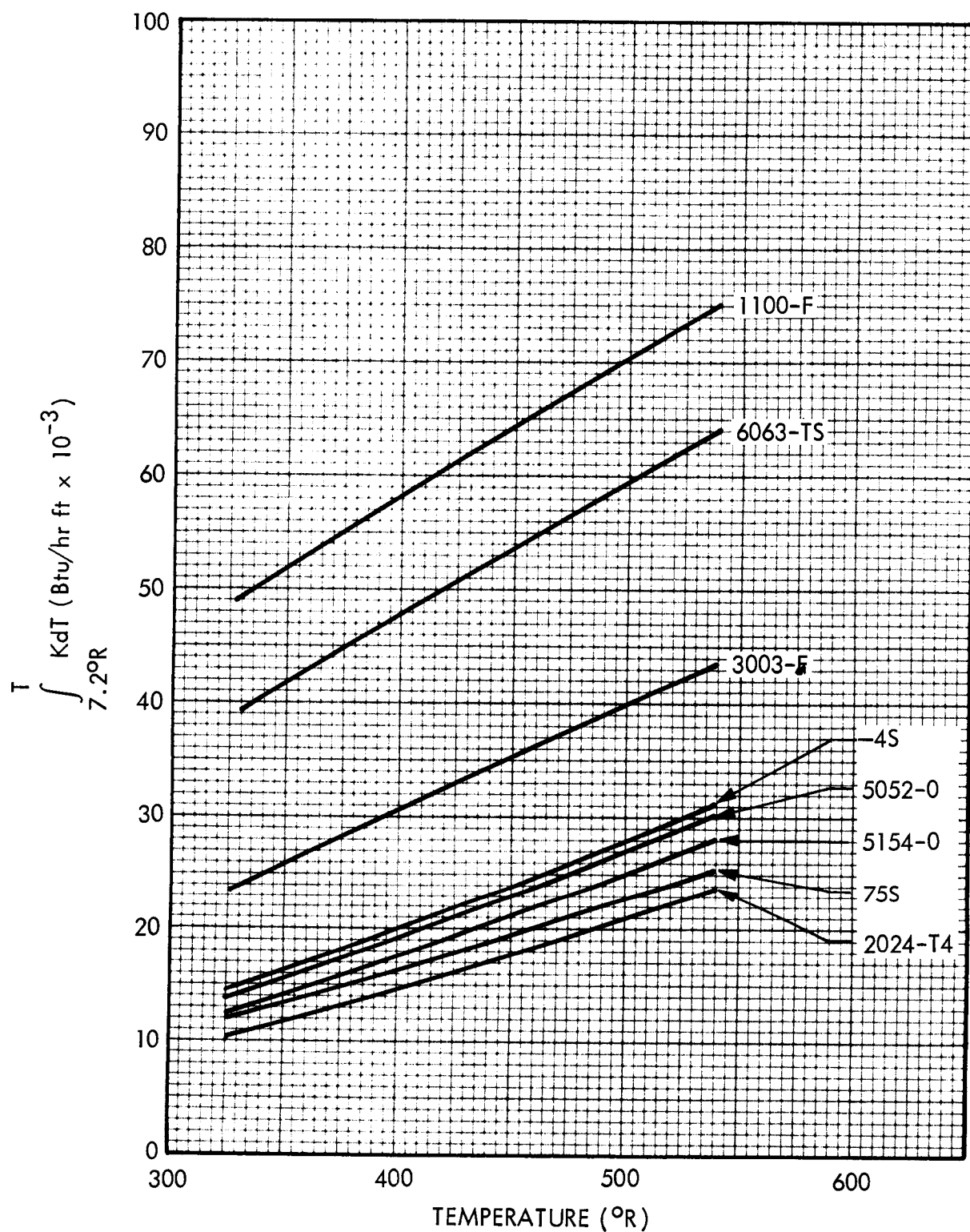


Fig. 2-5(d) Thermal Conductivity Integrals of Various Aluminum Alloys as a Function of Temperature

Thermal Conductivity Integrals of Titanium
as a Function of Temperature

Titanium - 99.99% pure, single crystal, Associates Electric Industries

Titanium Alloy - Rem-Cru, RC 130-B, 4.7% Mn, 3.99% Al, 0.14% C

All data were obtained from Ref. 104.

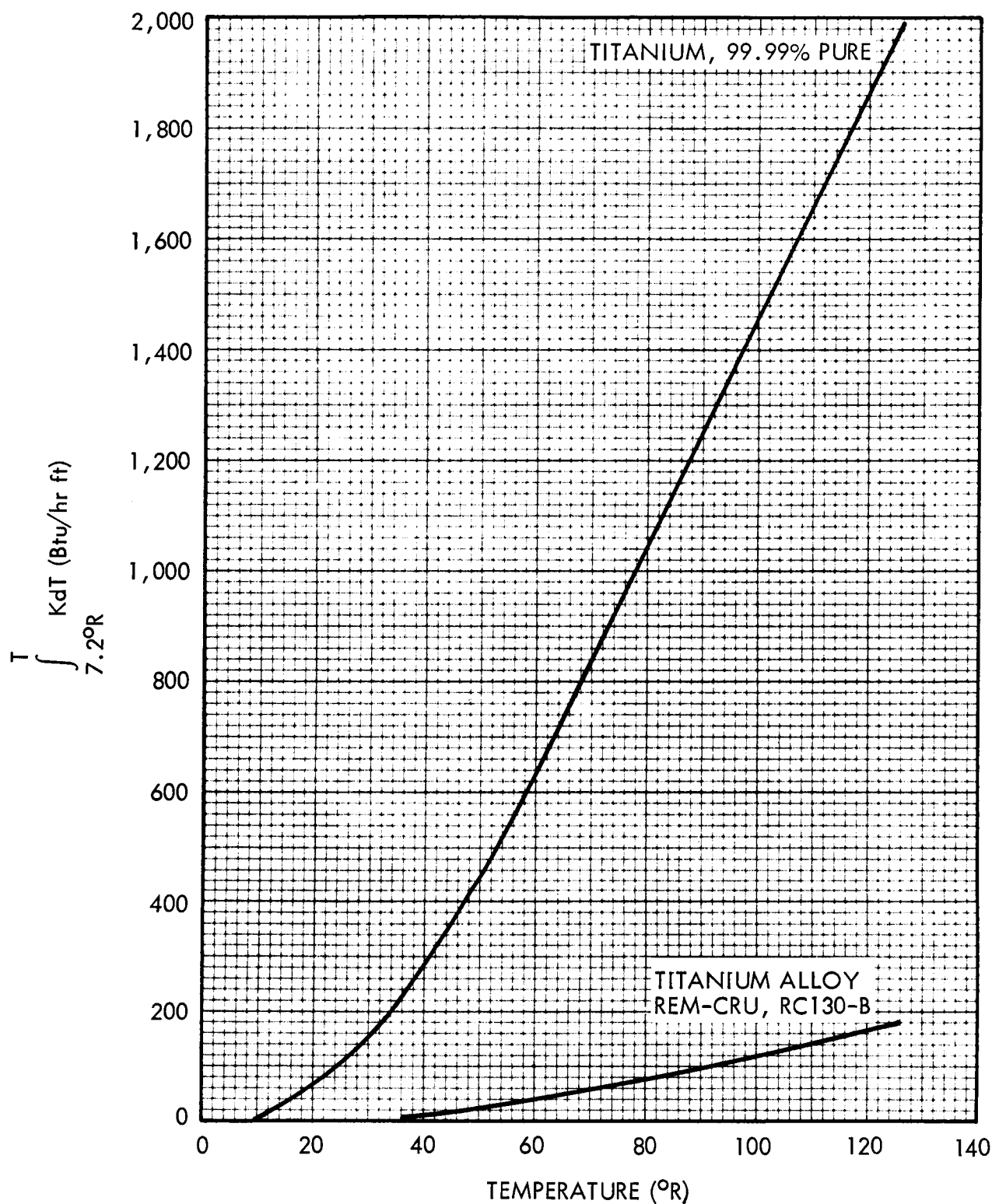


Fig. 2-6(a) Thermal Conductivity Integrals of Titanium as a Function of Temperature

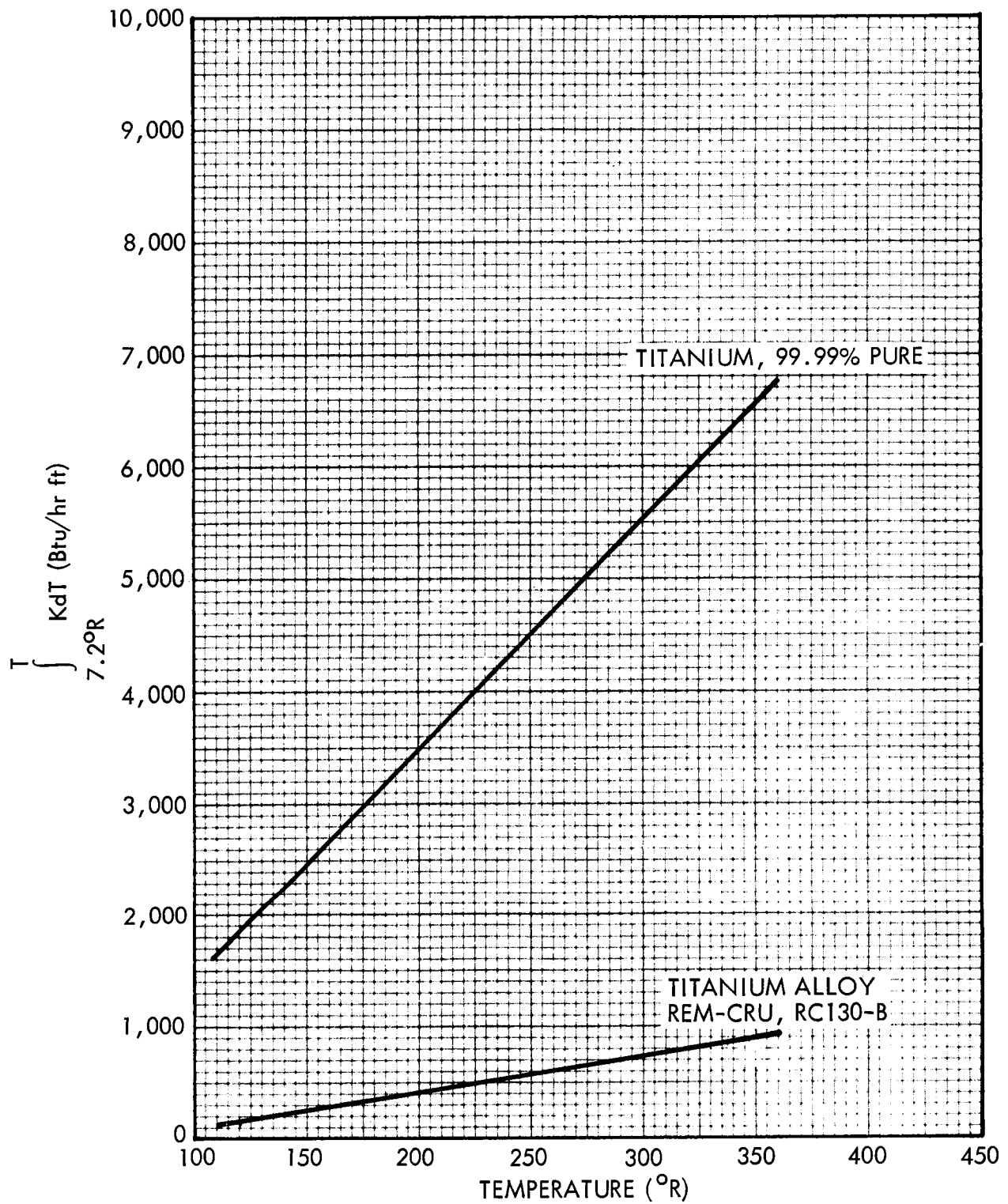


Fig. 2-6(b) Thermal Conductivity Integrals of Titanium as a Function of Temperature

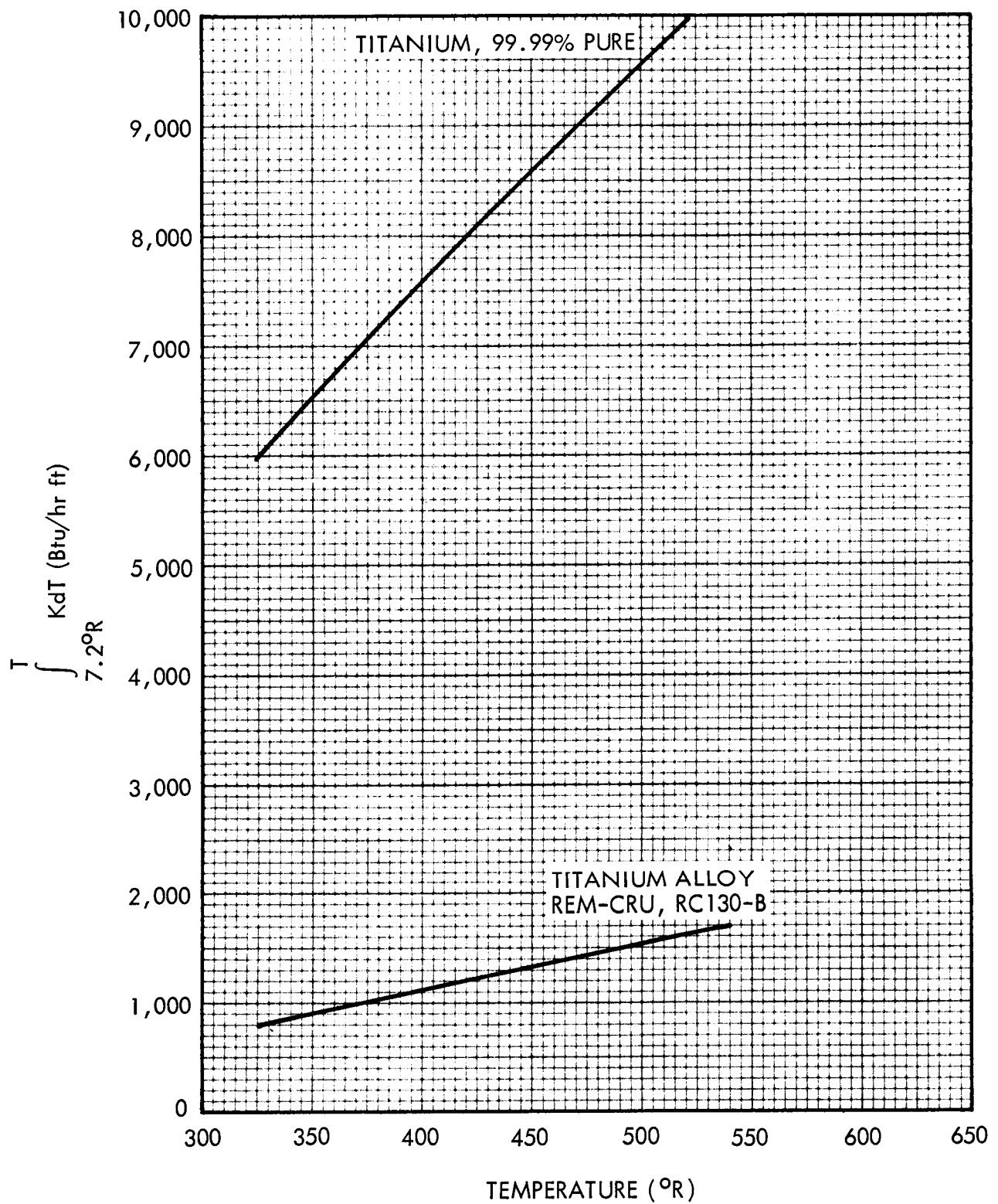


Fig. 2-6(c) Thermal Conductivity Integrals of Titanium as a Function of Temperature

Thermal Conductivity Integrals of Several Commercial Titanium

Alloys

4Al-3Mo-1V - 4.4% Al, 1.0% V, 3.0% Mo, 0.1% Fe, 0.03% C, 0.011% N

2.5Al-16V - 2.75% Al, 14.95% V, 0.21% Fe, 0.03% C, 0.015% N

6Al-4V - 5.89% Al, 3.87% V, 0.15% Fe, 0.02% C, 0.015% N

13V-11Cr-3Al - 3.5% Al, 13.9% V, 10.4% Cr, 0.25% Fe, 0.04% C, 0.025% N

All data were obtained from Ref. 105.

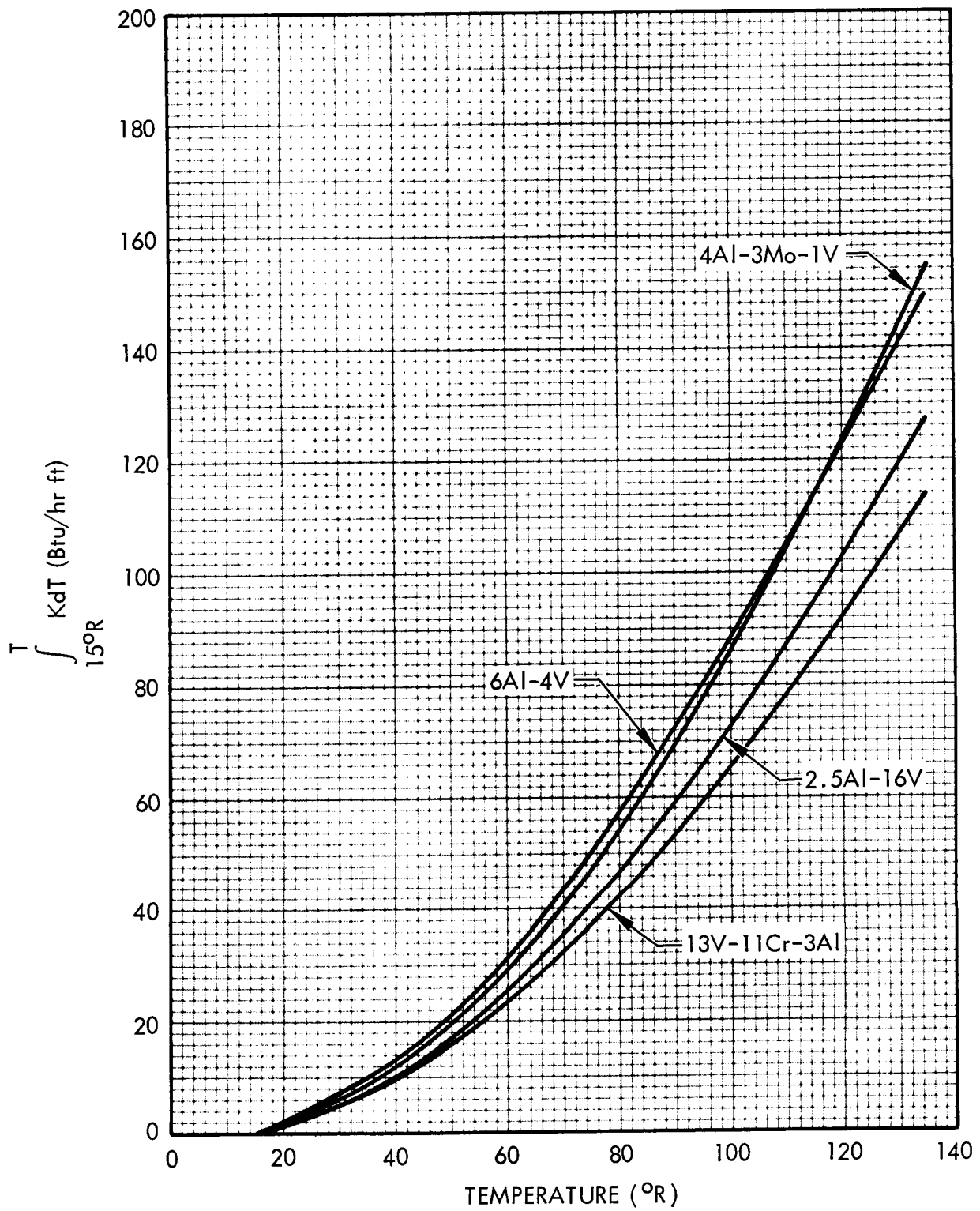


Fig. 2-7(a) Thermal Conductivity Integrals of Several Commercial Titanium Alloys

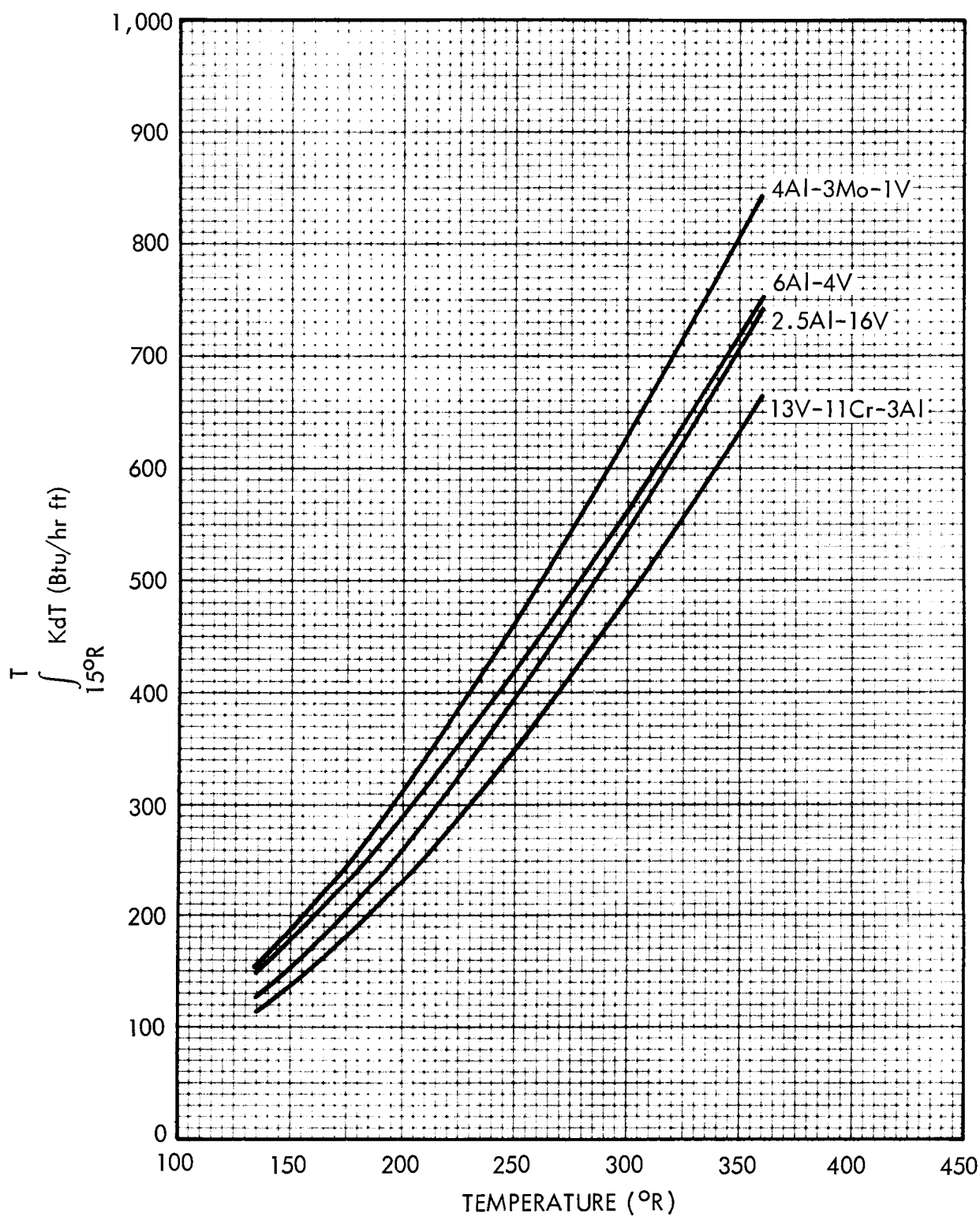


Fig. 2-7(b) Thermal Conductivity Integrals of Several Commercial Titanium Alloys

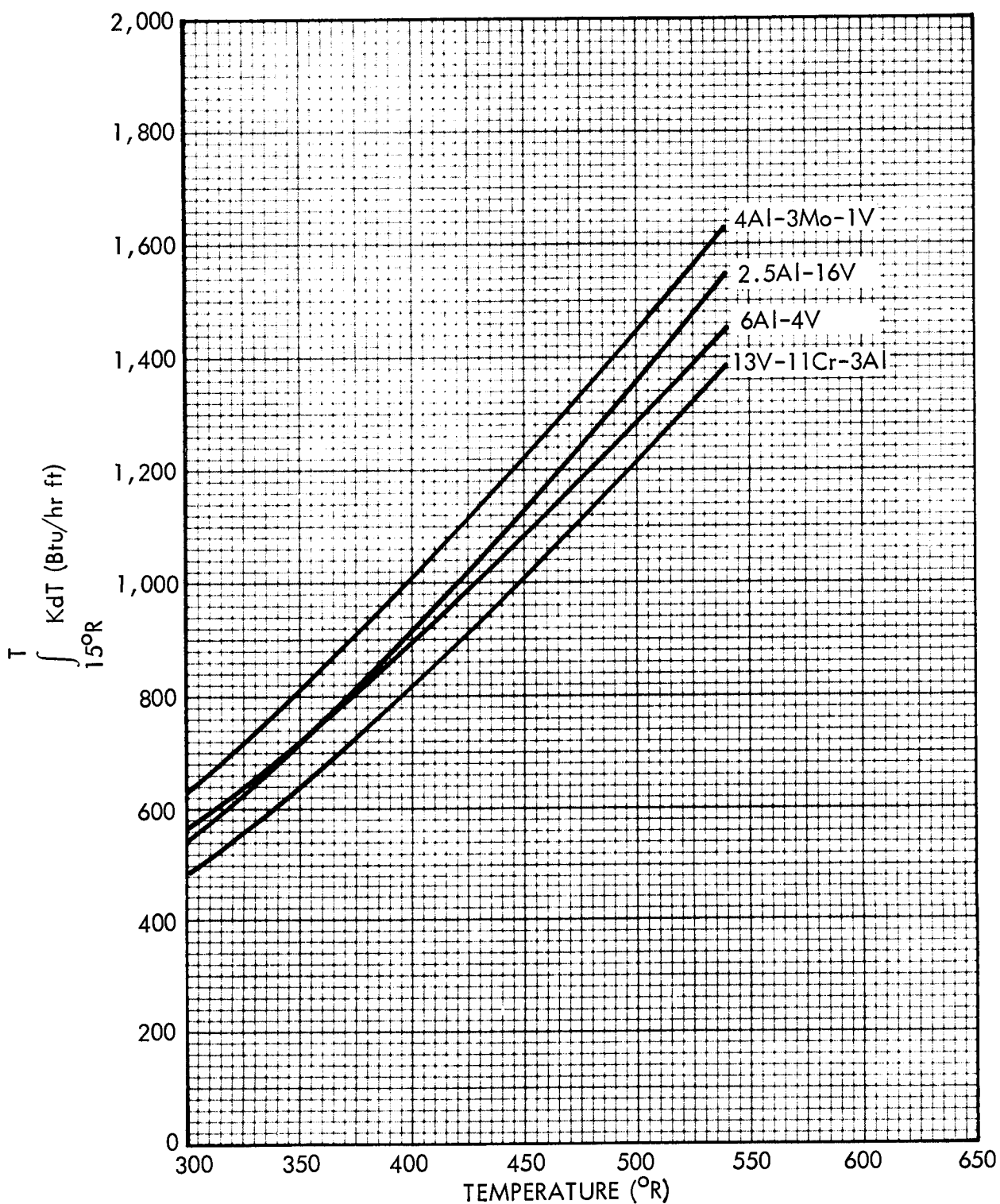


Fig. 2-7(c) Thermal Conductivity Integrals of Several Commercial Titanium Alloys

Thermal Conductivity Integrals of Ferrous Alloys
as a Function of Temperature

410 - 12.6% Cr, 0.36% Si, 0.32% Mn, 0.12% Ni, 0.09% C, 0.06% Cu, 0.03% N,
0.01% P

Stainless - Average value for close curves of types 303, 304, 316, 347, and
"stainless" as compiled in NBS Circular 556

All data were obtained from Ref. 104.

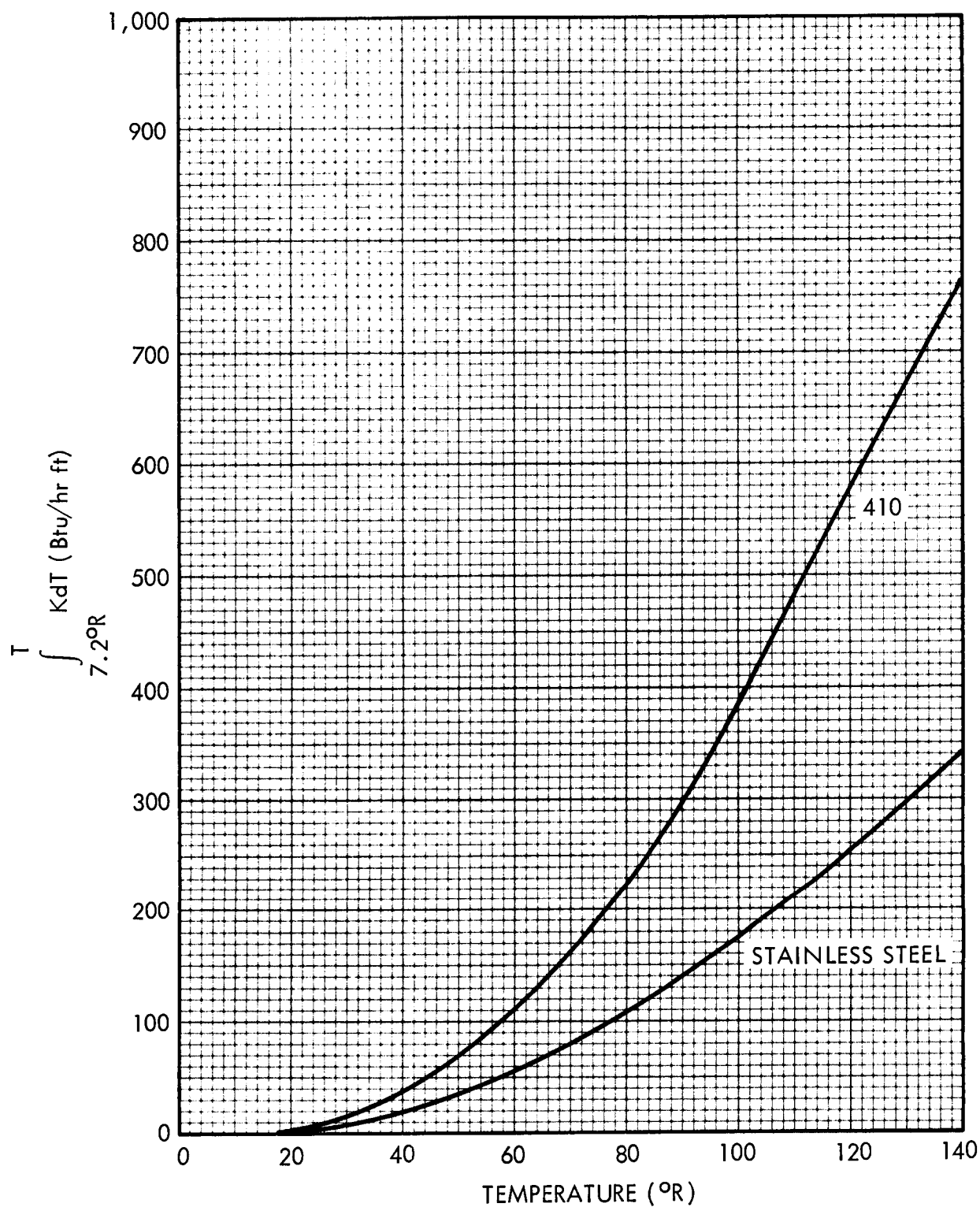


Fig. 2-8(a) Thermal Conductivity Integrals of Ferrous Alloys as a Function of Temperature

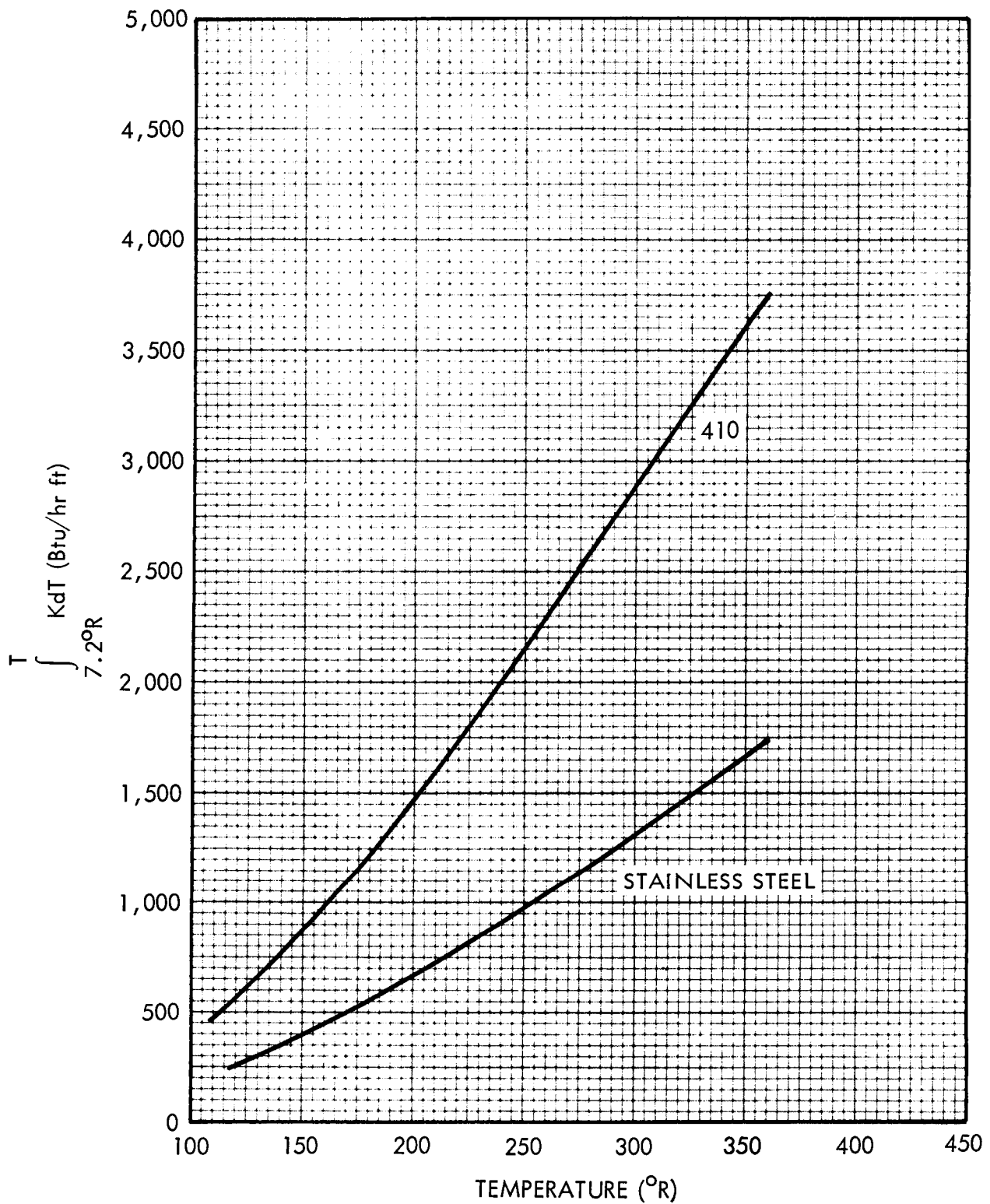


Fig. 2-8(b) Thermal Conductivity Integrals of Ferrous Alloys as a Function of Temperature

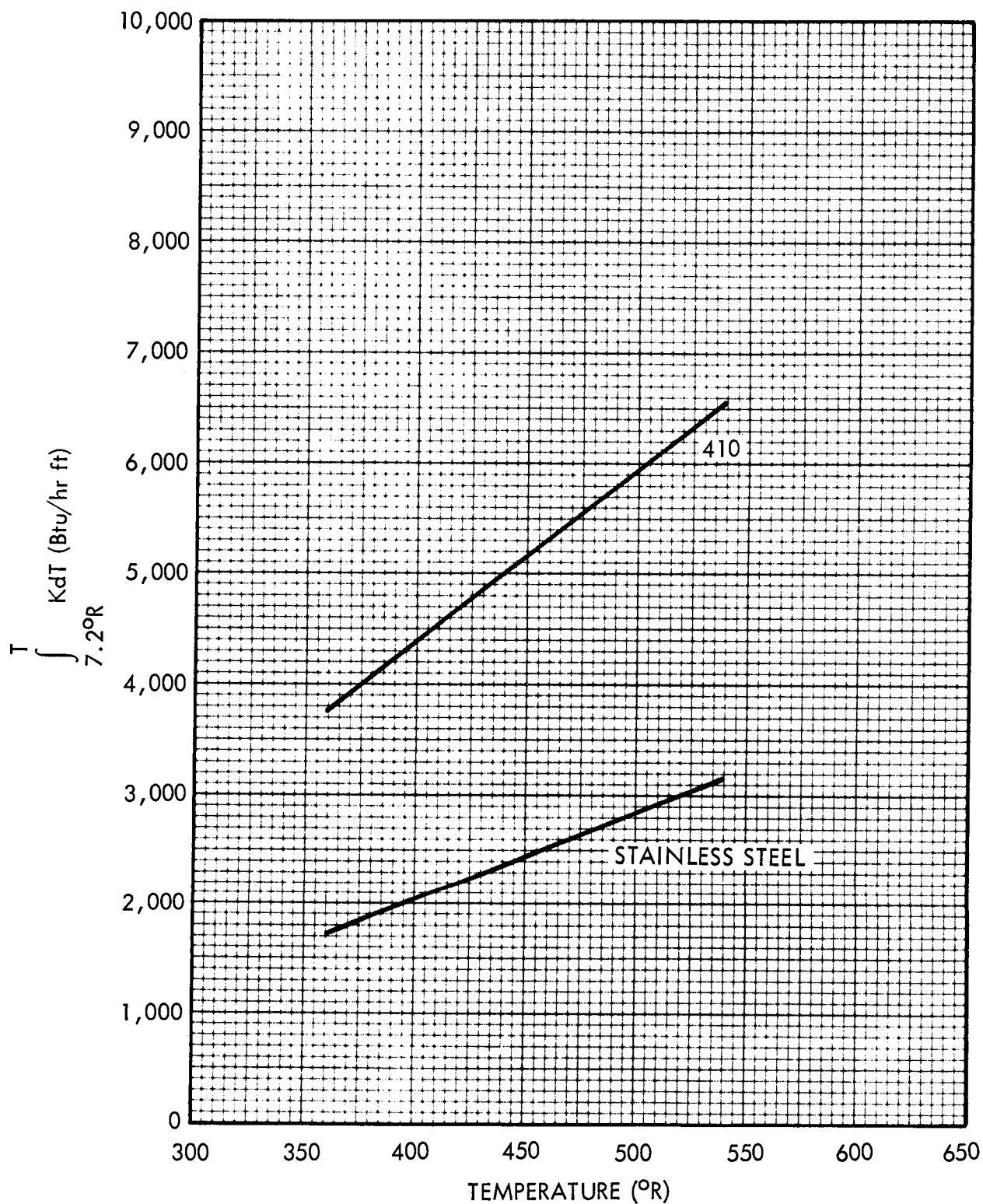


Fig. 2-8(c) Thermal Conductivity Integrals of Ferrous Alloys as a Function of Temperature

Specific Heat of Metals as a Function of Temperature

The stainless-steel alloys 316 and 347 are classified as 18-8 austenitic stainless steels. These contain 18 percent chromium and 8 percent nickel.

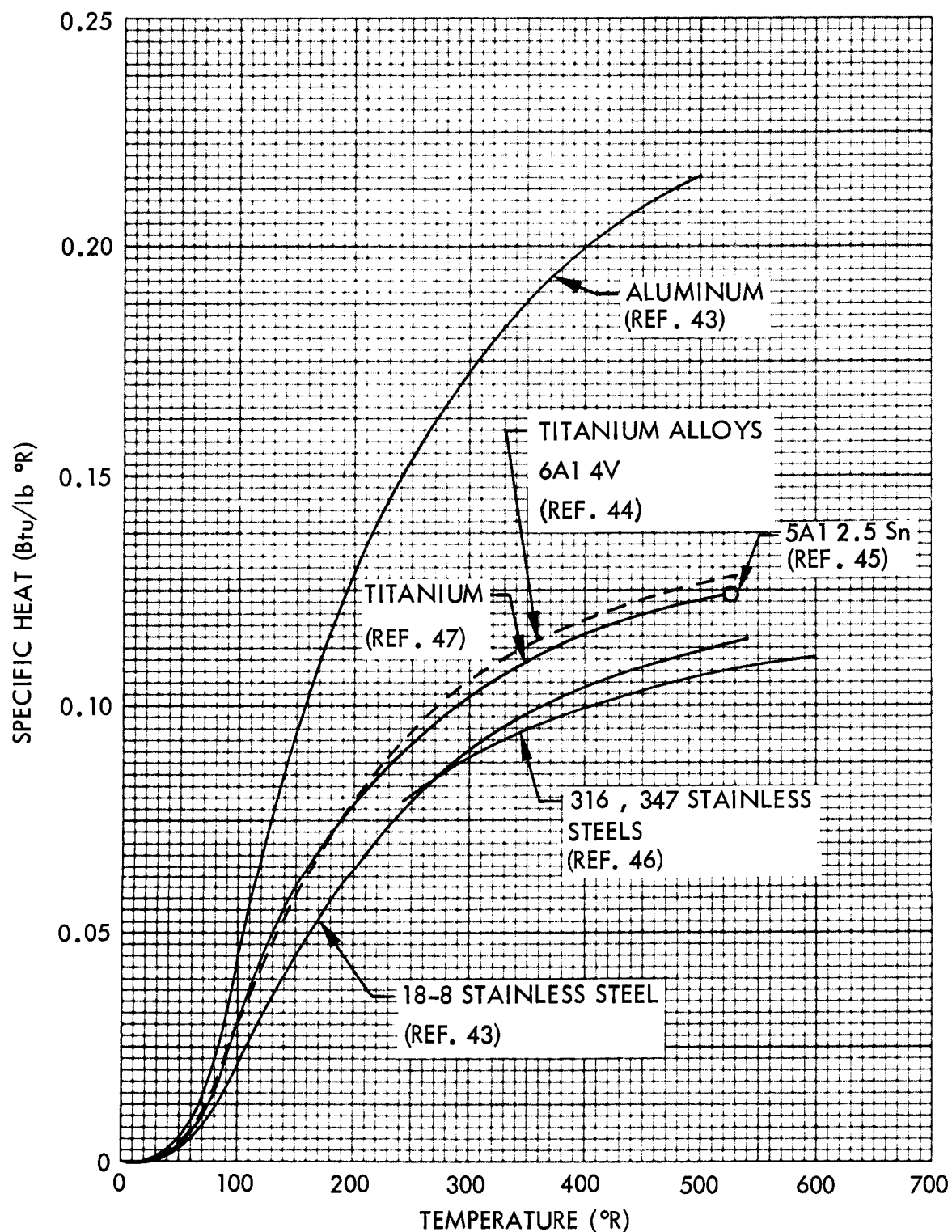


Fig. 2-9 Specific Heat of Metals as a Function of Temperature

Emittance of Metals as a Function of Temperature

Values of emittance depend markedly on the type of material, surface roughness, degree of oxidation, and temperature.

The No. 1 finish requires a 15- μ in. rms surface; the No. 8 finish requires a 2- μ in. rms surface.

The data for 2024 and 7075 aluminum alloy apply to "clean and smooth surfaces scrubbed with soap, washed with water, dried, wiped with toluene and then with alcohol", according to Refs. 48 and 49.

The data for 347 stainless steel apply to a surface cleaned as noted above.

Fig. 2-11 shows the variation of emittance with temperature for chemically cleaned copper and 1/4-mil thick aluminum foil. The aluminum foil is typical of that found in some multilayer insulation composites.

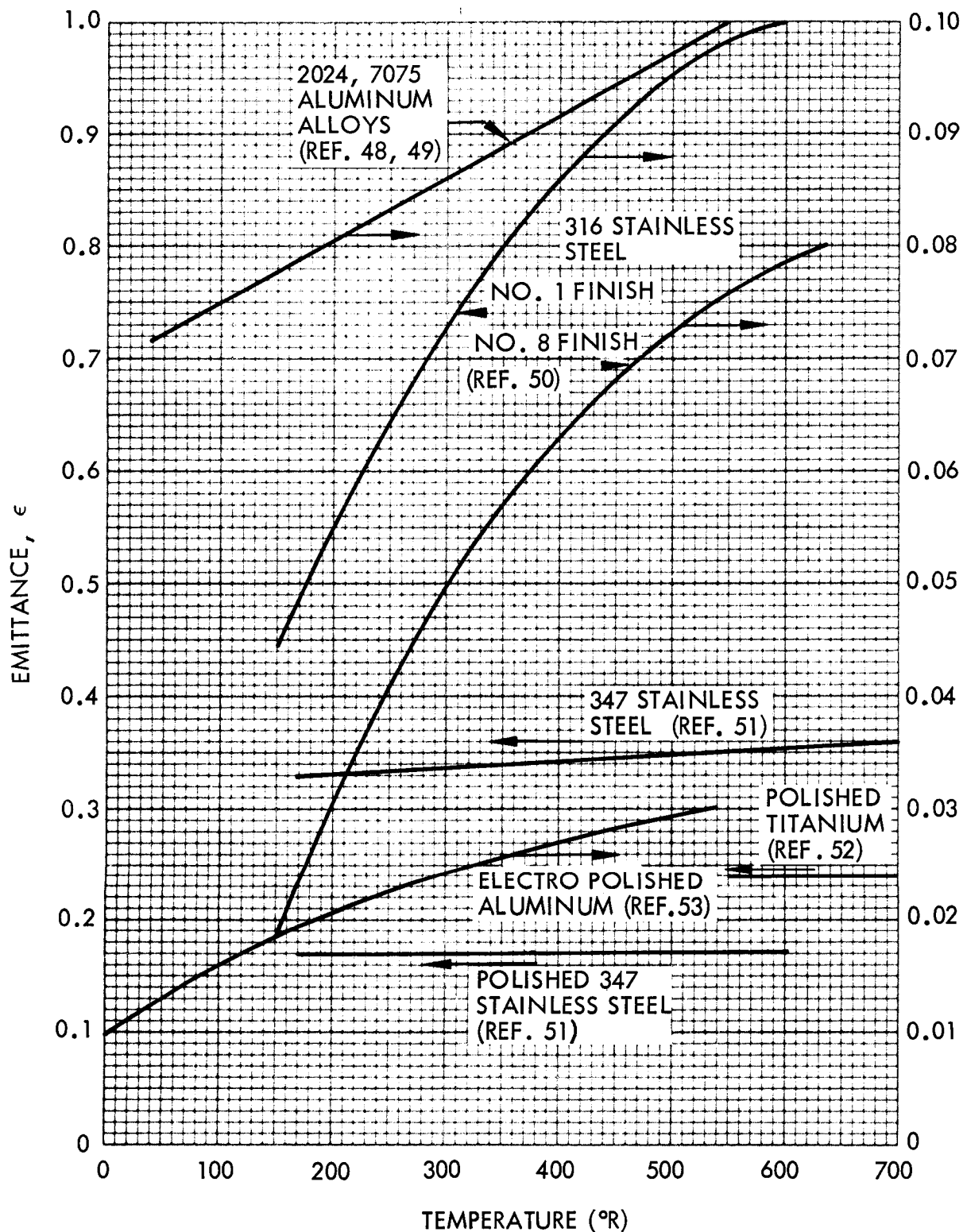


Fig.2-10 Emittance of Metals as a Function of Temperature

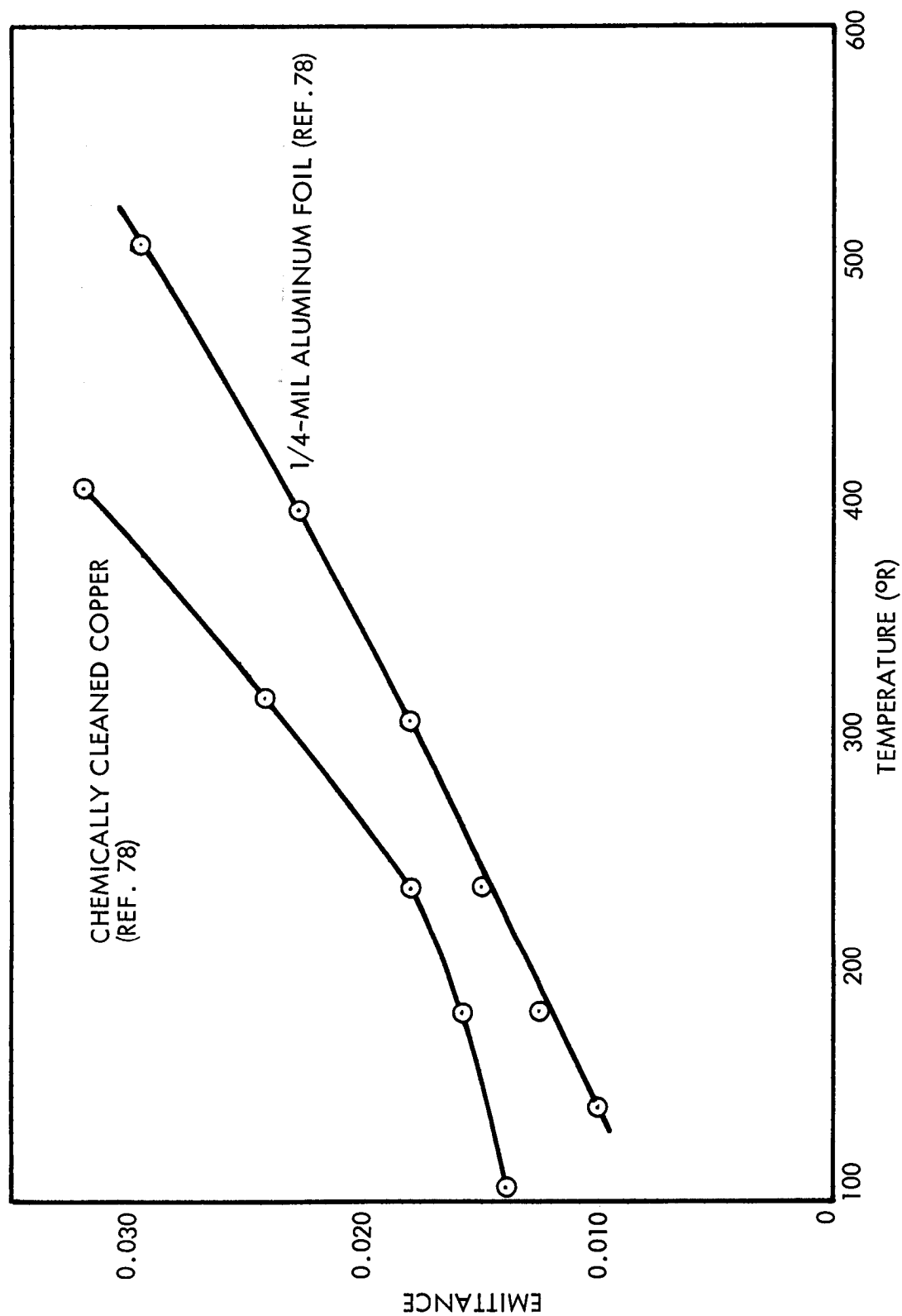


Fig. 2-11 Emissivity of Chemically Cleaned Copper and 1/4-mil Thick Aluminum Foil as a Function of Temperature

3. FIBERGLASS LAMINATES

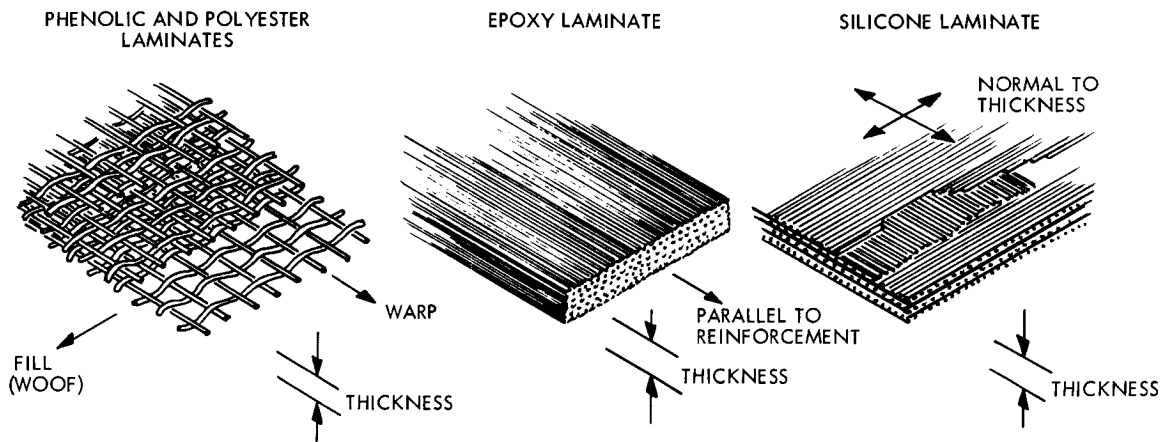
The use of fiberglass laminates is common for standoffs around structures. In the future, it may become feasible to use this class of materials for plumbing lines and propellant-tank support structures.

The property data provided in this section are for phenolic, epoxy, silicone, and polyester laminates. The data presented include density, linear expansion, thermal conductivity, and specific heat.

Table 3-1

CHARACTERISTICS OF FIBERGLASS LAMINATES

Resin Type	Key	Resin Trade Name	Reinforcement System				Layup	Resin Content (%)	Density (lb/cu. ft)
			Trade Name	Style	Form	Finish			
Phenolic	PH	CTL-91-LD	E Glass	181	Fabric	Volan A	Parallel laminate	23	102
Epoxy	E	DOW DER-332	YM-31-A Glass	—	Roving	HTS	Unidirectional	29	124
Silicone	S	DC-2106	E Glass	—	Roving	140 HTS	Cross-plyed at 90°	Not Given	116
Polyester	P	Paraplex P-43	E Glass	181	Fabric	Volan A	Parallel laminate	36	110



Linear Thermal Expansion of Fiberglass Laminates as a Function of Temperature

Information about the following laminates appears in the figure:

<u>Laminate</u>	<u>Reinforcement</u>	<u>Key</u>
Phenolic	Glass fabric	PH
Epoxy	Parallel glass fiber	E
Silicone	90° cross-plyed	S
Polyester	Glass fabric	P

Directions are keyed as follows in the figure:

<u>Direction</u>	<u>Key</u>
Warp	W
Fill	F
Thickness	T
Normal to thickness	⊥
Parallel to reinforcement	

See Table 3-1 for more detailed description of samples.

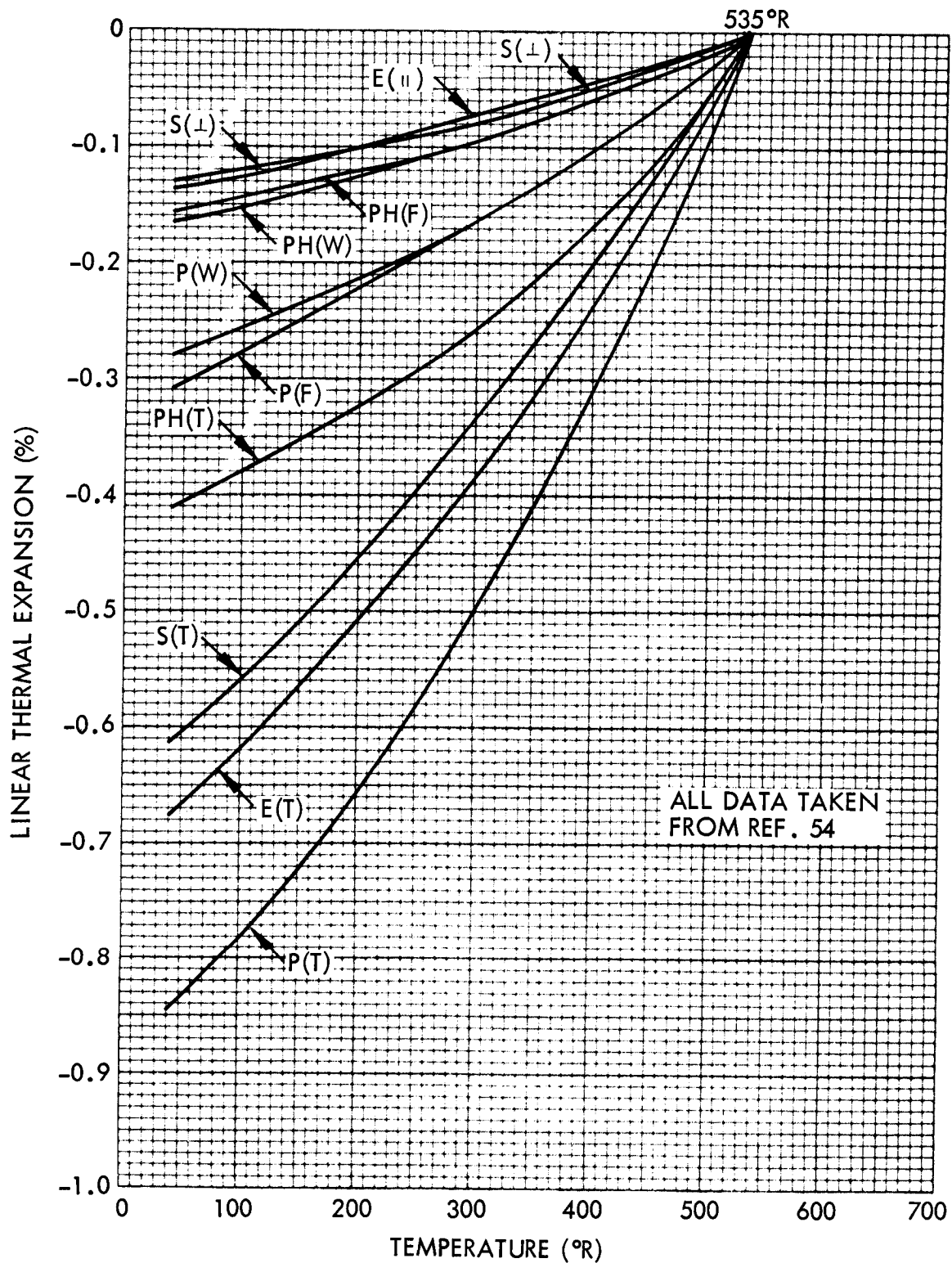


Fig. 3-1 Linear Thermal Expansion of Fiberglass Laminates as a Function of Temperature

Thermal Conductivity of Fiberglass Laminates as a Function of Temperature

The tests were conducted in a helium atmosphere.

Information about the following laminates appears in the figure:

<u>Laminate</u>	<u>Reinforcement</u>	<u>Key</u>
Phenolic	Glass fabric	PH
Epoxy	Parallel glass fiber	E
Silicone	90° Cross-plyed	S
Polyester	Glass fabric	P

Directions are keyed as follows in the figure:

<u>Direction</u>	<u>Key</u>
Thickness	T
Normal to thickness	⊥
Parallel to reinforcement	

See Table 3-1 for more detailed description of samples.

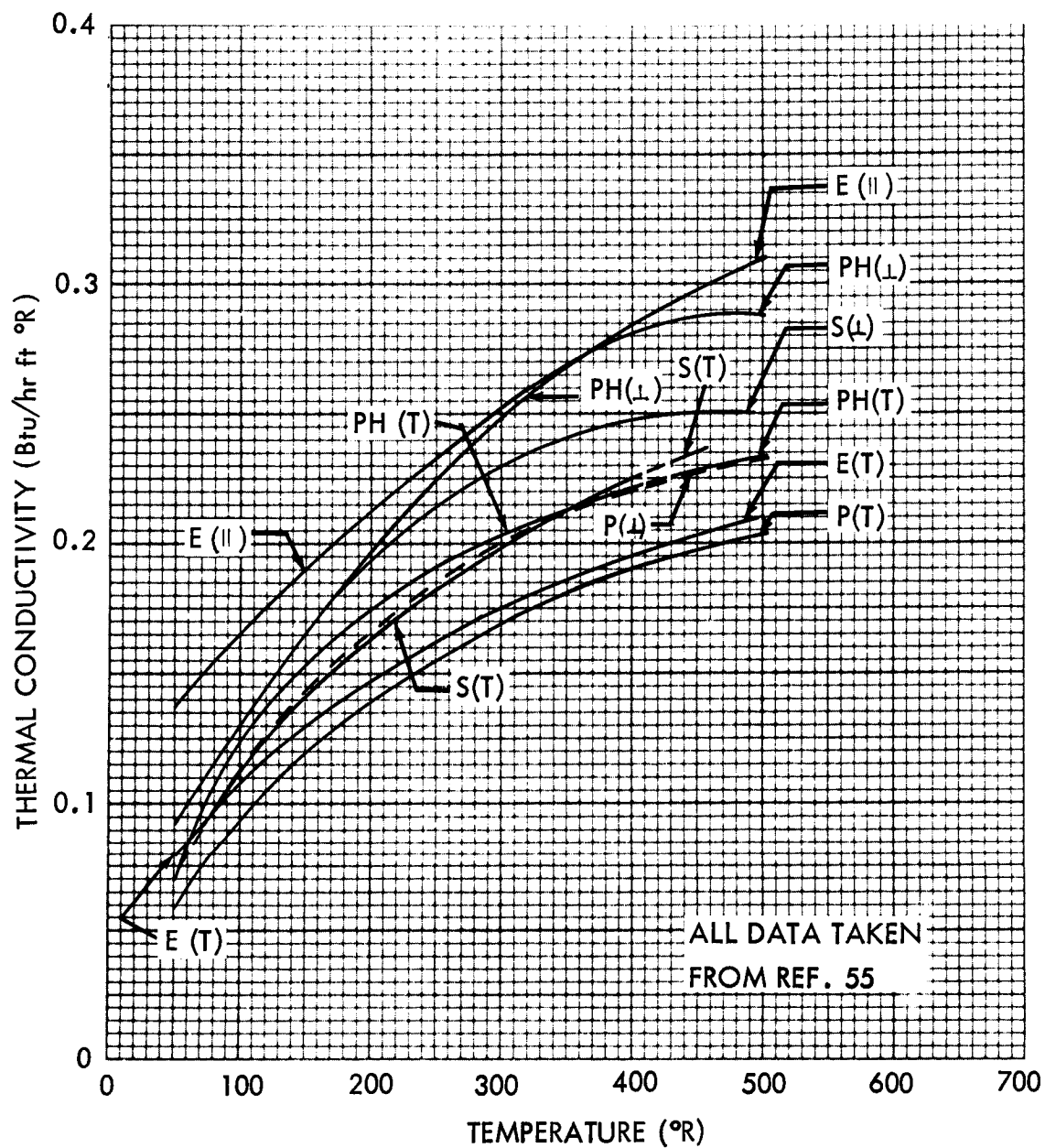


Fig. 3-2 Thermal Conductivity of Fiberglass Laminates as a Function of Temperature

Thermal Conductivity Integrals of Glass and Plastics
as a Function of Temperature

Glass - Average value of quartz, Pyrex, and borosilicate glasses

Nylon - Imperial Chem. Ind.; drawn monofilament

Perspex - An English organic glass thermoplastic similar to Lucite or
Plexiglas

Teflon - Extruded

All data were taken from Ref. 104.

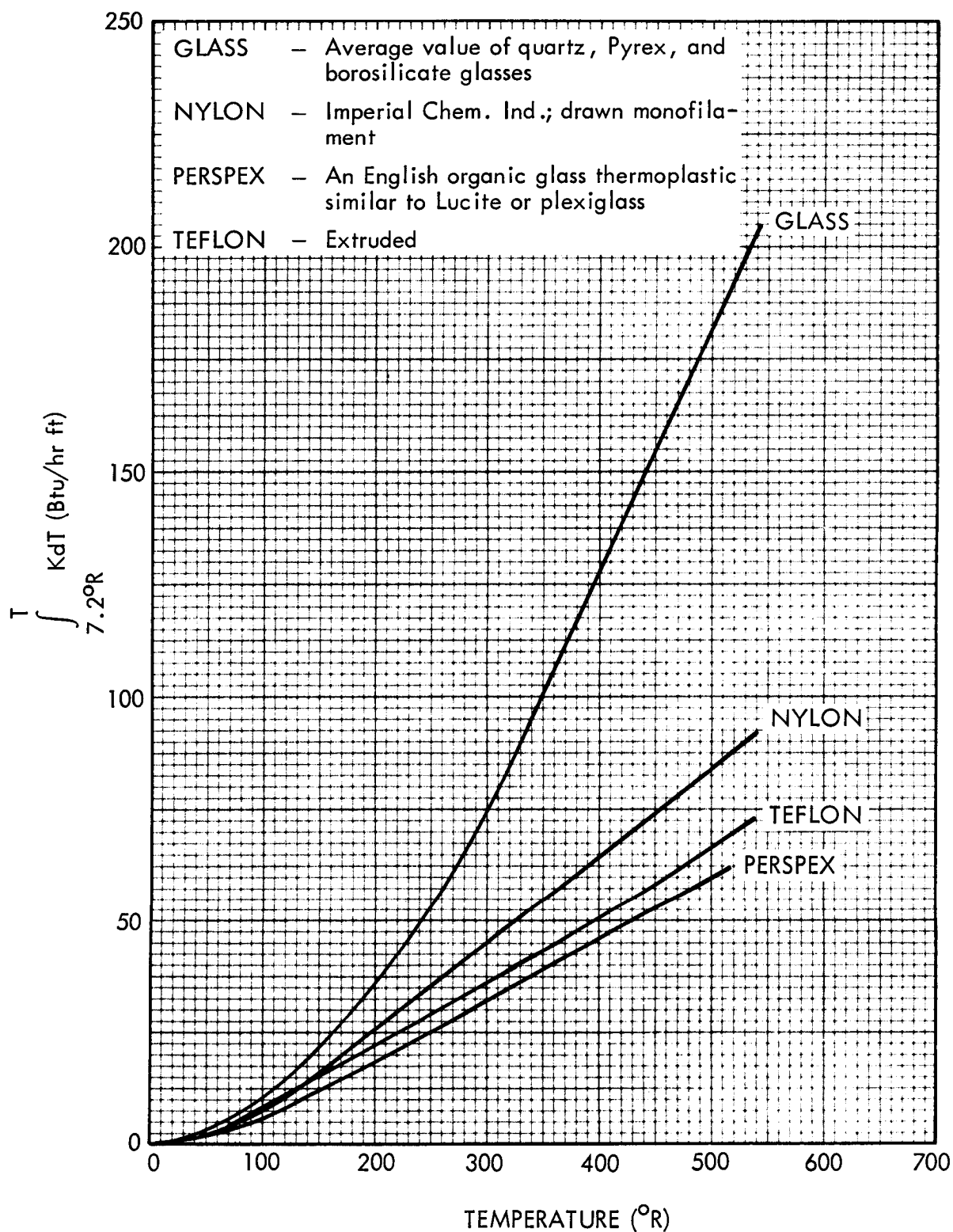


Fig. 3-3 Thermal Conductivity Integrals of Glass and Plastic as a Function of Temperature

Specific Heat of Fiberglass Laminates as a Function of Temperature

Information about the following laminates appears in the figure:

<u>Laminate</u>	<u>Reinforcement</u>	<u>Key</u>
Phenolic	Glass fabric	PH
Epoxy	Parallel glass fiber	E
Silicone	90° cross-ply	S
Polyester	Glass fabric	P

See Table 3-1 for more detailed description of samples.

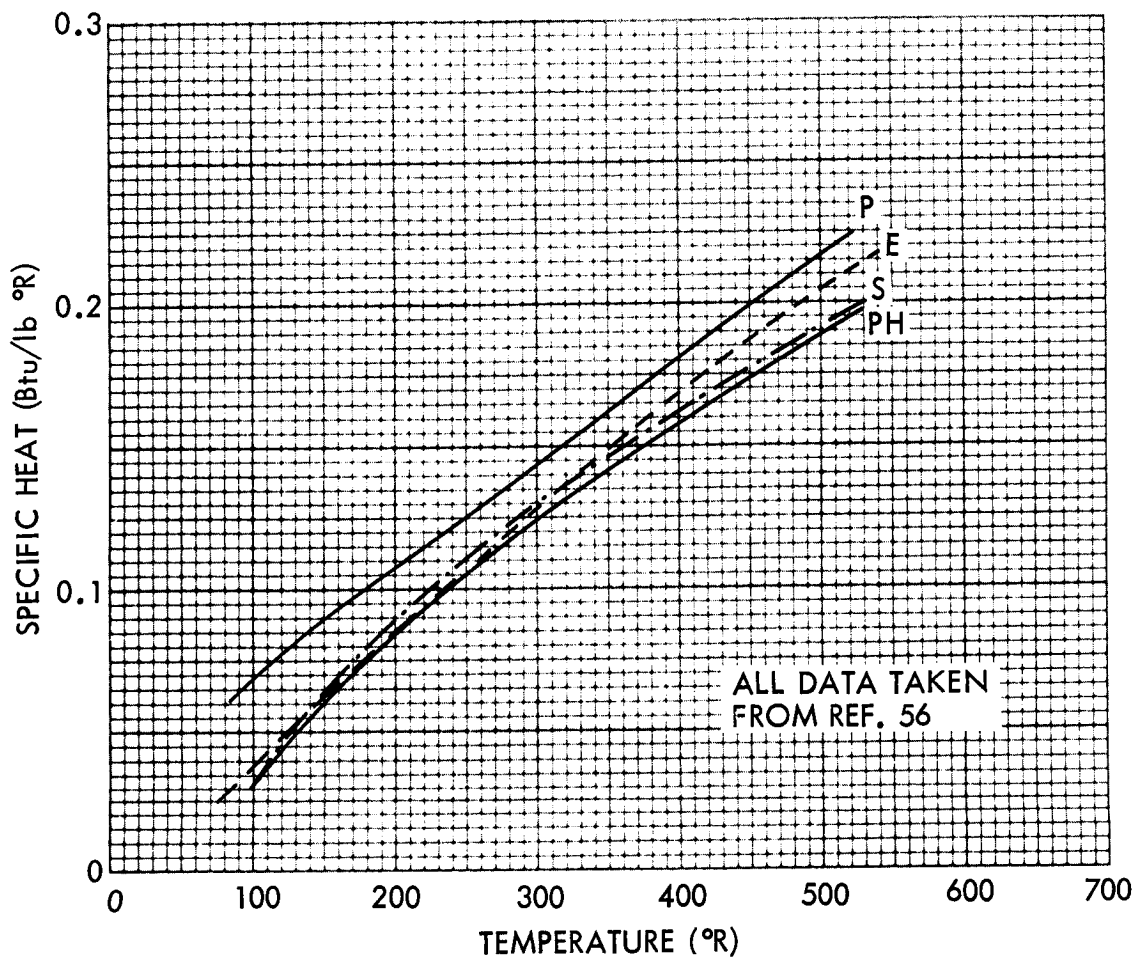


Fig. 3-4 Specific Heat of Fiberglass Laminates as a
Function of Temperature

4. MULTILAYER INSULATIONS

4.0 INTRODUCTION

Included in this section are the various physical, thermodynamic, and gas dynamic properties of multilayer insulation materials alone and in combinations. Also included is a section on practical attachment methods of insulation systems to flight-type tankage. This section includes thermal transport properties of two attachment techniques. In order to give the thermal analyst a better appreciation of the limitations of existing thermal transport data, a detailed description of present testing techniques is presented in Section 4.5.

Current practice within the aerospace community is to define an effective thermal conductivity for multilayer insulation as a thermal transport property upon which calculations and prediction of the insulation thermal performance can be made. This parameter, an extension of the thermophysical property known as thermal conductivity (k), is based on one-dimensional conductive heat transfer analog of the actual process. The actual heat transfer mechanism in a direction normal to the insulation layers is most generally a complicated function of both the radiative and conductive modes of heat transfer. In practice, however, the effective thermal conductivity is defined from the one-dimensional steady-state Fourier heat conduction equation

$$q = \frac{k A \Delta T}{L}$$

where q is the heat flow along the path of cross-sectional area A and length L over which there is a temperature gradient of ΔT . This equation generally applies to the heat transport data obtained from the flat-plate calorimeter (see Sec. 4.5) where the parameters q , A , L and ΔT are measured. For a test apparatus of the NBS-cryostat configuration (see Sec. 4.5), where the insulation specimen is in the form

of a cylinder with the heat flow being radially inward, the governing equation becomes

$$q = \frac{2\pi Lk \Delta T}{\ln \frac{r_o}{r_i}}$$

where r_o is the outer radius of the insulation and r_i the inner radius.

To reiterate, these equations do not govern the actual thermal energy transport mechanism; they, or similar equations representing only the conductive mechanism, can be utilized only in conjunction with experimental data as an analog of the actual processes.

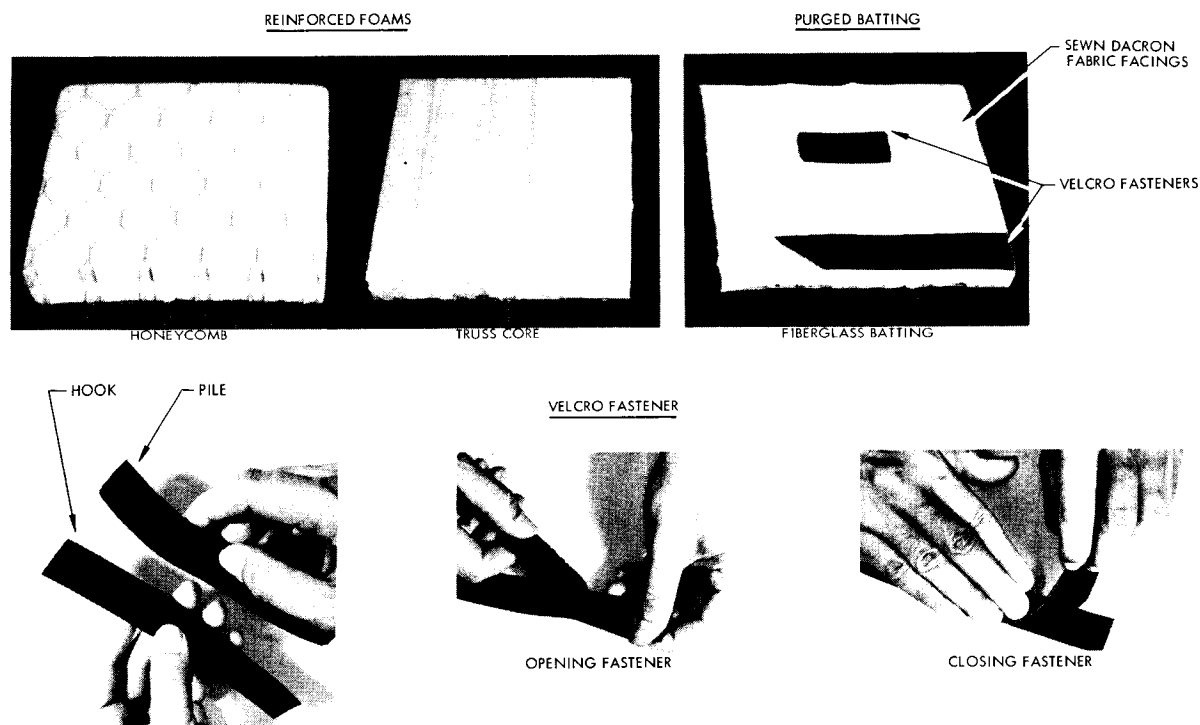
The thermal energy transport data for insulations presented in this section are in the form of effective thermal conductivities. Typically, these data are available only with cold-boundary temperatures of 36 and 140° R, and warm-boundary temperatures near room temperatures. In this form the data can be used quite effectively to compare the performance of various insulation systems. However, it should be recognized that these data cannot be utilized directly to obtain temperature distributions throughout an insulation system. Additionally, one cannot accurately predict the thermal performance of an insulation system utilizing a nodal set up where thermal conductivities are required for boundary temperatures other than those for which test data are available. Estimates of the effective thermal conductivity dependence on temperature can be made if temperature distribution through the insulation is known. Estimates of this dependence have been made by Wang (Ref. 80) and also in Volume I of this final report (Ref. 114).

4.1 SUBSTRATES

Two types of substrate materials are commonly considered for application to liquid hydrogen tankage for preventing the liquefaction of ambient gas in the multilayers during ground hold. These materials comprise sealed reinforced foams and purged fiberglass batting.

The closed-cell foam cryopumps during fill of the propellant tank, thereby providing a relatively low thermal conductivity. Use of fiberglass batting as a substrate reduces heat transfer by gaseous convection and by radiation.

This section provides data about thermal conductivity and specific heat.



Thermal Conductivity of Substrate Materials as a Function of Temperature

After liquid hydrogen fill, the temperature at the outer surface of the substrate insulation should be slightly above the liquefaction temperature for oxygen, 162°R ; consequently, the data were plotted over the temperature range 40 to 180°R .

Because of the scatter in foam data, a thermal conductivity range was plotted rather than a single curve. These data are for unreinforced foams.

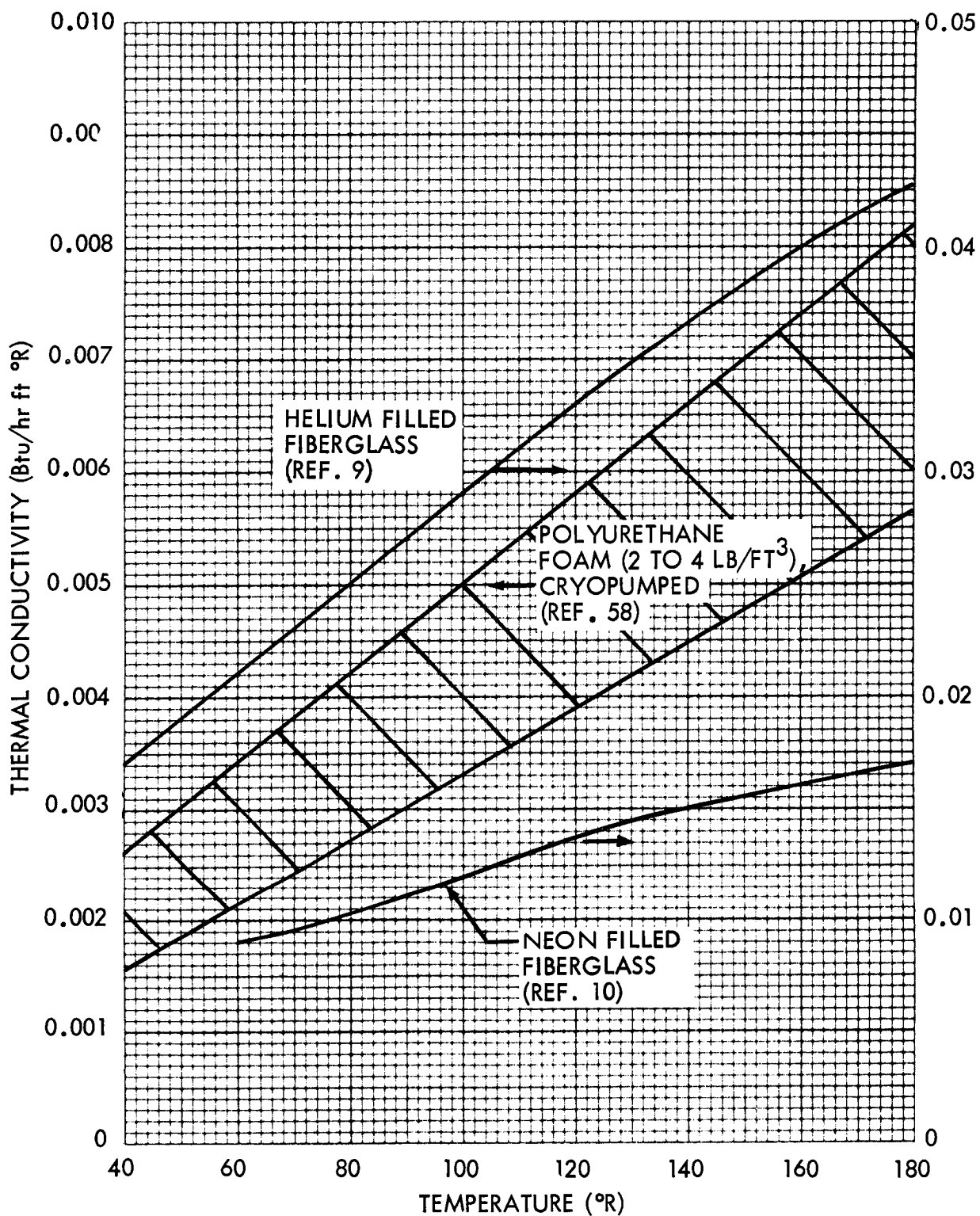


Fig. 4.1-1 Thermal Conductivity of Substrate Materials as a Function of Temperature

Thermal Conductivity of Fiberglass Batting as a Function of Nitrogen Gas
Pressure and Batting Density

The data apply to fiberglass batting composed of AA fibers, 0.03 to 0.05 mil in diameter.

The 0.5 lb/ft³ density is the lowest density available on a standard commercial order.

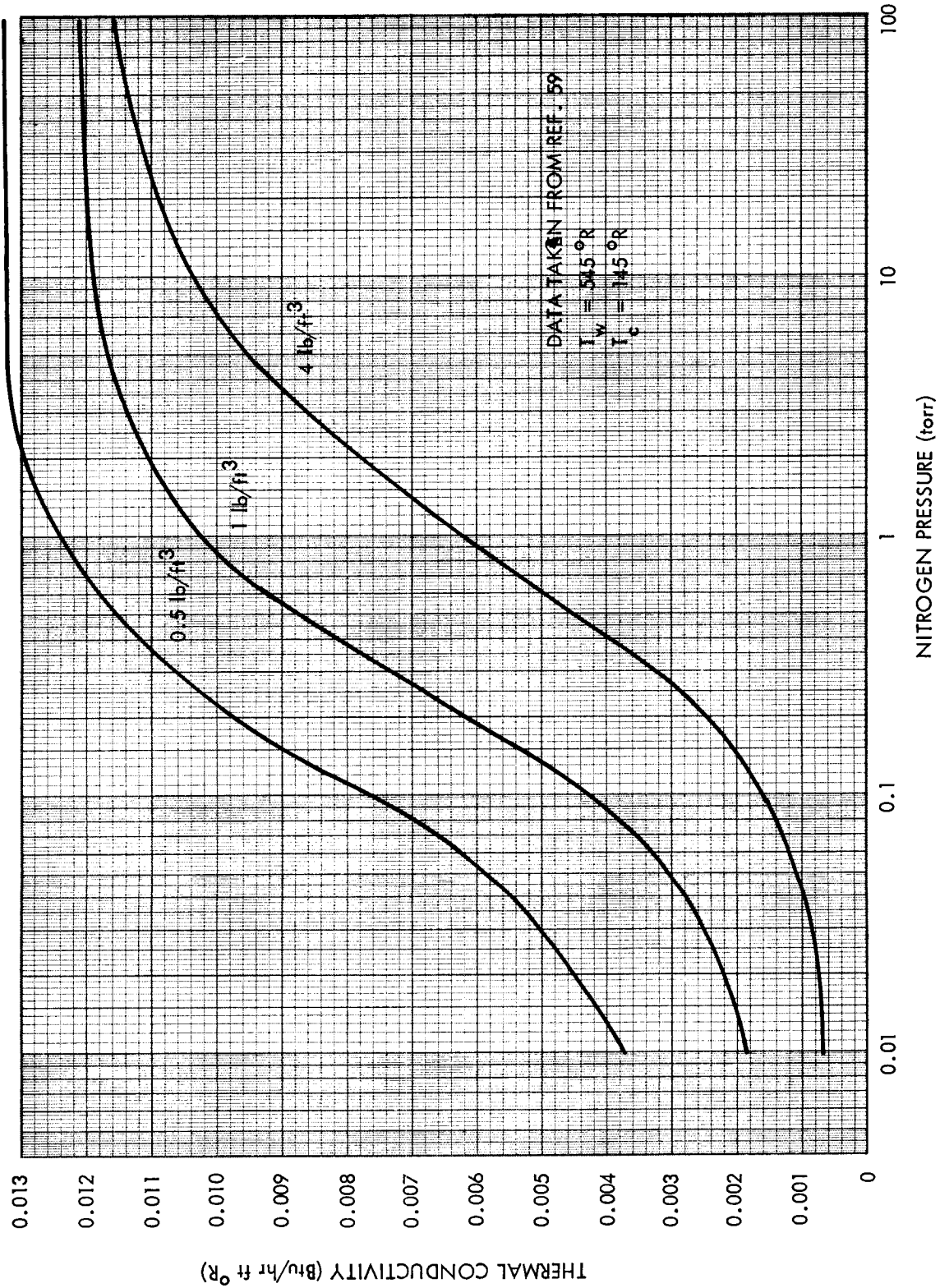


Fig. 4.1-2 Thermal Conductivity of Fiberglass Batting as a Function of Nitrogen Gas Pressure and Batting Density

Specific Heat of Substrate Materials as a Function of Temperature

The specific heat of aluminum foil with Dexiglas paper spacers is given in Ref. 60. With the relative weights of the two materials and the specific heat of aluminum from Fig. 2-3, the specific heat of the glass fibers was calculated. The specific heat of foam at low temperature was not found in the literature.

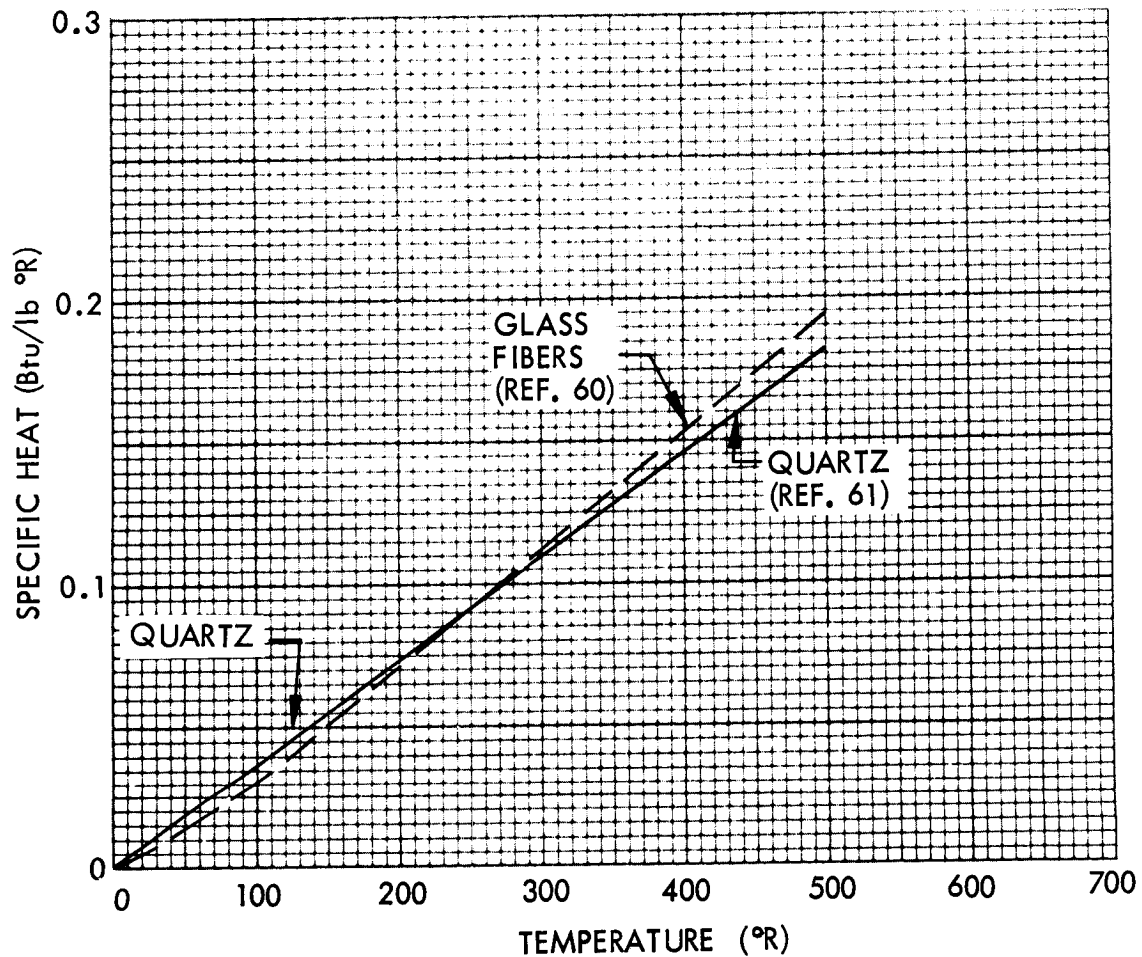
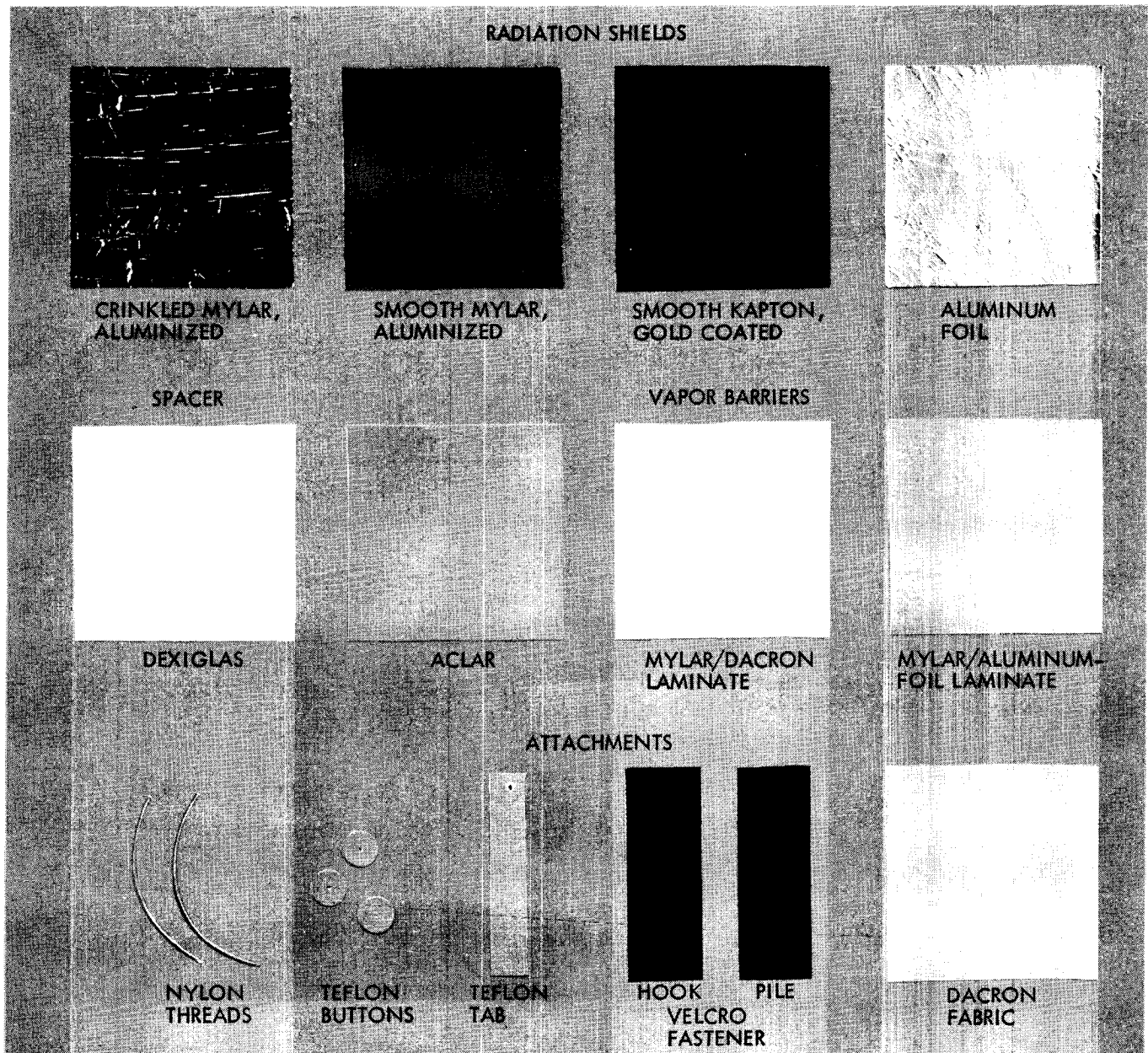


Fig. 4.1-3 Specific Heat of Substrate Materials as a Function of Temperature

4.2 MULTILAYER-INSULATION-SYSTEM MATERIALS

Data are presented here for the following applications of material: radiation shields, spacers, vapor barriers, and attachments. The properties considered are density, weight/area, maximum operating temperature, linear thermal expansion, thermal conductivity, specific heat, and emissivity of radiation shields.



Properties of Multilayer-Insulation-System Materials

The thicknesses shown in Table 4.2-1 are typical of multilayer materials being considered. The radiation-shield thickness of 0.25 mil is about as thin as is practical for commercial production. Sheets of 0.15-mil Mylar are available in limited widths at higher cost. The dexiglas paper spacer, 2.8 mil thick, is fragile, and must be handled with care. The thickness of the vapor barrier is dictated either by purge pressure and size of the tank (for purge systems), or by the allowable gas-permeation rates for passive and evacuated systems.

Ascent heating dictates the maximum temperature that the insulation will experience during the flight.

Table 4.2-1

PROPERTIES OF MULTILAYER-INSULATION-SYSTEM MATERIALS

Material	Polymer Classification	Typical Thickness (mil)	Density (lb/ft ³)	Weight/Area (lb/ft ²)	Maximum Continuous Operating Temperature (°R)	Zero Strength Temperature (°R)	Melting Point (°R)
RADIATION SHIELD SUBSTRATES							
Mylar	Polyester	0.25	87	1.81 x 10 ⁻³	760 (300°F)	938	940
Kapton (H-Film)	Polyimide	0.25	89	1.85 x 10 ⁻³	1210 (750°F)	1960	None
Aluminum Foil		0.25	168	3.49 x 10 ⁻³		-	1680 (1220°F)
SPACER							
Dexiglas Paper (Glass Fibers)		2.8	14.0	3.3 x 10 ⁻³	1060 (600°F)	-	-
Tissuglas Paper (Glass Fibers)		0.6	15.4	.8 x 10 ⁻³	1060 (600°F)	-	-
Silk Netting		3.5	4.1	1.2 x 10 ⁻³	-	-	-
Foam	Polyurethane	20.0	2.0	3.3 x 10 ⁻³	-	-	-
ATTACHMENTS							
Nylon 66	Polyamide	-	71	-	735 (275°F)	-	-
Teflon (TFE 7)	Fluorocarbon	-	137	-	960 (500°F)	-	None
VAPOR BARRIER MATERIALS							
Aclar 33C	Chlorofluorocarbon	5	134	56 x 10 ⁻³	810 (350°F)	-	-
Trilaminare of Mylar/Mylar/Dacron	Polyesters	0.35/ 0.35/3	87	14.6 x 10 ⁻³	760 (300°F)	-	-
Trilaminare of Mylar/Al Foil/Mylar	Polyester	0.5/ 1/0.5	-	21.1 x 10 ⁻³	760 (300°F)	-	-

Linear Thermal Expansion of Multilayer-Insulation-System Materials as a
Function of Temperature

Some curves were adjusted slightly so that zero percent expansion falls at 530° R. This shift does not affect the relative value of thermal expansion between two temperatures.

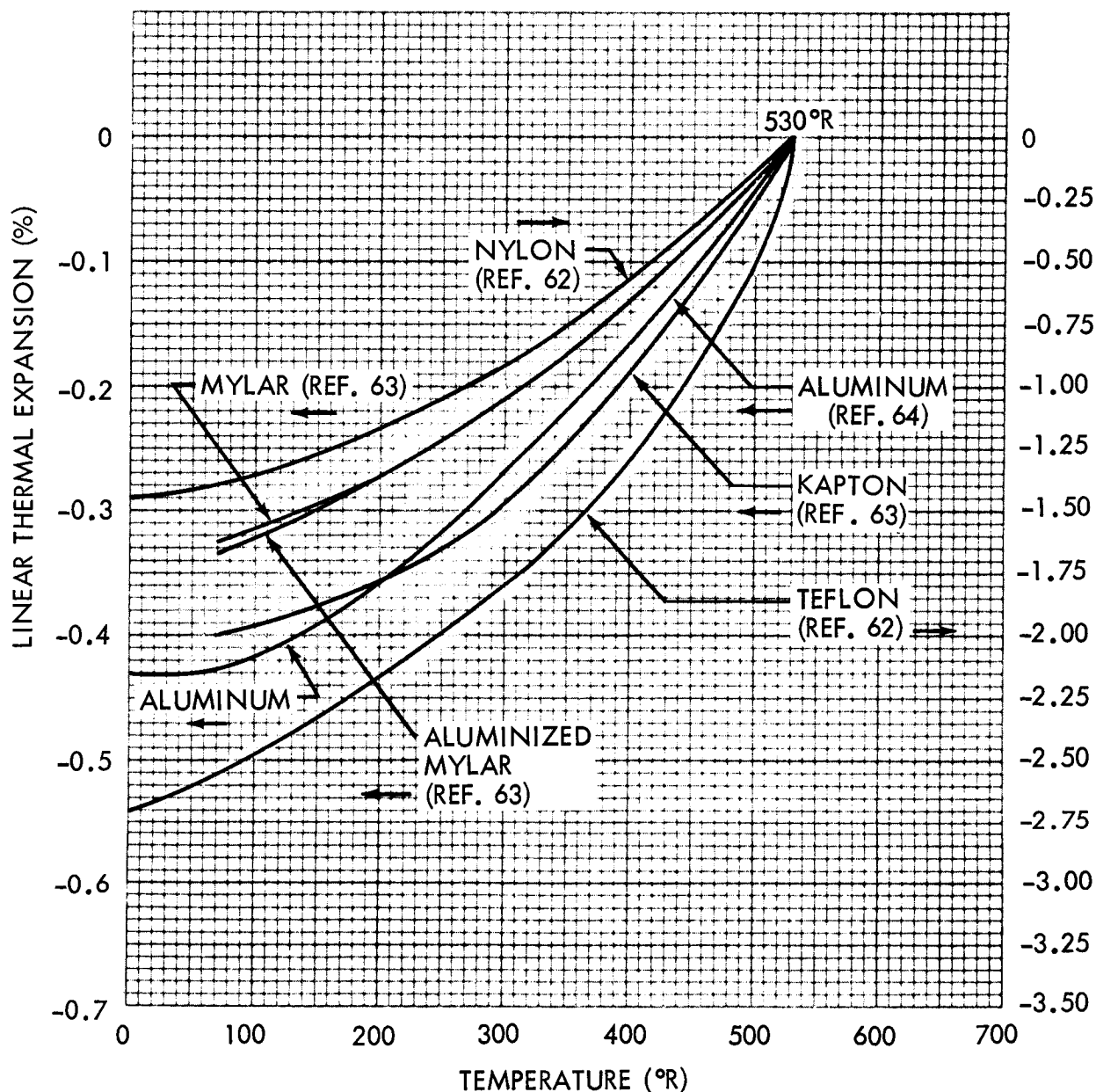


Fig. 4.2-1 Linear Thermal Expansion of Multilayer-Insulation-System Materials as a Function of Temperature

Thermal Conductivity of Multilayer-Insulation-System Materials as a
Function of Temperature

Two curves are given in Ref. 69 for the thermal conductivity of Mylar: these differ by about 50 percent. One curve is essentially linear, whereas the other curve has the shape shown on the opposite page. The latter curve was chosen for use, since it followed the trend exhibited by the other polymers, Nylon and Teflon. This curve was shifted a factor of 1.9 to coincide with du Pont values given in Ref. 70.

The thermal conductivity of aluminum at low temperature varies markedly as a function of the purity. For a 99.996 percent pure single crystal, the thermal conductivity rises from 160 at 200°R to 3000 at 40°R. The reference curve given here, however, is for commercial grade (99 percent pure) aluminum foil, since the aluminum foil used for radiation shields is a commercial grade.

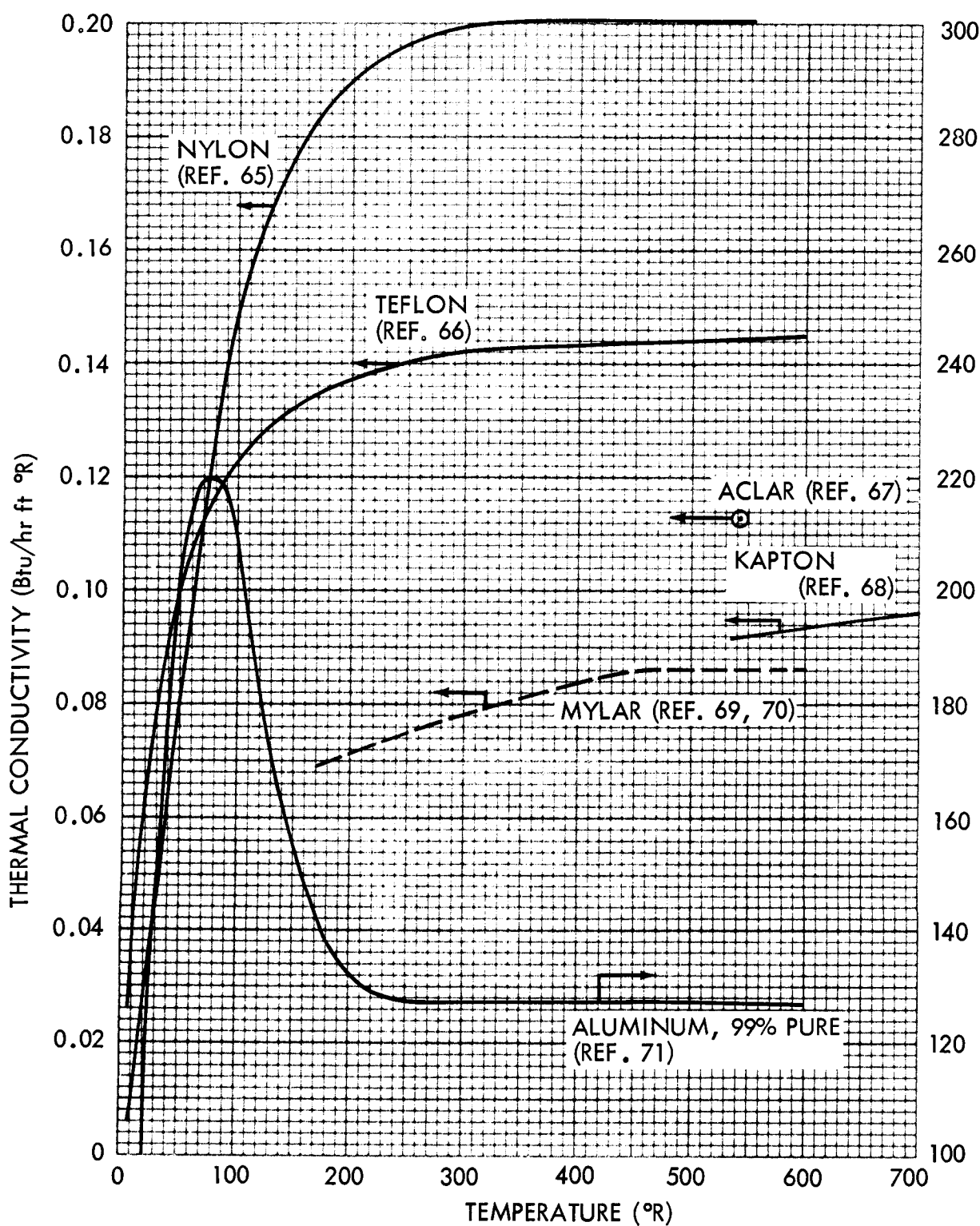


Fig. 4.2-2 Thermal Conductivity of Multilayer-Insulation-System Materials as a Function of Temperature

4.2-7

Effective Thermal Conductivity of Spacer Materials

Thermal conductivity data were obtained using a flat-plate calorimeter for both Dexiglas and Tissuglas, which are both made of pressed borosilicate glass fiber of less than 1 micron in diameter. These glass fibers are randomly oriented in the manufacturing process with a 7 percent cellulose binder for Tissuglas. The nominal thickness of Dexiglas is 2.8 mil whereas that of Tissuglas is 0.6 mil.

All data were obtained from Ref. 106 unless otherwise noted.

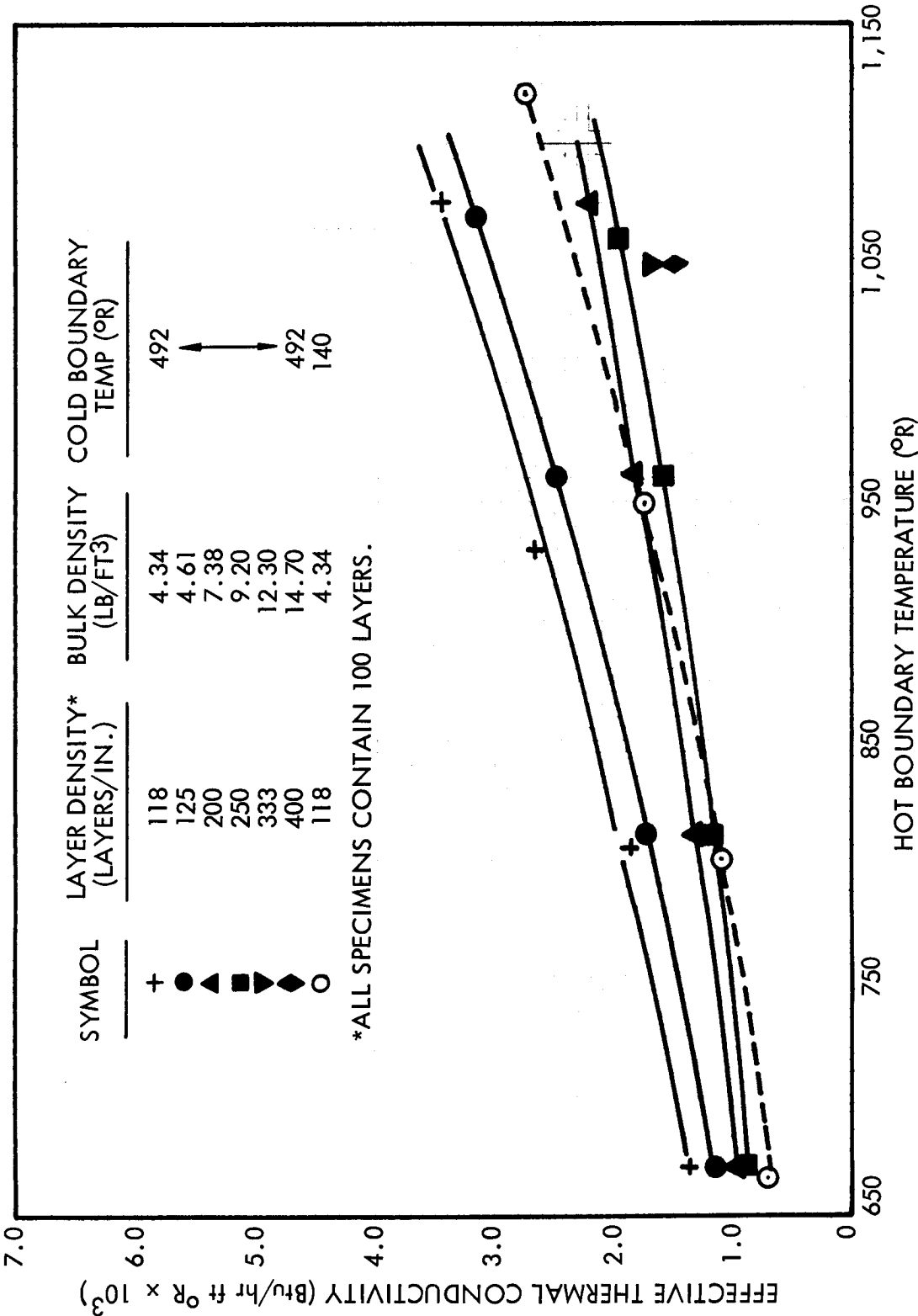


Fig. 4.2-3 Effective Thermal Conductivity of Dexiglas Spacer Material as a Function of Hot-Boundary Temperature and Bulk Density

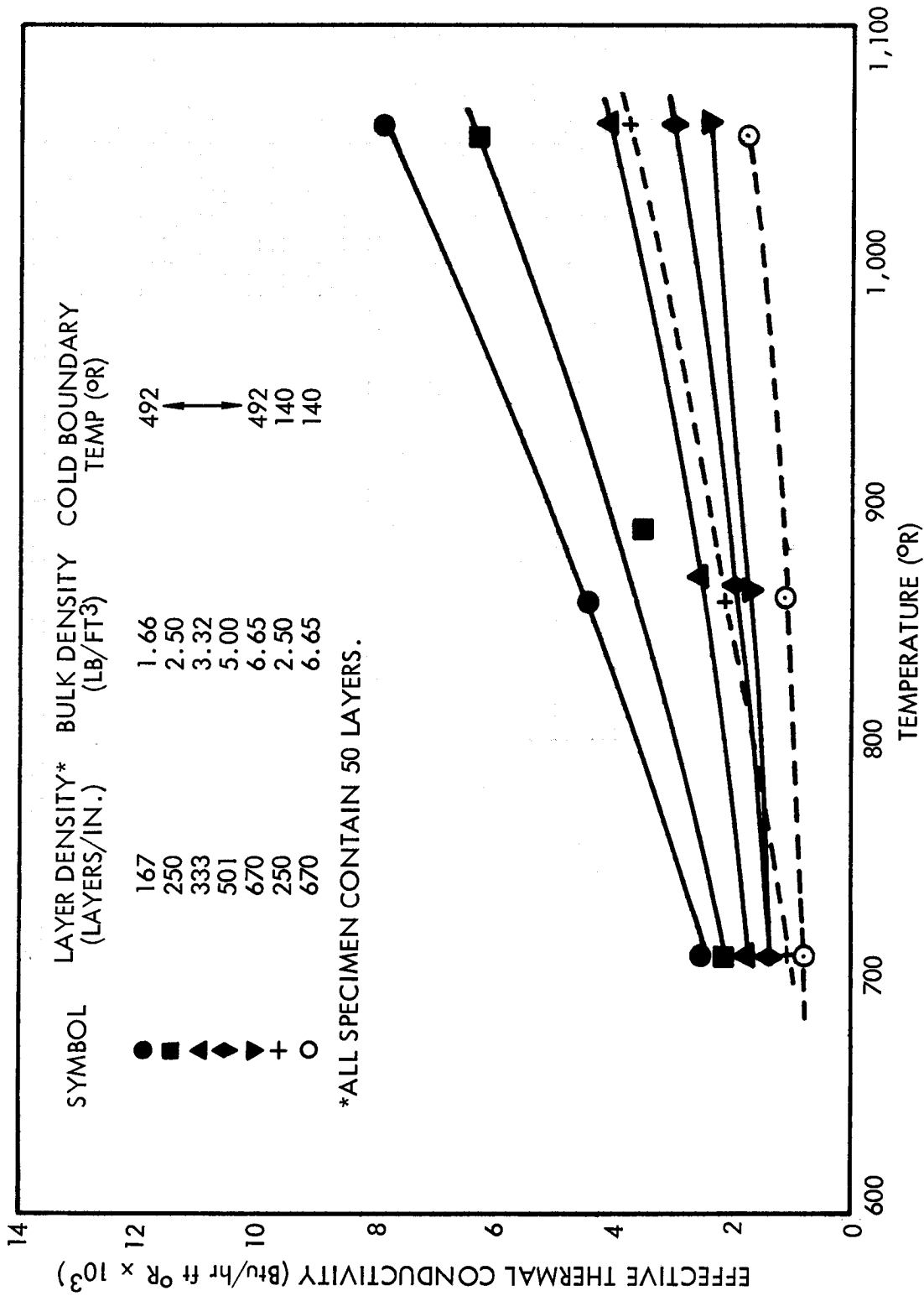


Fig. 4.2-4 Effective Thermal Conductivity of Tissuglass Spacer Material vs Hot-Boundary Temperature and Bulk Density

Scattering Cross Section of Spacer Materials
as a Function of Wavelength

Correlation of radiation heat transfer data for multilayer insulation fiberglass spacer materials have been successfully accomplished with the following equation (Ref. 106):

$$q_{\text{rad}} = \frac{2n^2\sigma (T_H^4 - T_C^4)}{(a + 2s)t}$$

where

n = Material index of refraction

σ = Stefan-Boltzmann Constant

T_H = Hot-boundary temperature

T_C = Cold-boundary temperature

a = Radiation absorption cross section per unit path length of radiation

s = Radiation scattering cross section per unit path length of radiation

t = Insulation thickness

Experimentally determined values for the scattering cross section of Tissuglas and Dexiglas are presented. Data were obtained from Ref. 106.

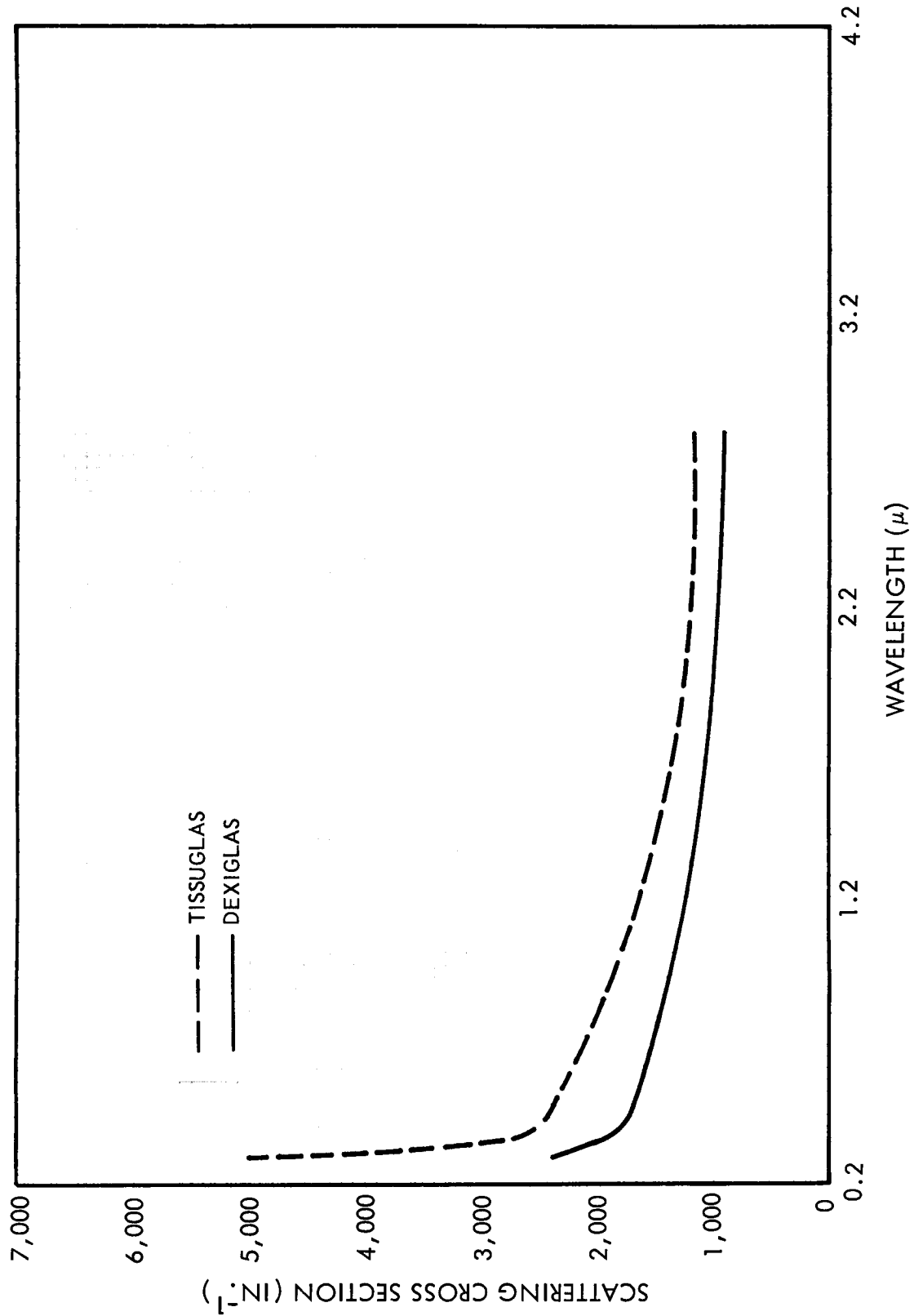


Fig. 4.2-5 Scattering Cross Sections of Tissuglas and Dexiglas Spacer Materials as a Function of Wavelength

Specific Heat of Multilayer-Insulation-System Materials as a
Function of Temperature

The Mylar curve was faired in to follow the general trend of Teflon, another polymer material.

Reference 60 gives the specific heat of aluminum foil with Dexiglas paper spacers. With the relative weights of the two materials and the specific heat of aluminum known, the specific heat of Dexiglas was calculated.

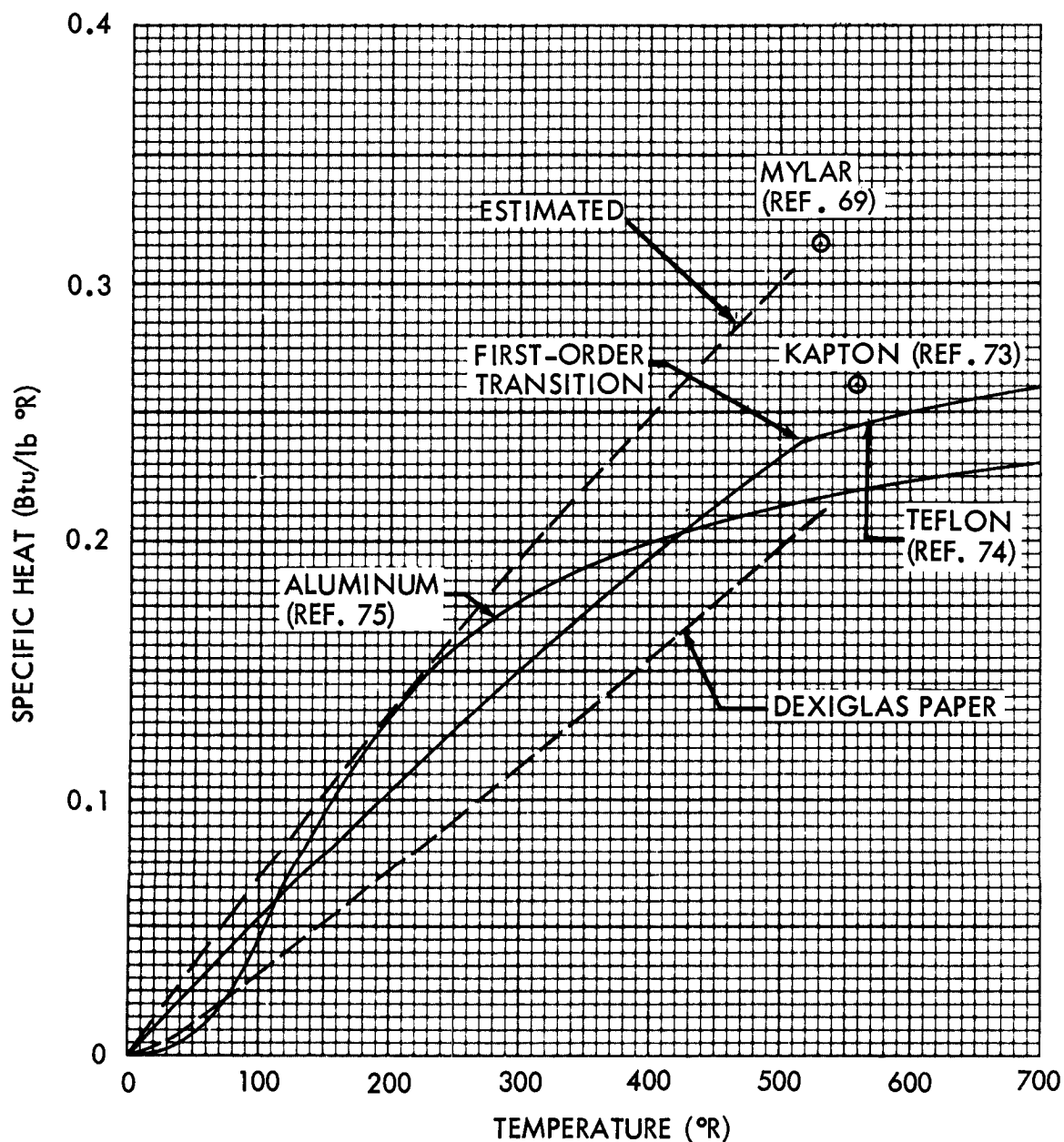


Fig. 4.2-6 Specific Heat of Multilayer-Insulation-System Materials as a Function of Temperature

Emittance of Radiation Shields as a Function of Temperature

Information about 1/4-mil aluminum foil taken from Linde multilayer insulation sample is shown in the figure.

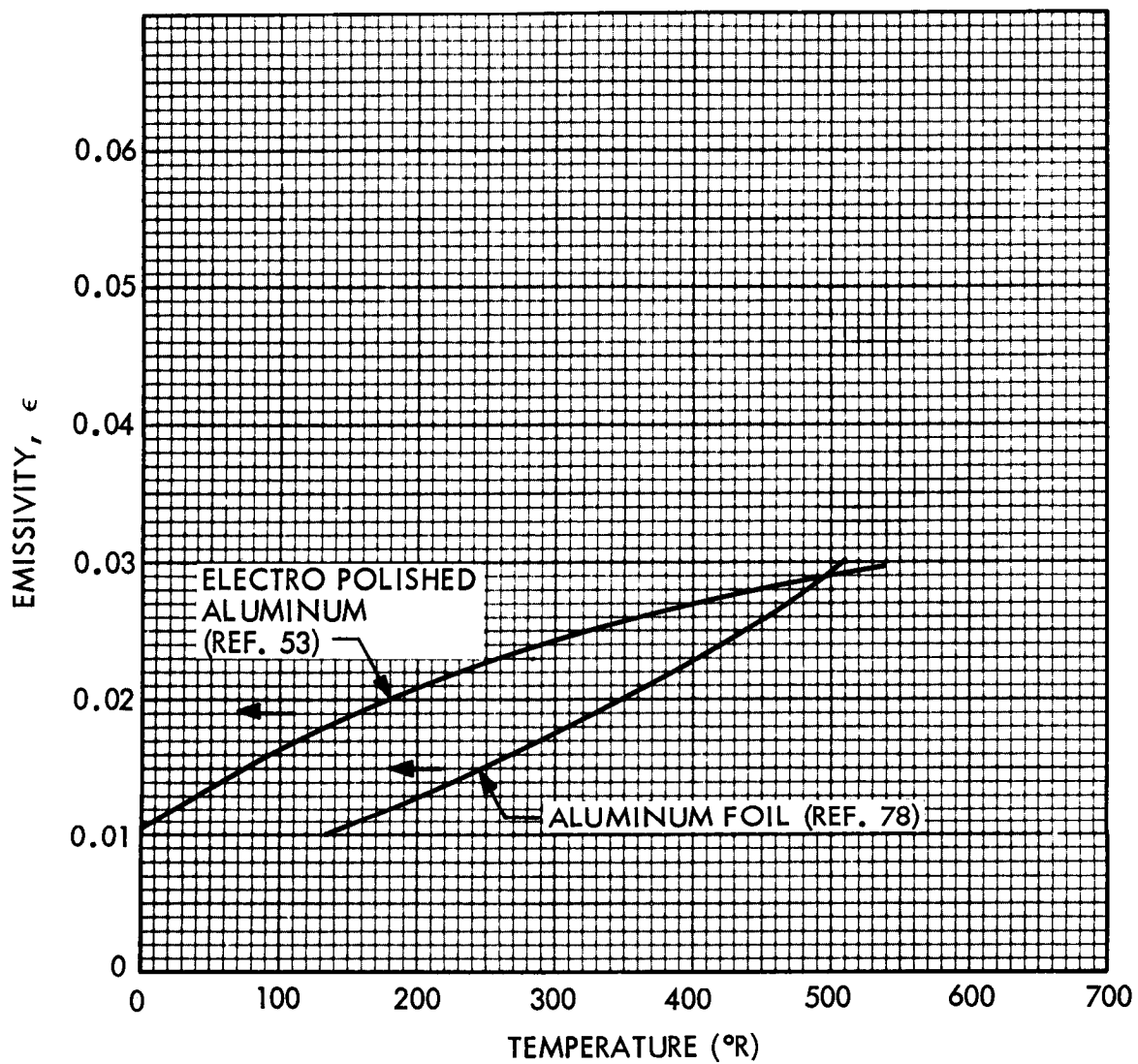


Fig. 4.2-7 Emissivity of Radiation Shields as a Function of Temperature

Emittance of Vacuum Deposited Metallic Films on Mylar Substrate
as a Function of Film Thickness

In order to minimize radiation heat transport normal to multilayer insulation systems, it is desirable to have a completely opaque metallized film on the radiation shields. The film thicknesses required for opacity (minimum emittance) are shown for aluminum, gold, and silver.

All data were obtained from Ref. 107.

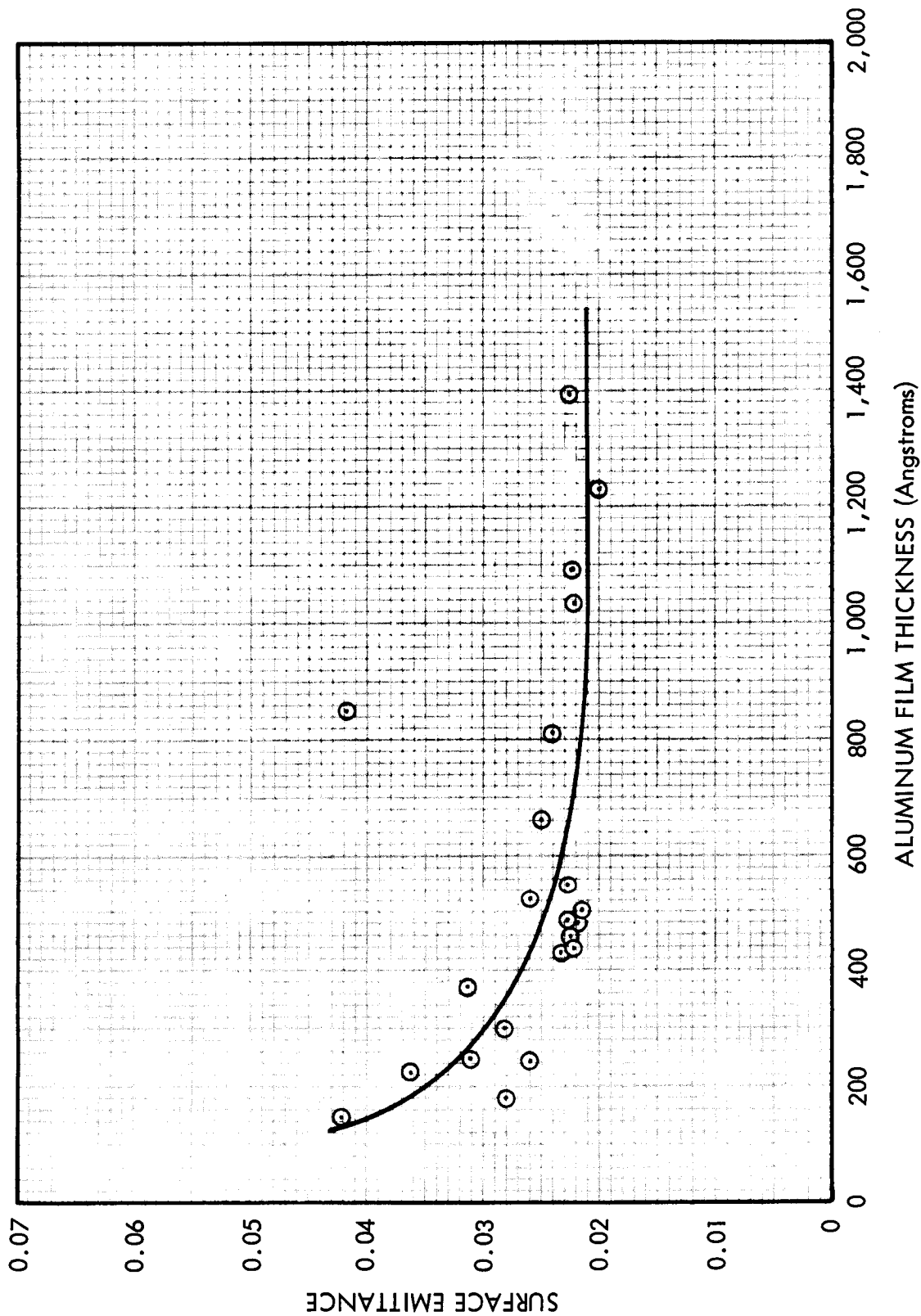


Fig. 4.2-8 Aluminized Mylar Surface Emittance vs Coating Thickness

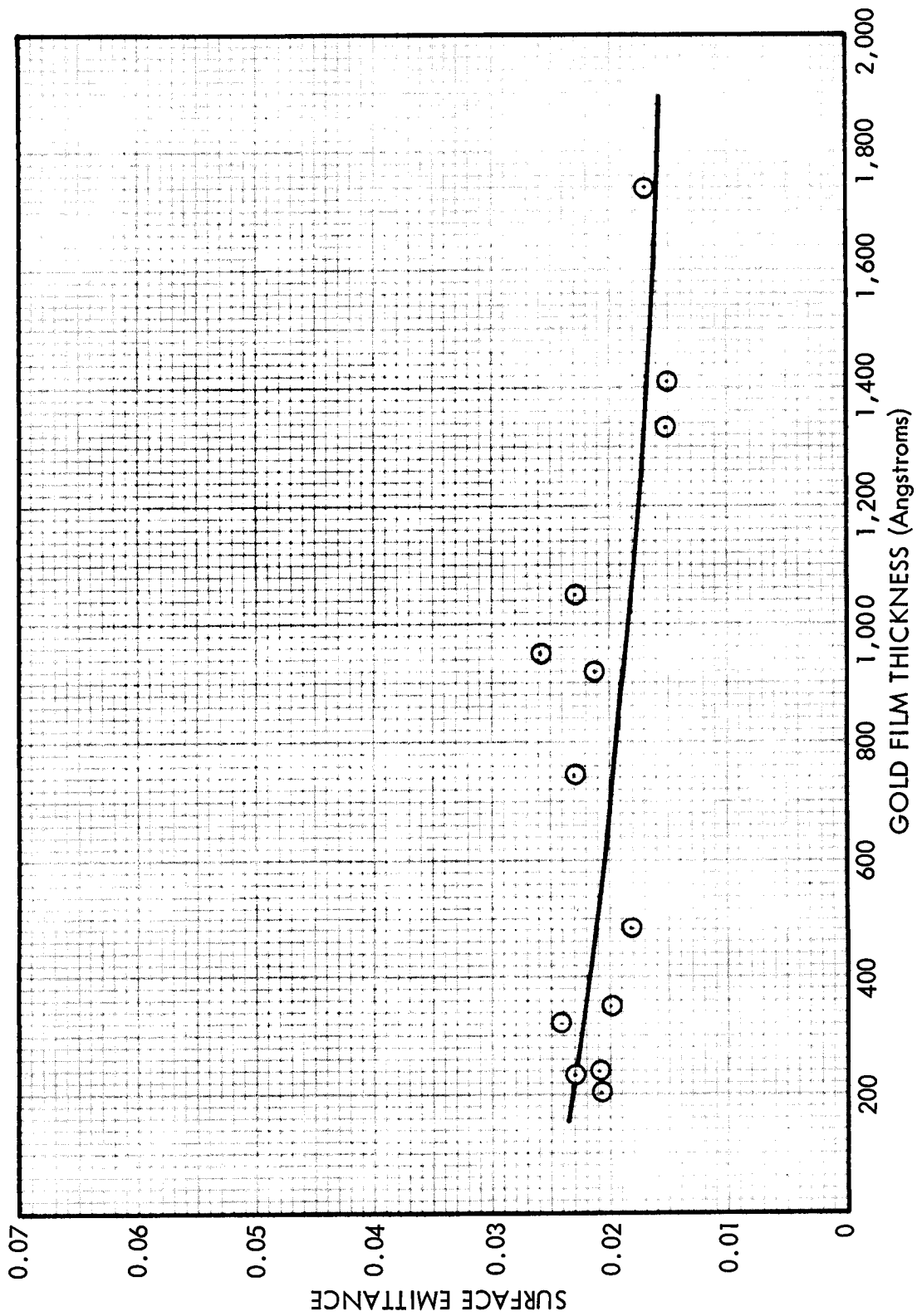


Fig. 4.2-9 Emittance of Gold Deposited on Mylar vs. Deposition Thickness

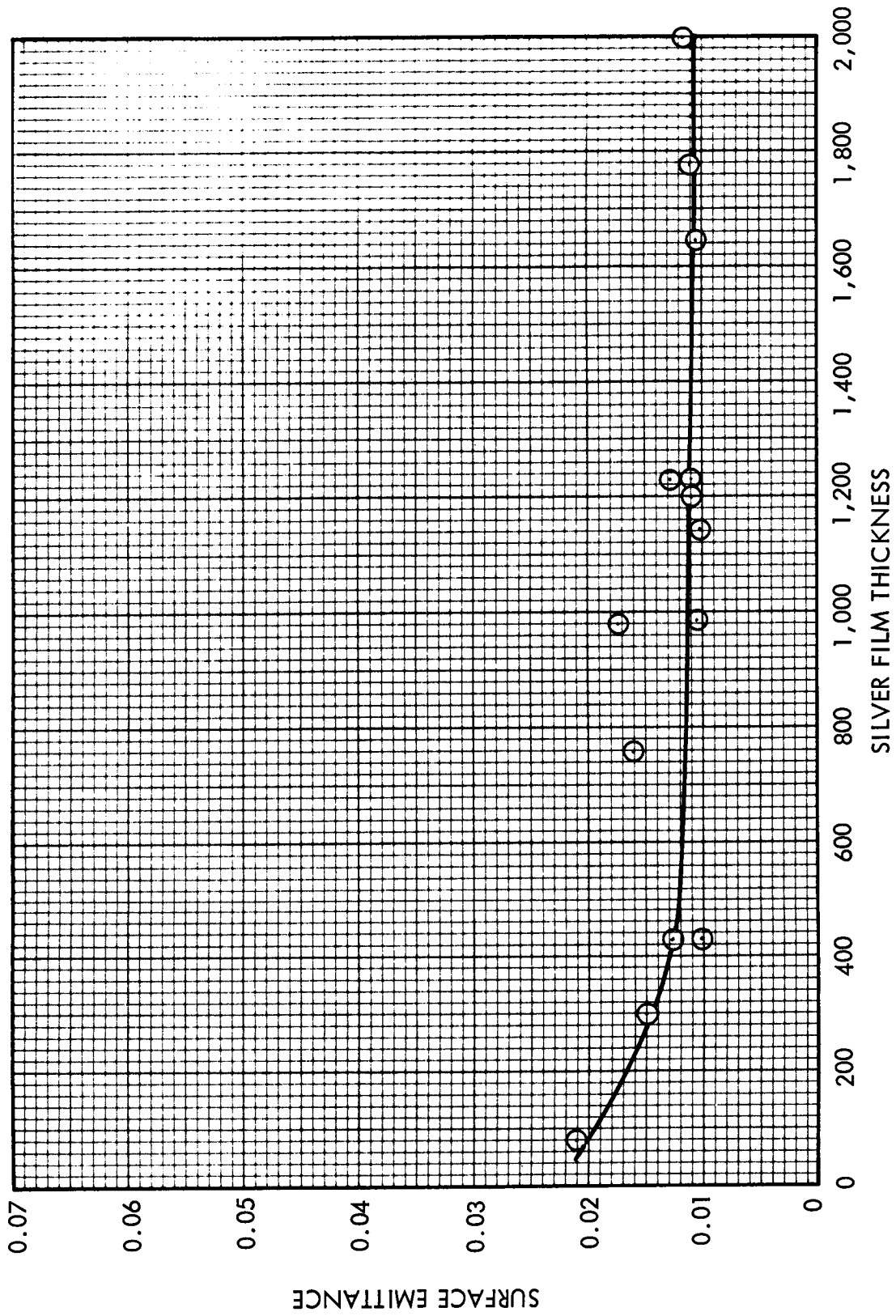


Fig. 4.2-10 Emittance of Silver Deposited on Mylar vs Deposition Thickness

Total Hemispherical Emittances of Vacuum Deposited Metallic Film
on a Kapton Substrate as a Function of Temperature and Film Thickness

The effect of temperature on the emittance of typical radiation shield material is presented. Data were obtained from Ref. 108.

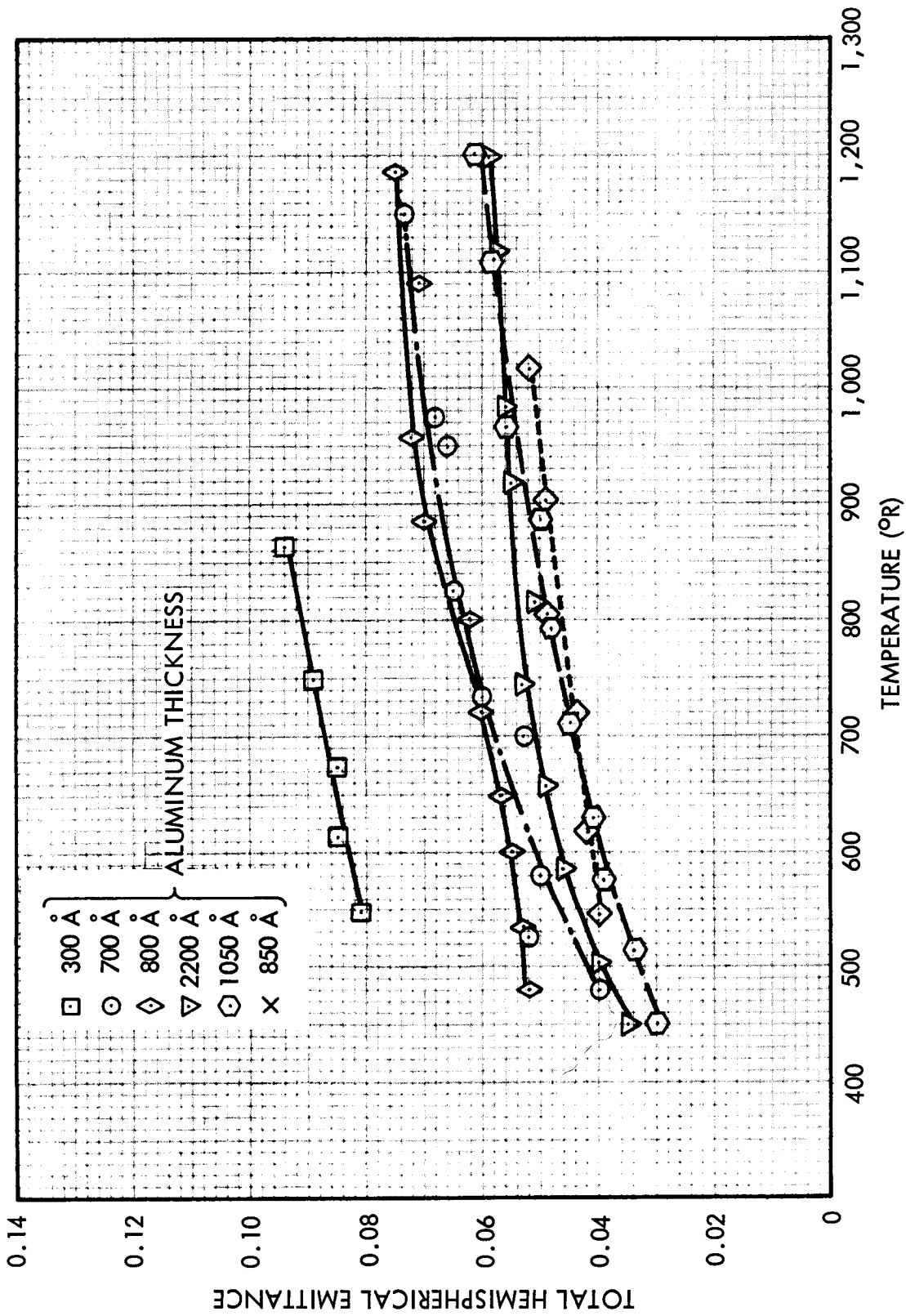


Fig. 4.2-11 Total Hemispherical Emittance of Vacuum Deposited Aluminum on Kapton as a Function of Temperature and Deposit Thickness

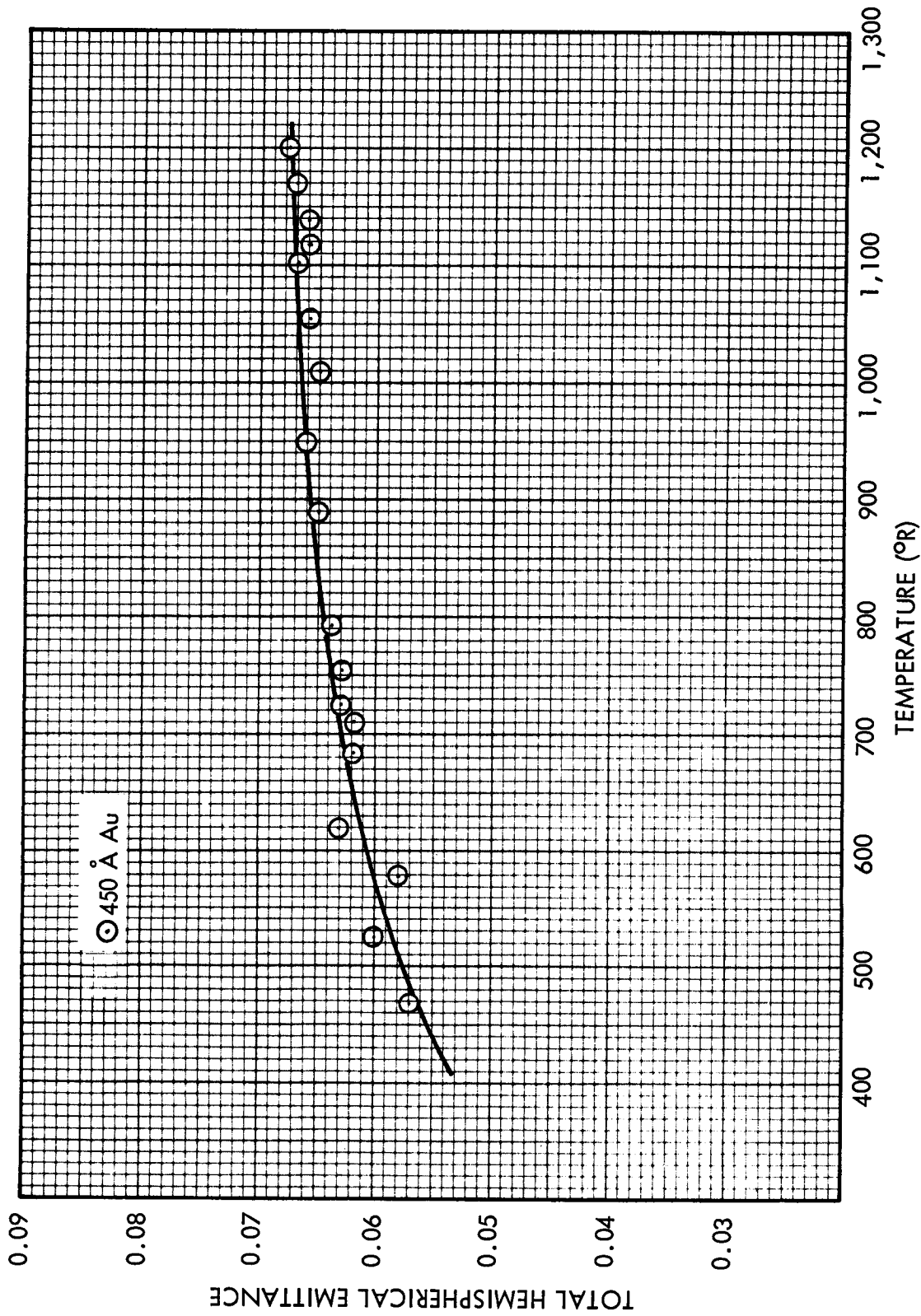


Fig. 4.2-12 Total Hemispherical Emittance of Vacuum Deposited Gold on Kapton

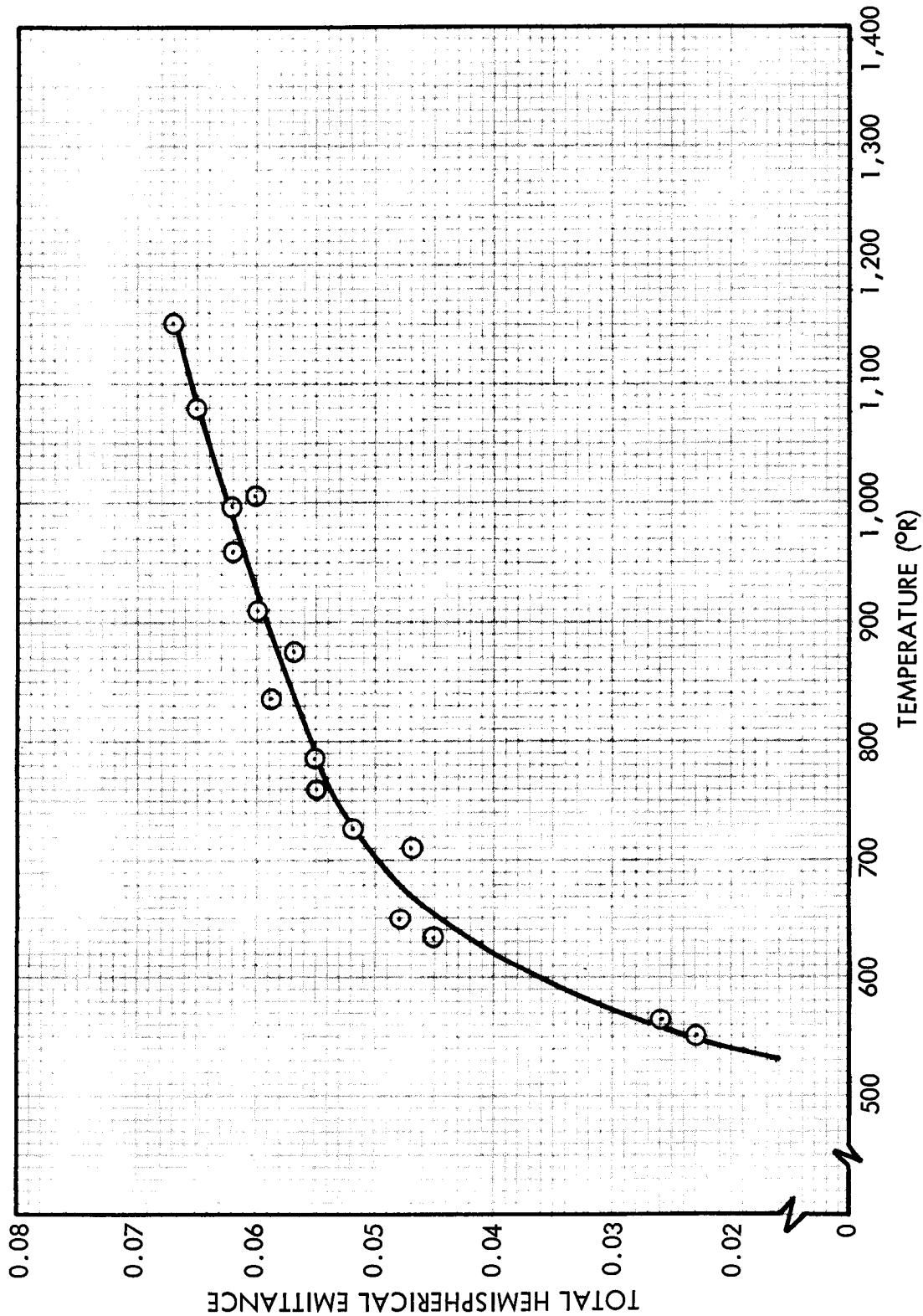


Fig. 4.2-13 Total Hemispherical Emittance of Vacuum Deposited Silver on Kapton

Metallized Film Thickness
as a Function of Film Electrical Resistance

Throughout the metallizing industry it is a standard practice to refer to or call out a metallized film thickness by an analogous surface film resistance in ohms per square. The reason for this is that direct measurement requires very expensive and elaborate equipment due to the small film thicknesses involved, whereas the film surface resistance can be measured quite readily.

The correspondence between film surface resistance and film thickness for aluminum, gold, and silver is presented (Ref. 113).

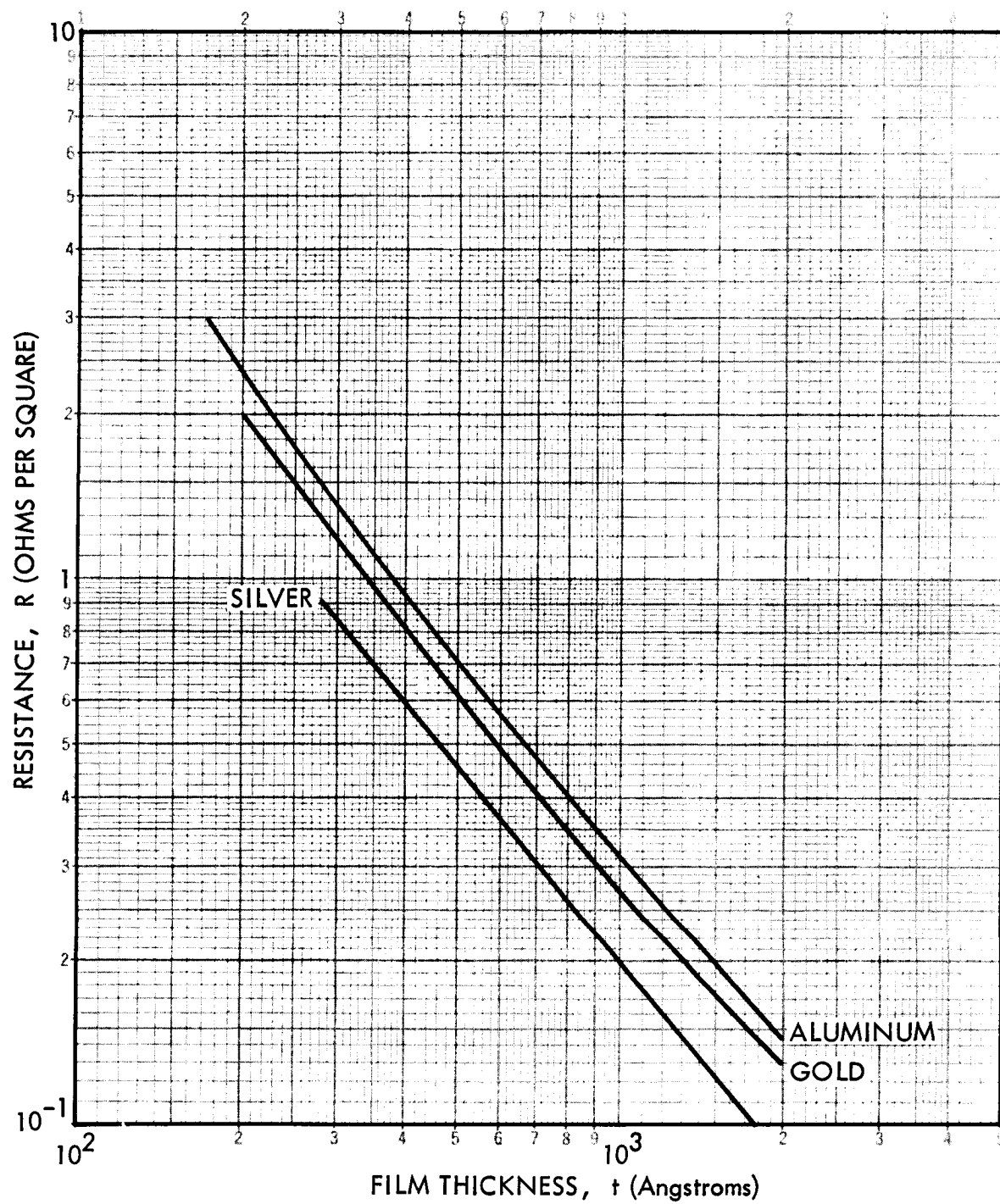


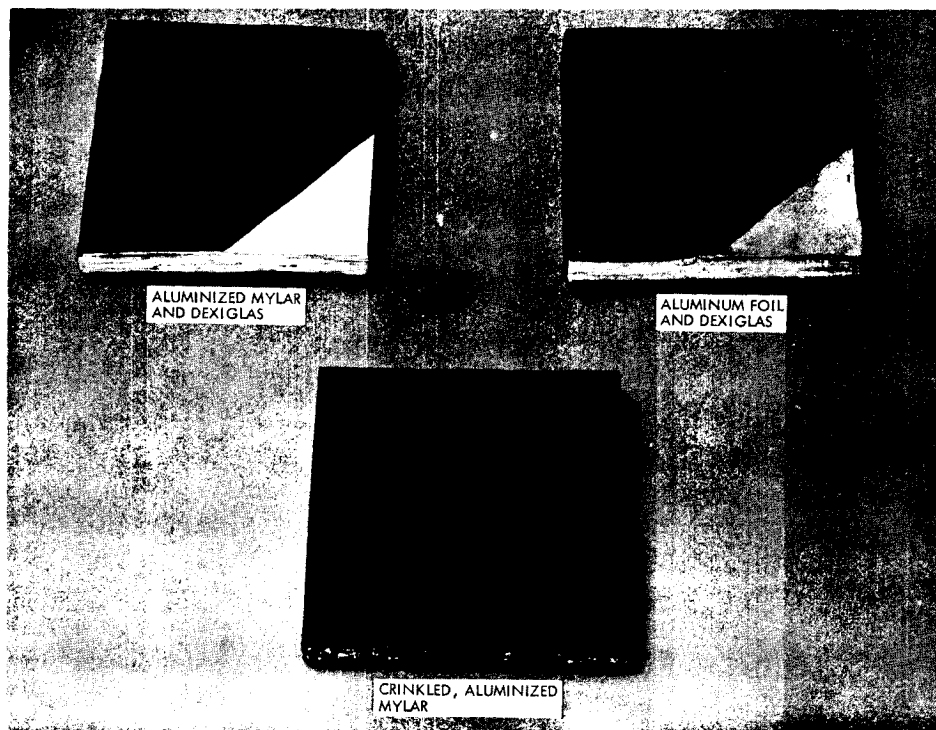
Fig. 4.2-14 Thickness of Aluminum, Gold, and Silver Films as a Function of Film Electrical Resistance

4.3 MULTILAYER COMPOSITES

The properties of the following multilayer insulation composites are provided in this section:

- Dimplar
- 1/4-mil Mylar, aluminized two sides, with a 2.8-mil Dexiglas paper spacers
- 1/4-mil aluminum foil, with a 2.8-mil Dexiglas paper spacers
- 1/4-mil crinkled Mylar, aluminized one side
- 1/4-mil Mylar, aluminized two sides, with 3.5-mil silk netting spacers
- 1/4-mil Mylar, aluminized two sides, with 20-mil foam spacers

The properties given are weight/area ratio, apparent density, thermal conductivity as a function of layer density, the product of apparent density and thermal conductivity, thermal conductivity as a function of warm-side temperature, thermal conductivity parallel to the layers, thermal conductivity as a function of pressure, gas flow conductance values, the effect of mechanical compression on heat flux, and specific heat.



4.3-1

Unit Weight of Multilayer Composites
as a Function of Number of Radiation Shields

Information about the following composites appears in the figure:

<u>Composite</u>	<u>Key</u>
1/4-mil aluminum foil and 2.8-mil Dexiglas paper spacers	FOIL + PAPER
1/4-mil Mylar, aluminized two sides, with 2.8-mil Dexiglas paper spacers	MYLAR + PAPER
1/4-mil crinkled Mylar, aluminized one side	CRINKLED MYLAR
1/4-mil Mylar, aluminized two sides, with 0.6-mil Tissuglas spacers	MYLAR + TISSUGLAS
1/4-mil Mylar, aluminized two sides, with 20-mil foam spacers	MYLAR + FOAM
1/2- and 1-mil Mylar, aluminized two sides, with 1/2- and 1-mil Mylar, aluminized two sides, and dimpled	DIMPLAR, 1/2 mil (1 mil)
1/4-mil Mylar, aluminized two sides, with 2 layers of 3.5-mil silk netting	MYLAR + SILK

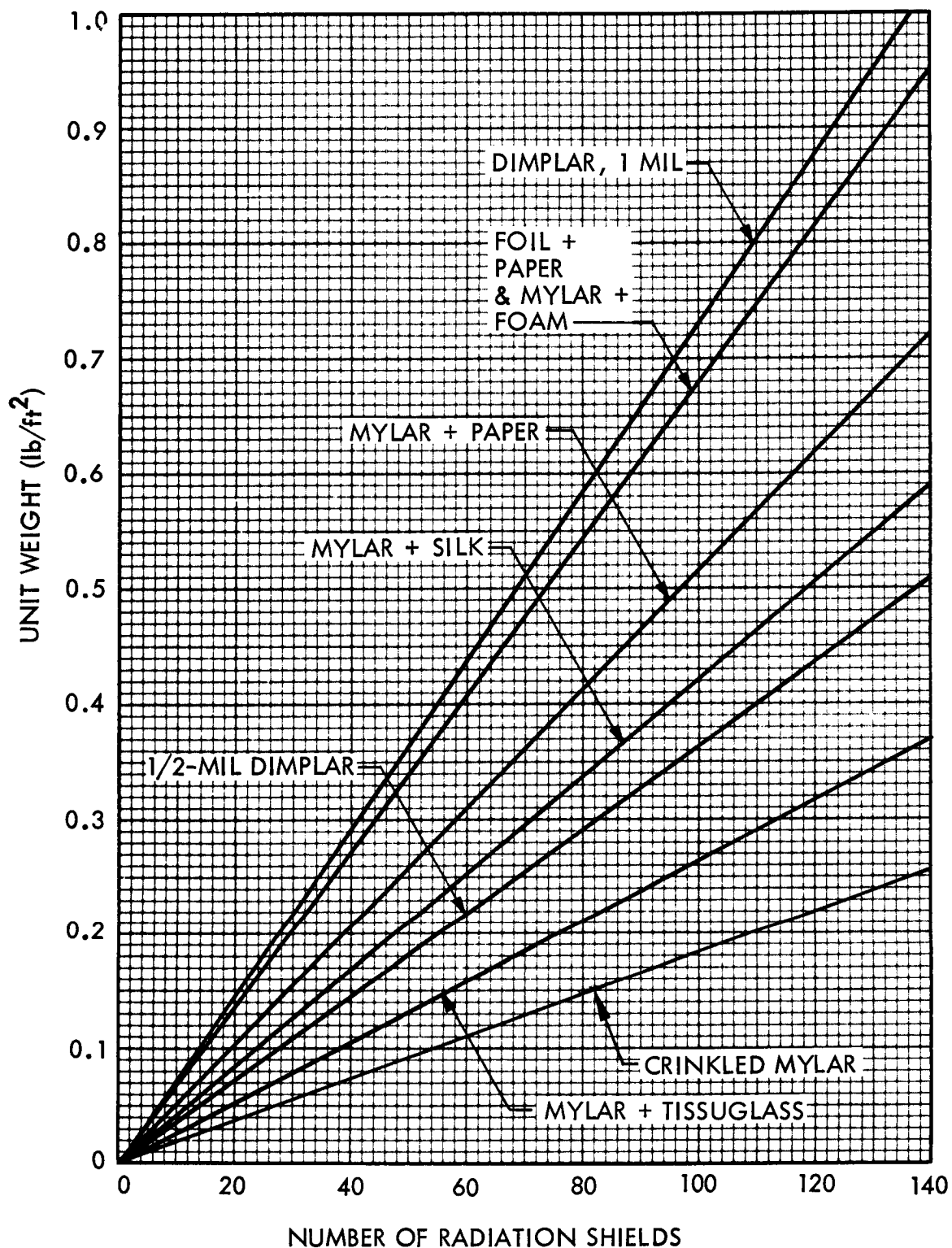


Fig. 4.3-1 Unit Weight of Multilayer Composites as a Function of Number of Radiation Shields

4.3-3

Nominal Density of Multilayer Composites
as a Function of Layer Packing Density

Information about the following composites appears in the figure:

<u>Composite</u>	<u>Key</u>
1/4-mil aluminum foil, with 2.8-mil Dexiglas paper spacers	FOIL + PAPER
1/4-mil Mylar, aluminized two sides, with 2.8-mil Dexiglas paper spacers	MYLAR + PAPER
1/4-mil crinkled Mylar, aluminized one side	CRINKLED MYLAR
1/4-mil Mylar, aluminized two sides, with 0.6-mil Tissuglas spacers	MYLAR + TISSUGLAS
1/4-mil Mylar, aluminized two sides, with 20-mil foam spacers	MYLAR + FOAM
1/2- and 1-mil Mylar, aluminized two sides, with 1/2- and 1-mil Mylar, aluminized two sides, and dimpled	(DIMPLAR, 1/2 MIL (1 MIL)
1/4-mil Mylar, aluminized two sides, with 2 layers of 3.5-mil silk netting	MYLAR + SILK

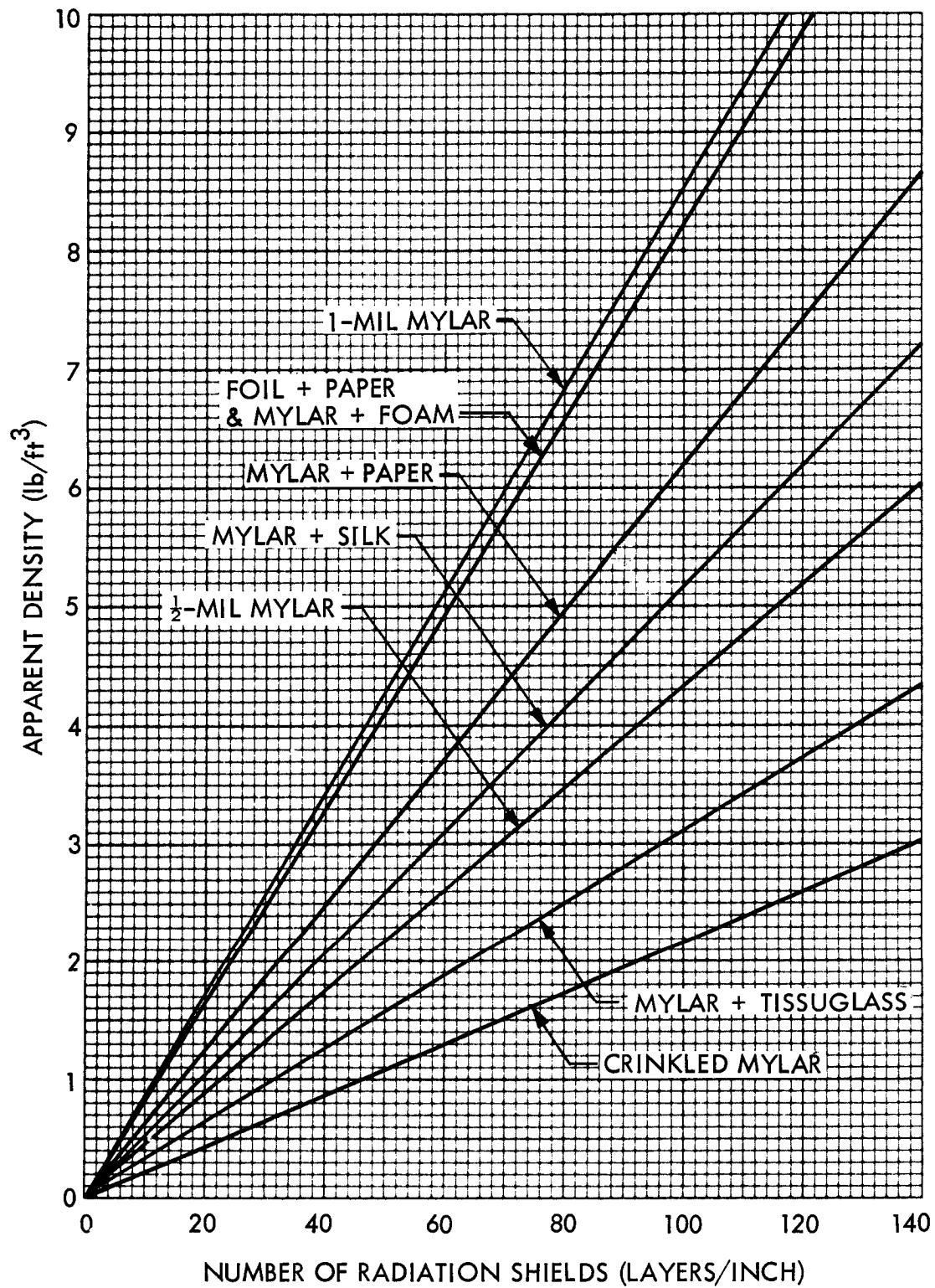


Fig. 4.3-2 Nominal Density of Multilayer Composites as a Function of Layer Packing Density

Effective Thermal Conductivity* of Multilayer Composites
as a Function of Layer Packing Density

Information about the following composites appears in the following figures:

<u>Composite</u>	<u>Key</u>	<u>Reference</u>	<u>Method of Obtaining Data</u>
1/4-mil Mylar, aluminized two sides, with 2.8-mil Dexiglas paper spacers	MYLAR + PAPER	72	NBS-Cryostat
1/4-mil crinkled Mylar, aluminized one side	CRINKLED MYLAR	79	Flat-Plate Calorimeter
1/4-mil Mylar, aluminized two sides, with 2 layers of 3.5-mil thick silk netting, 14×14 mesh	MYLAR + SILK	107	Flat-Plate Calorimeter
1/2-mil Mylar, aluminized two sides, with 1/2-mil Mylar, aluminized two sides, and dimpled	DIMPLAR	72, 108, 109, 110	NBS-Cryostat and Flat-Plate Calorimeter
1/4-mil Mylar, aluminized two sides, with 20-mil, 2.0 lb/ft ³ Freon blown polyurethane foam	MYLAR + FOAM	79, 107	Flat-Plate Calorimeter

*See Section 4.0 for definition

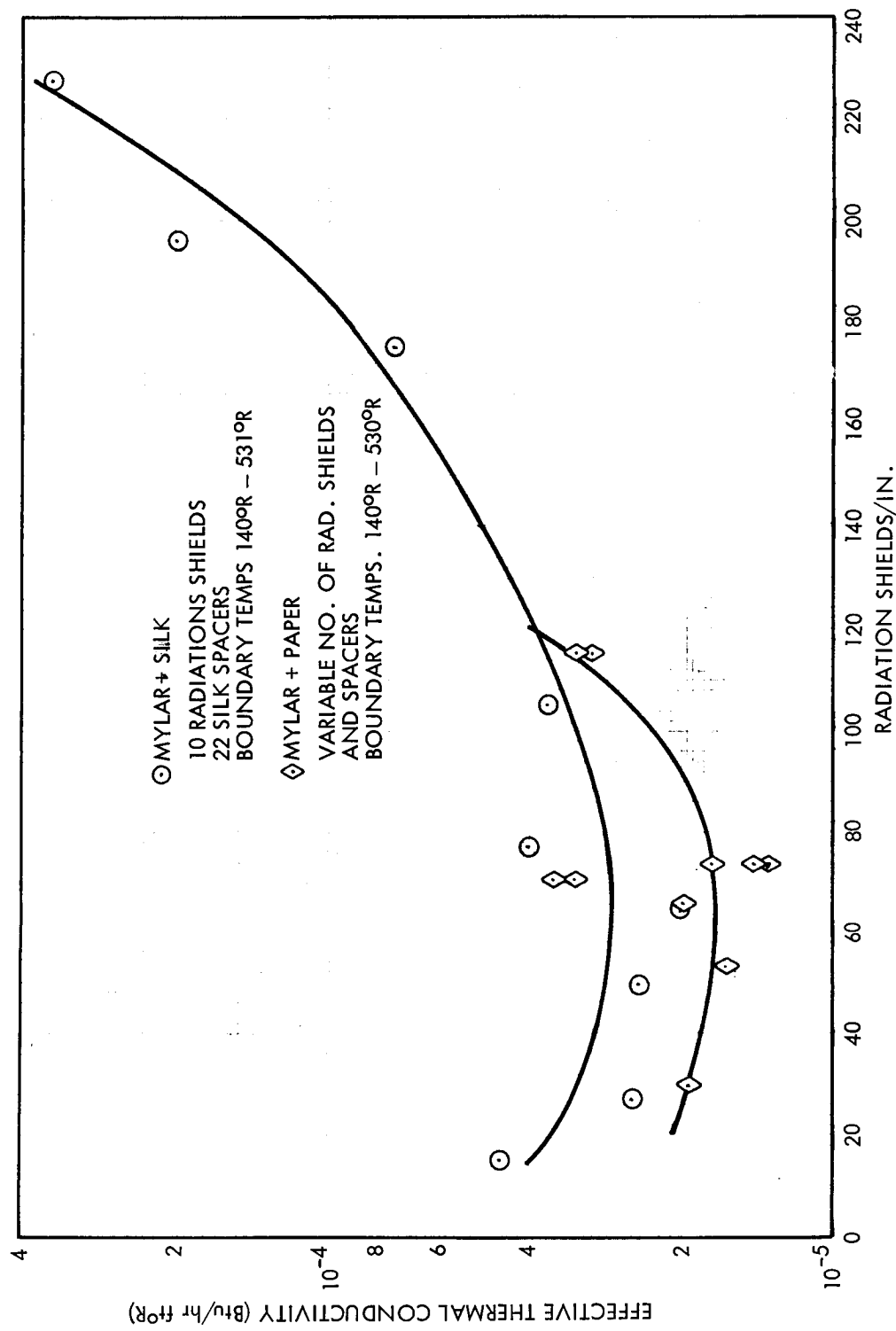


Fig. 4.3-3 Effect of Layer Density on Thermal Conductivity

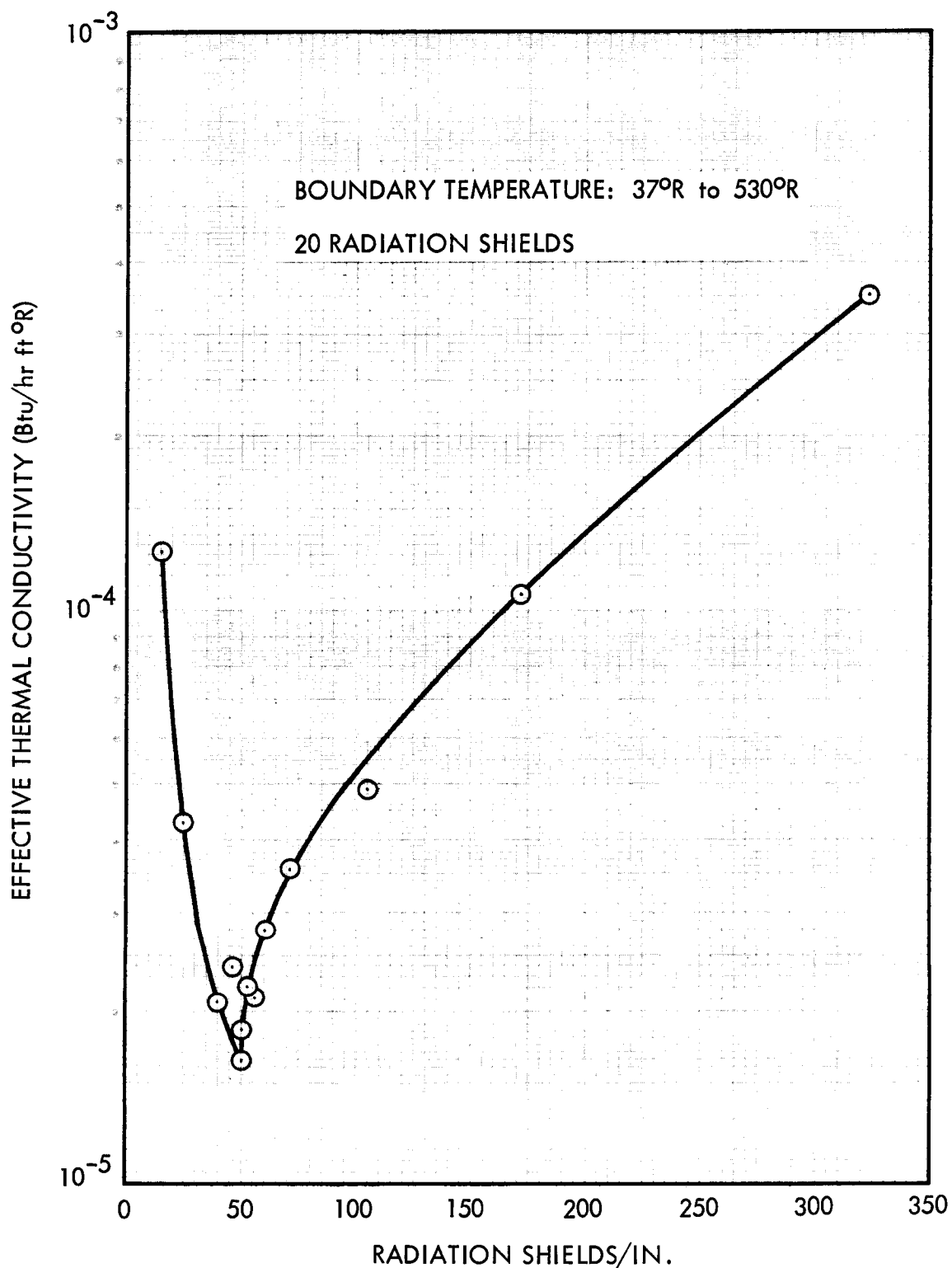


Fig. 4.3-4 Effect of Layer Density on Thermal Conductivity for Singly-Aluminized Crinkled Mylar

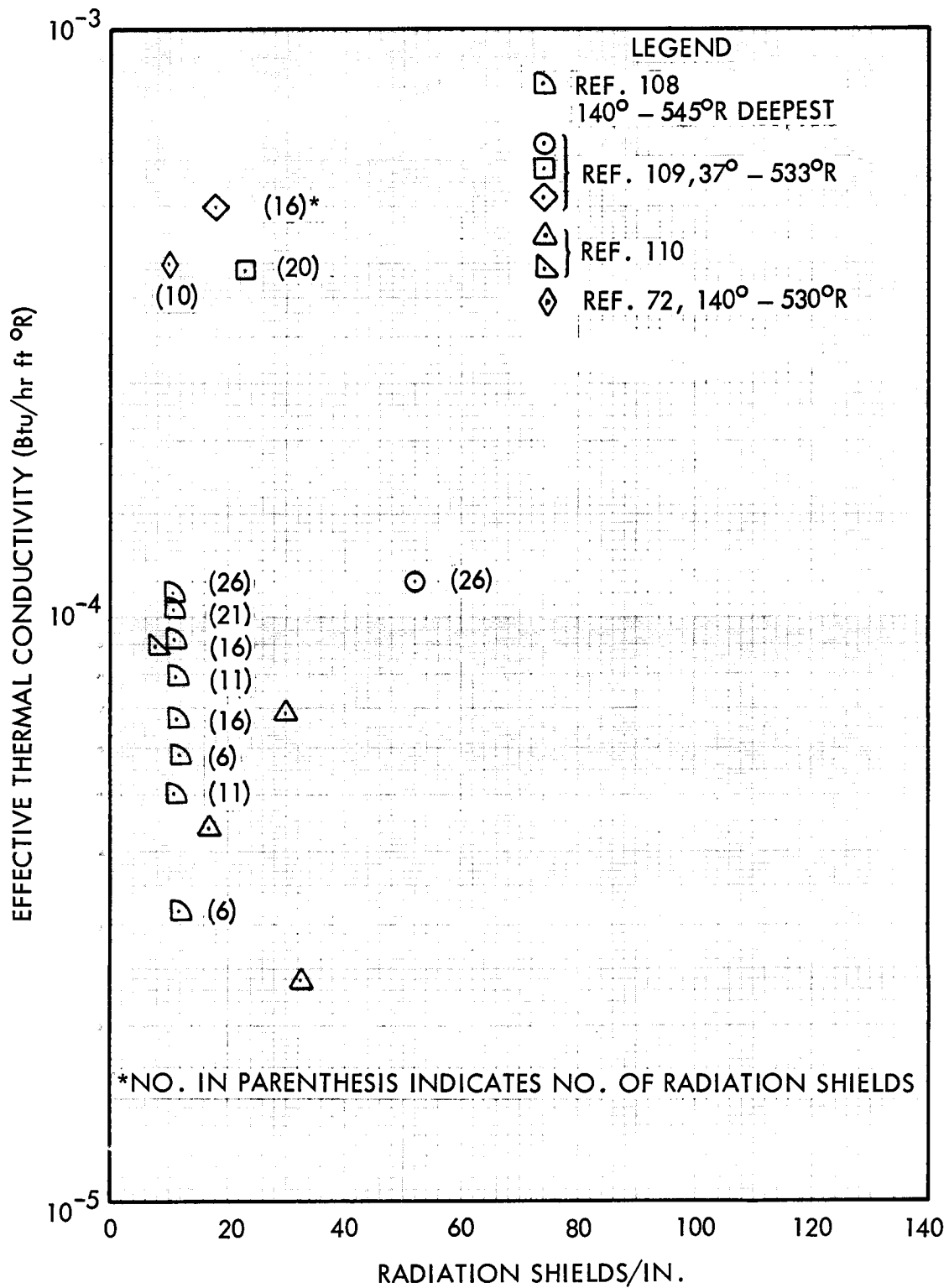


Fig. 4.3-5 Effect of Layer Density on Dimplar Thermal Conductivity

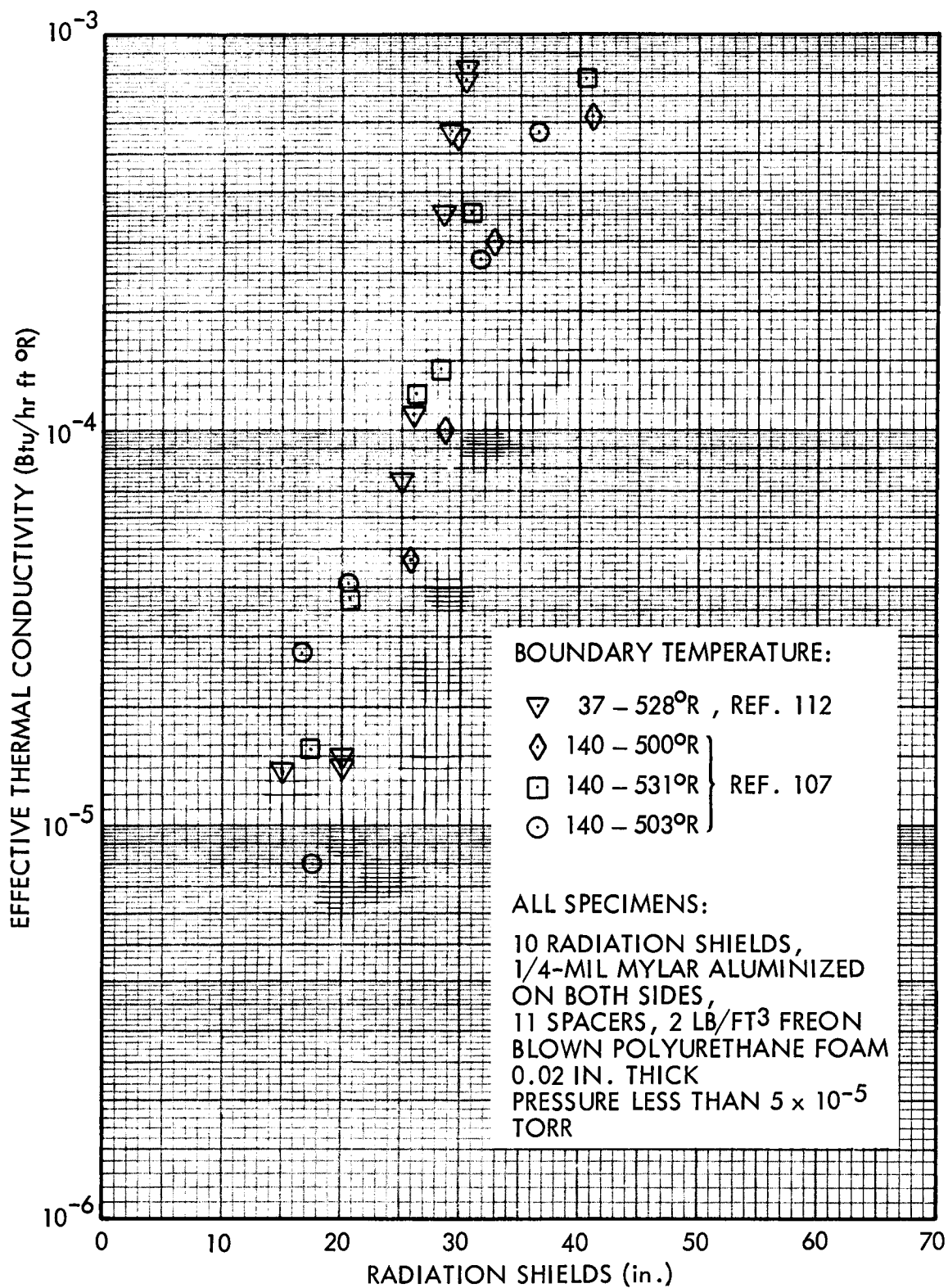


Fig. 4.3-6 Layer Density Effect on Thermal Conductivity of Mylar + Foam

Nominal-Density/Thermal-Conductivity Product of Multilayer Composites
as a Function of Layer Packing Density

The ordinates of Fig. 4.3-2 through 4.3-6 were multiplied together to obtain the curves in the accompanying figure. Extreme care should be exercised in utilizing these curves, particularly on a comparative basis. As an example, the compressive loads required to produce the higher $k\rho$ products of the Mylar-plus-Foam system are much higher than those of the other insulation systems shown. Additionally, several of the curves are not at the same boundary conditions. Due to the lack of standard testing techniques, it should also be recognized that data obtaining on different types of apparatus and by different investigators generally results in substantial differences in reported data.

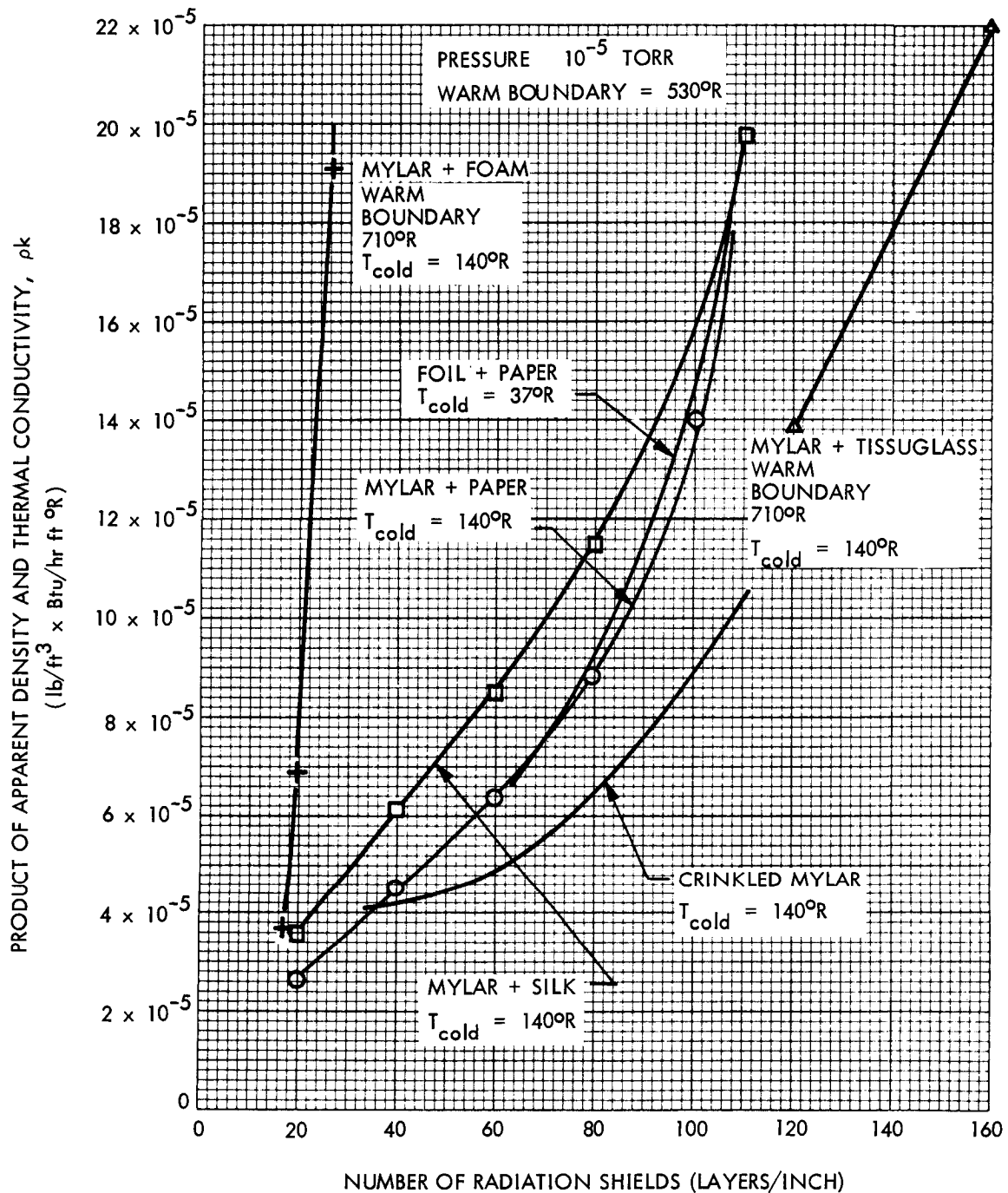


Fig. 4.3-7 Nominal-Density/Thermal-Conductivity Product of Multilayer Composites as a Function of Layer Packing Density

Thermal Conductivity of High-Temperature Multilayer Composites
as a Function of Warm-Side Temperature

All data shown were obtained on a flat-plate calorimeter.

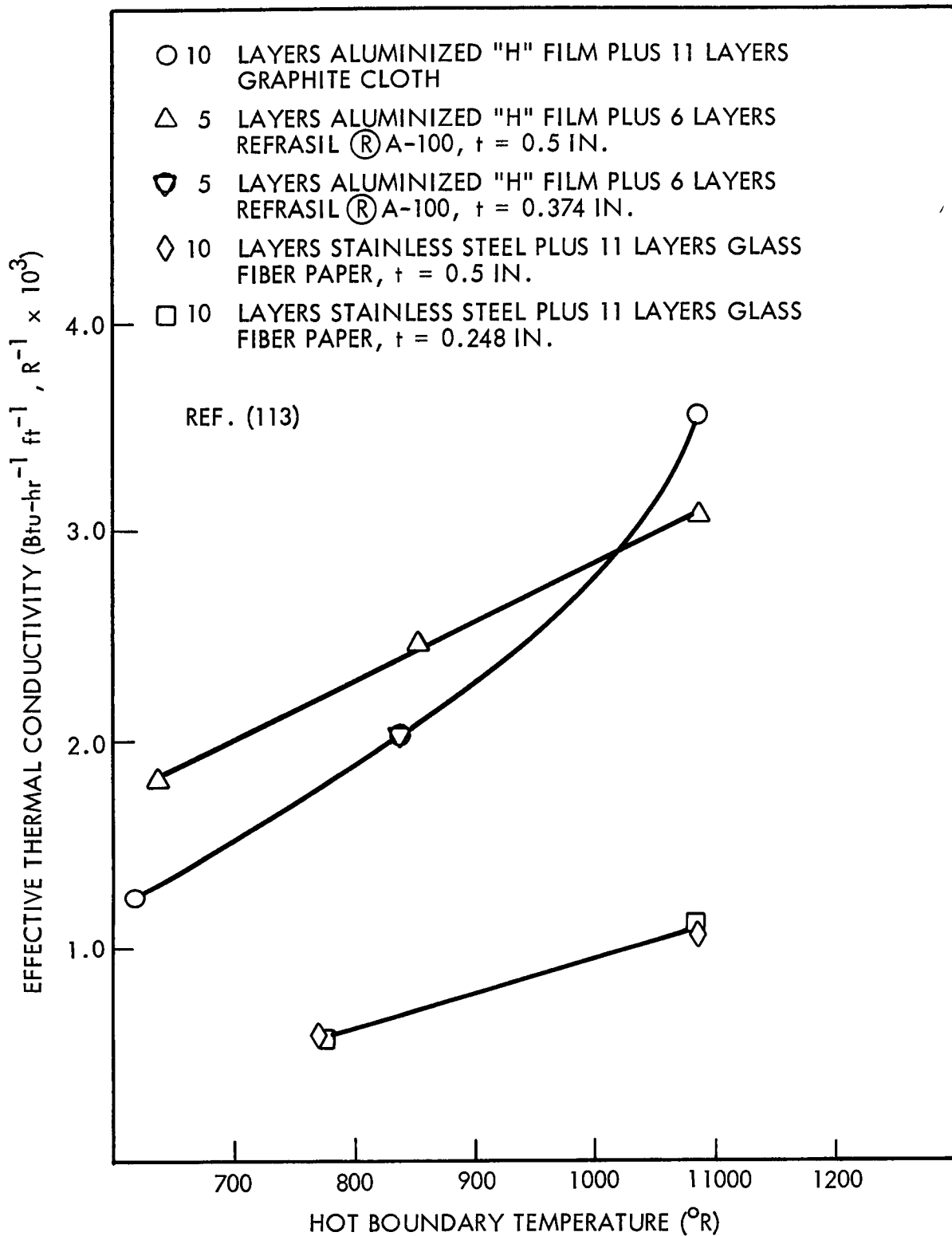


Fig. 4.3-8 Effective Thermal Conductivities of Several Combinations of Shield and Spacer Materials

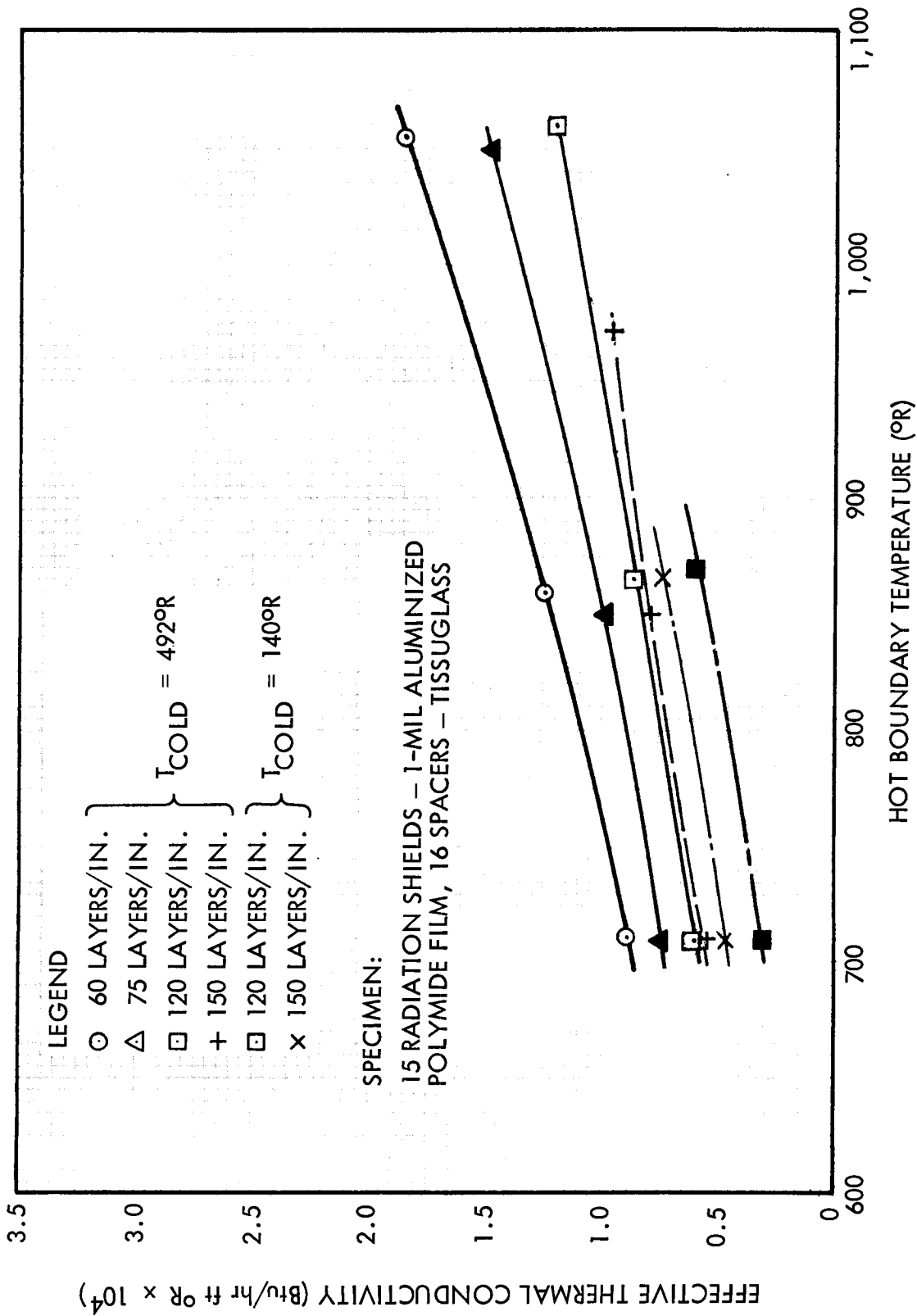


Fig. 4.3-9 Influence of Hot-Boundary Temperature on Effective Thermal Conductivity

Effective Thermal Conductivity* Parallel to Layers of Multilayer Insulation
as a Function of Temperature

<u>Materials Tested</u>	<u>Film Thickness</u>	<u>Layer Density</u>	<u>Ref.</u>
Double-aluminized Mylar Dexiglas	750 - 1000 Å	82 Layers/in.	114
NRC-2	300 Å	52 Layers/in.	114

*The effective thermal conductivity is based on the bulk material, i.e., the overall cross-sectional area of the test specimen. The effective thermal conductivity is determined from

$$k_e = \frac{Q L_s}{A_s (T_H - T_C)}$$

where Q is the heat rate being transported across the insulation specimen of length L_s and bulk cross-sectional area A_s , with a cold- and hot-boundary temperature of T_C and T_H , respectively.

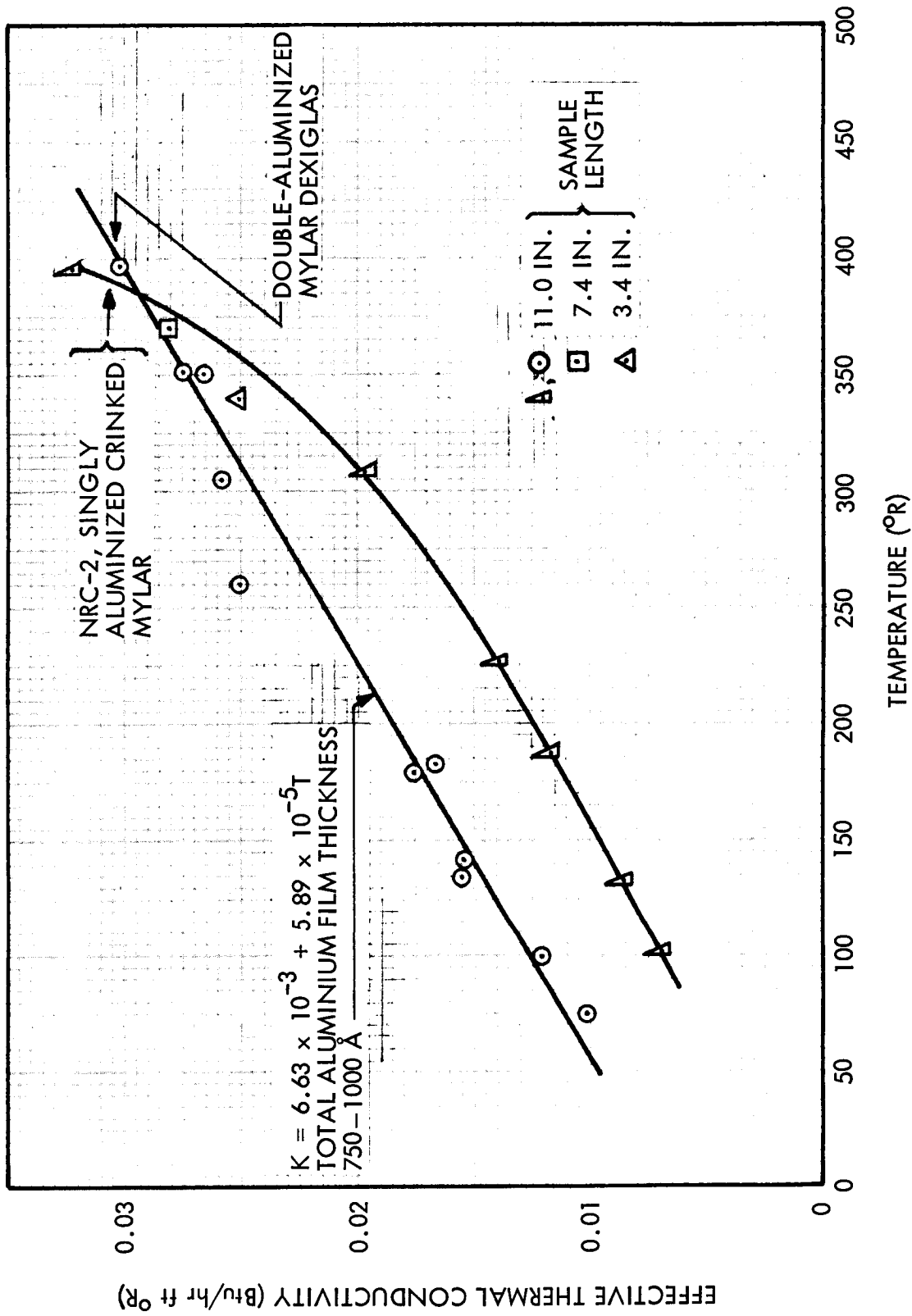


Fig. 4.3-10 Effective Thermal Conductivity of Multilayer Insulation System Measured Parallel to the Layers

Effective Thermal Conductivity Parallel to Layers of Aluminum
Foil as a Function of Temperature

The effective thermal conductivity parallel to multilayers is considerably higher than in the normal direction, mainly because of solid conduction along the radiation-shield layers. There are also small contributions from solid conduction along the spacer material and from radiation tunneling. Calculation of this anisotropic effect took into account only solid conduction along the aluminum foil. The effective thermal conductivity values were obtained by the following equation:

$$k_{\text{eff}} = \frac{N}{I} (k_{\text{Al}} \delta_{\text{Al}})$$

where

N = number of foil radiation shields

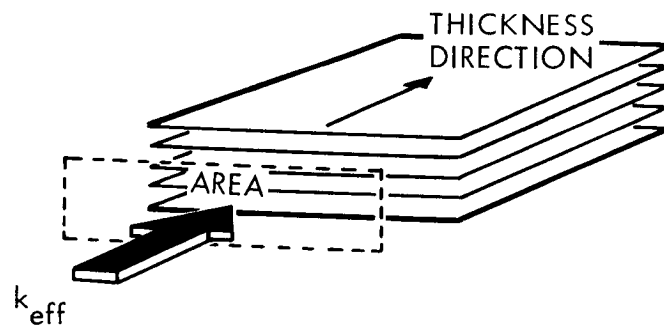
I = nominal multilayer thickness

k_{Al} = thermal conductivity of aluminum (See Fig. 4.2-2)

δ_{Al} = aluminum foil thickness (0.25 mil)

NOTE

Effective k value applies to the nominal area and thickness direction shown below.



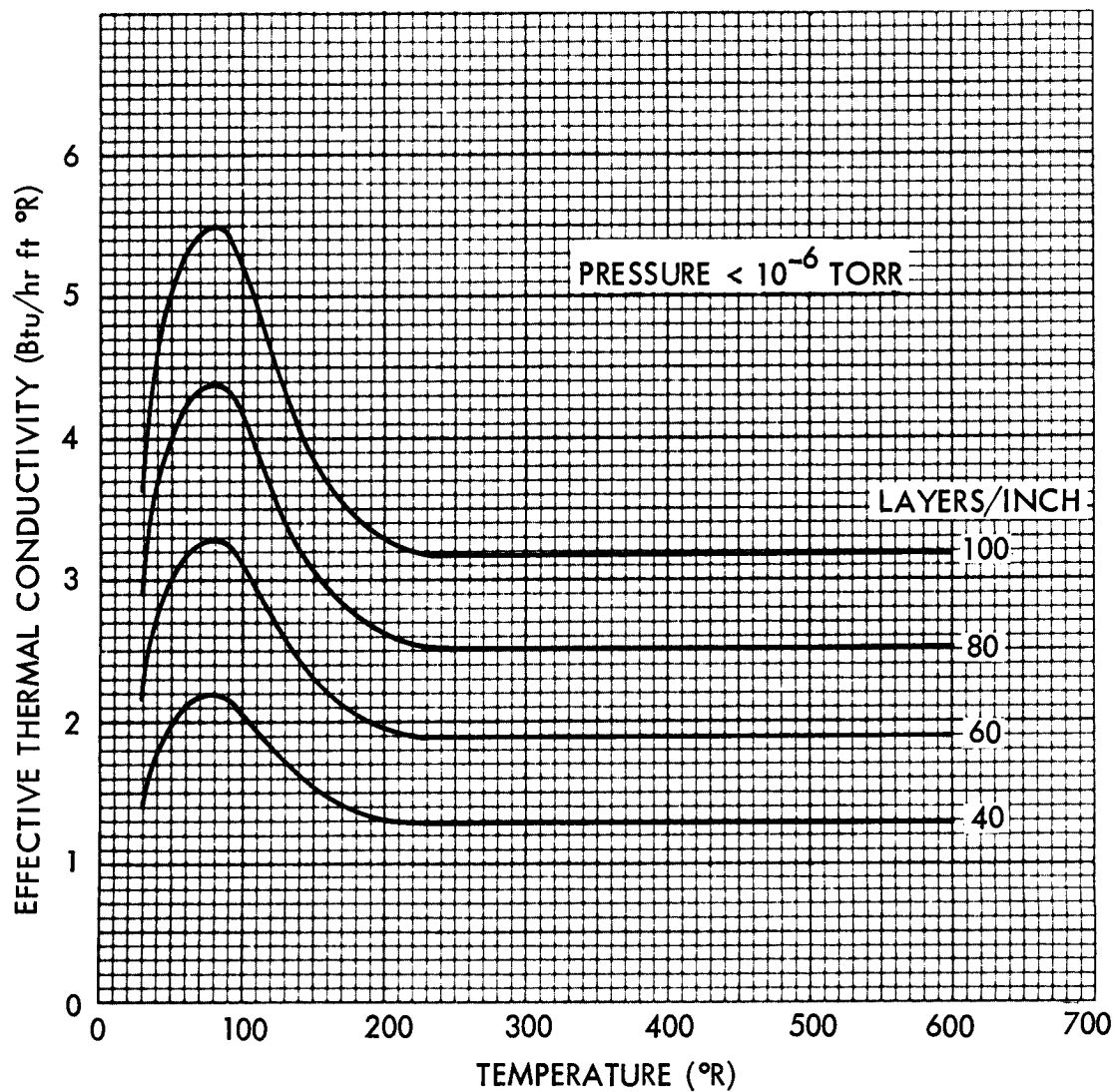


Fig. 4.3-11 Effective Thermal Conductivity Parallel to Layers of Aluminum Foil as a Function of Temperature

4.3-23

Thermal Conductivity of Multilayer Composites as a Function of Gas Pressure

Information about the following composites appears in the figure:

<u>Composite</u>	<u>Layers/Inch</u>	<u>Key</u>	<u>Reference</u>
Aluminum foil and fiberglass paper spacers	36	(1) FOIL + PAPER	84
Aluminum foil and fiberglass paper spacers	Not specified	(2) FOIL + PAPER	83
1/4-mil Mylar, aluminized two sides, and 2.8-mil Dexiglas paper spacers, buttons on 4-in. centers	68	(3) MYLAR + PAPER	72
1/4-mil crinkled Mylar, aluminized one side	40	(4) CRINKLED MYLAR	85

The equilibrium thermal conductivity values at 10^{-5} torr have not been adjusted to correspond with those in previous figures. The normalized thermal conductivity ratio from Fig. 4.3-9 must be used to obtain values consistent with previous curves.

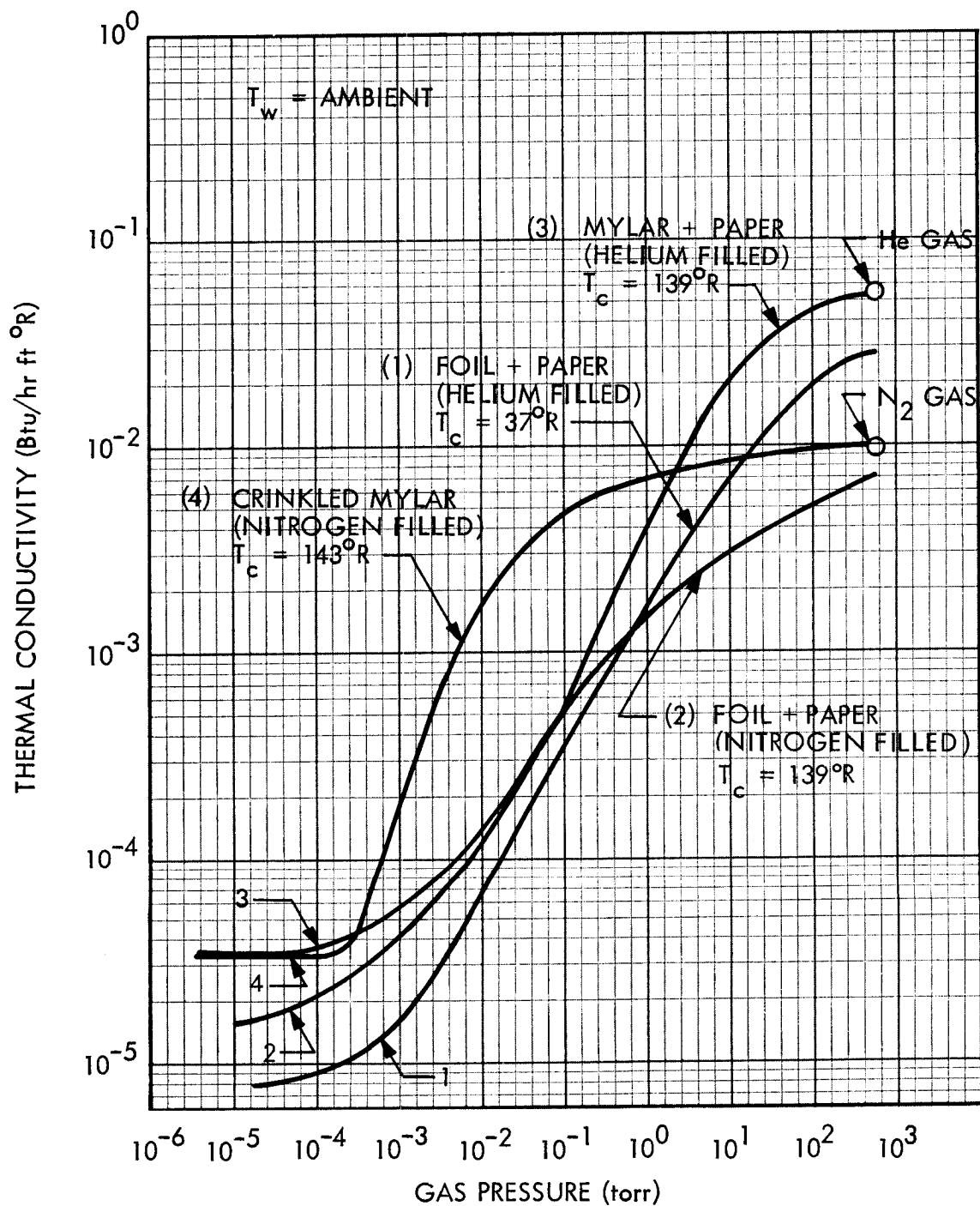


Fig. 4.3-12 Thermal Conductivity of Multilayer Composites as a Function of Gas Pressure

Normalized Thermal Conductivity of Multilayer Composites as a
Function of Gas Pressure

Information about the following composites appears in the figure:

<u>Composite</u>	<u>Layers/Inch</u>	<u>Key</u>	<u>Reference</u>
Aluminum foil and fiberglass paper spacers	36	(1) FOIL + PAPER	84
Aluminum foil and fiberglass paper spacers	Not specified	(2) FOIL + PAPER	83
1/4-mil Mylar, aluminized two sides, and 2.8-mil Dexiglas paper spacers, buttons on 4-in. centers	68	(3) MYLAR + PAPER	72
1/4 mil crinkled Mylar, aluminized one side	40	(4) CRINKLED MYLAR	85

These curves were calculated from the data in Fig. 4.3-8. The thermal conductivity at varying pressures was divided by the equilibrium thermal conductivity value at 10^{-5} torr.

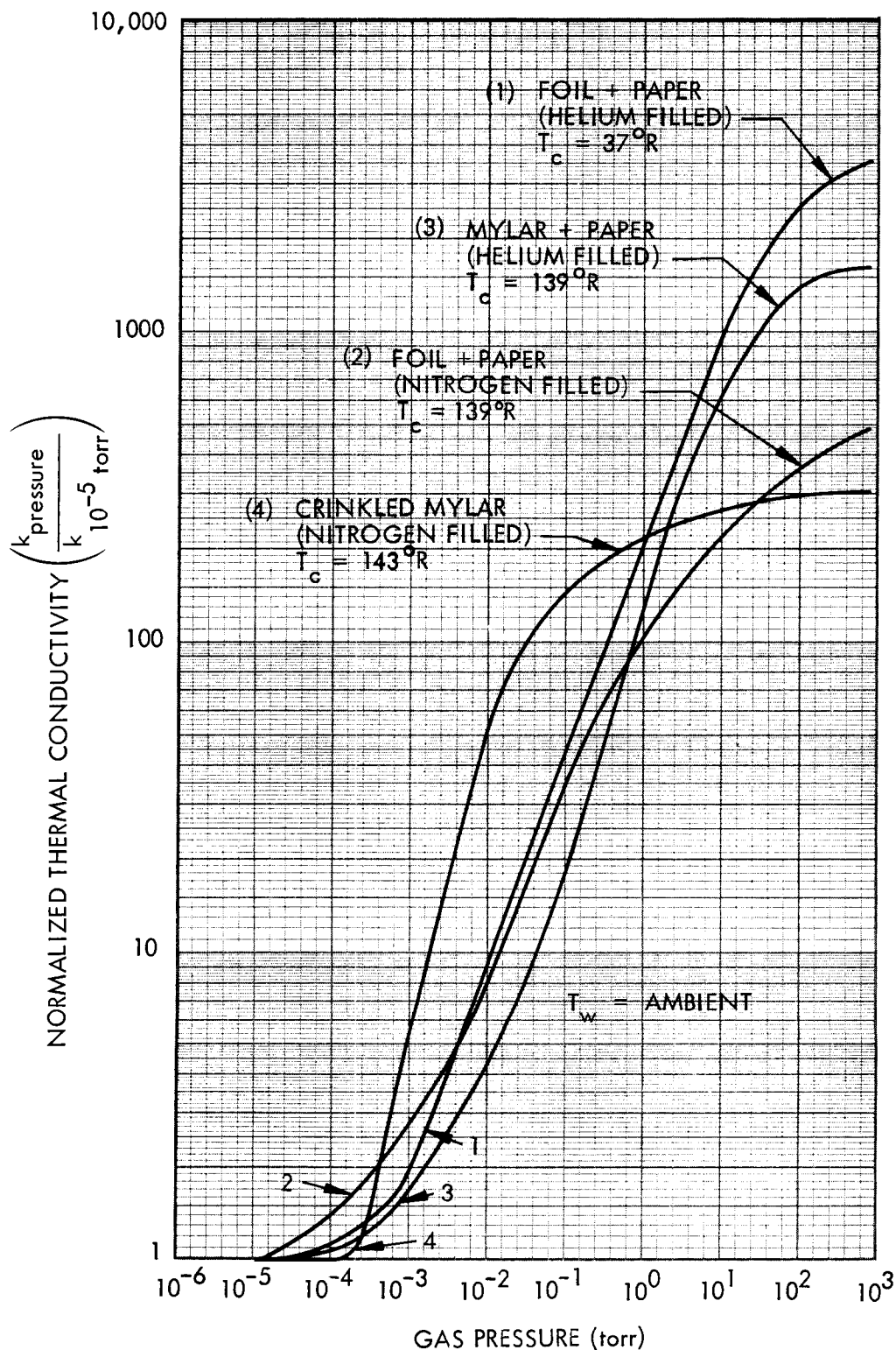


Fig. 4.3-13 Normalized Thermal Conductivity of Multilayer Composites as a Function of Gas Pressure

Permeability of Multilayer Composites as a Function of Layer Packing Density

Knowledge of the transient pressure decay of the purge gas within multilayer-insulations during ascent flight is required in order to evaluate the mechanical adequacy of the system and to predict the transient heating and associated propellant boil-off. The equation which describes the one-dimensional pressure decay along the multilayers in the continuum regime is:

$$\frac{P \partial^2 P}{\partial x^2} + \left(\frac{\partial P}{\partial x} \right)^2 = \frac{\mu \partial P}{K \partial \theta}$$

where x is the flow path length, μ is the gas viscosity, and K is the permeability of the purge gas through the multilayer system. The quantity K was experimentally determined (Ref. 92) for the selected multilayer systems cited below.

Information about the following composites appears in the figure:

<u>Composite</u>	<u>Key</u>
Linde SI-62 insulation	FOIL + PAPER
1/4-mil Mylar, aluminized two sides, and 2.8-mil Dexiglas spacers	MYLAR + PAPER
1/4-mil crinkled Mylar, aluminized one side	CRINKLED MYLAR

NOTE

Permeability is not a function of the type of purge gas or the gas temperature.

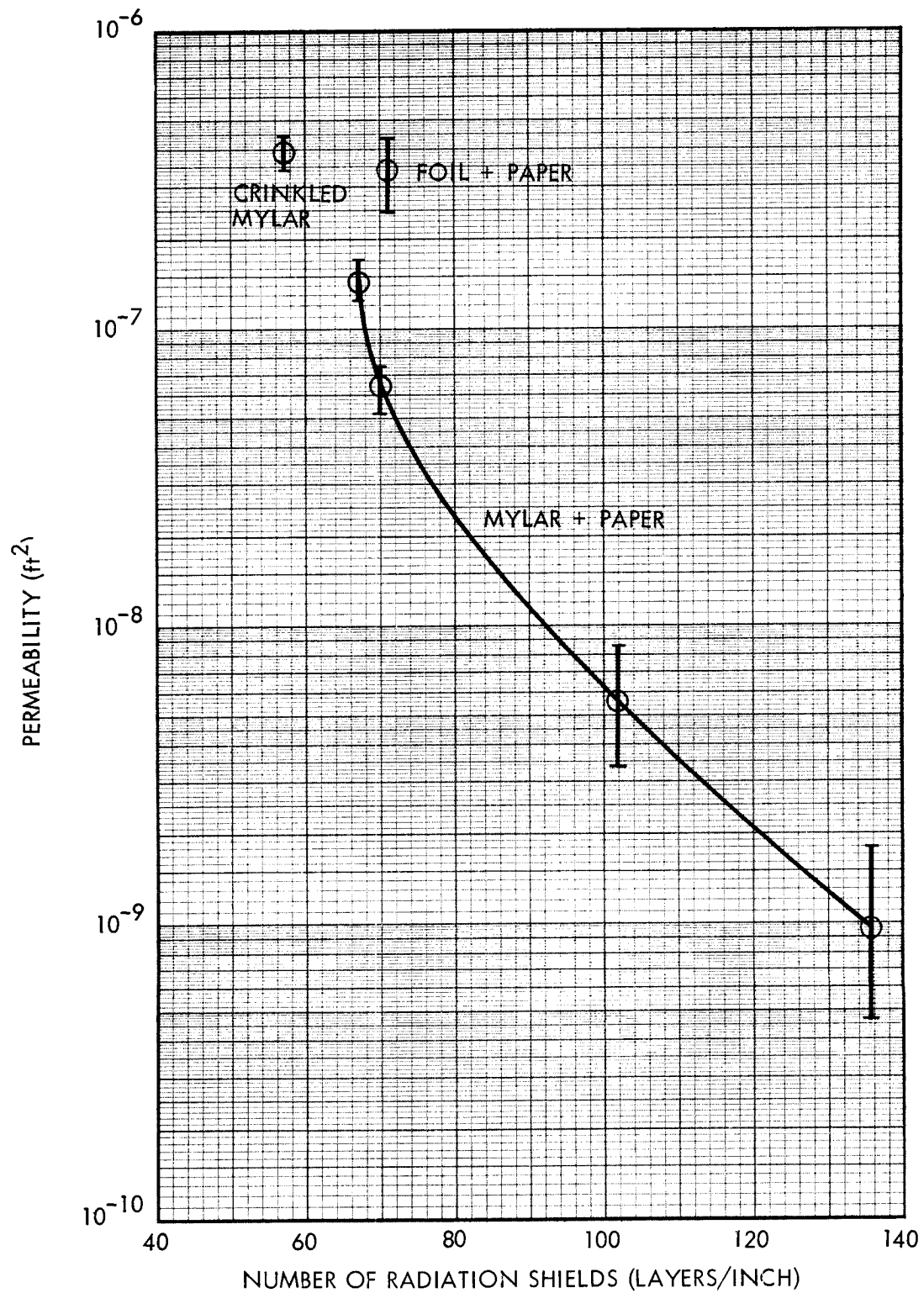


Fig. 4.3-14 Permeability of Multilayer Composites as a Function of Layer Packing Density

Diffusion Coefficients of Multilayer Composites as a
Function of Layer Packing Density

The diffusion equation describes the pressure decay of the purge gas along the multilayers in the free molecular flow regime. This equation for one-dimensional flow is as follows (Ref. 14):

$$D \frac{\partial^2 P}{\partial x^2} = \frac{\partial P}{\partial \theta}$$

The diffusion coefficient, D , was experimentally determined for selected multilayer insulation and layer densities.

The diffusion coefficient is a function of the type of purge gas and its temperature, as well as of the multilayer system and the layer density used. Data are presented in Table 4.3-1. Coefficients for other gases and temperatures can be obtained by solving the relation:

$$\frac{D}{D_{\text{He}}} = \left(\frac{T M_{\text{He}}}{T_{\text{He}} M} \right)^{1/2} = \left(\frac{T}{267 M} \right)^{1/2}$$

where M is the molecular weight, T is the temperature in $^{\circ}\text{R}$, and D_{He} is the diffusion coefficient for helium from Table 4.3-1. The measured effect of molecular weight on diffusion coefficient is plotted in Fig. 4.3-15 (Ref. 114).

Table 4.3-1
DIFFUSION COEFFICIENT DATA (REF. 114)

Sample 1: NRC-2 crinkled, singly-aluminized Mylar, 67 layers/in., 36 in. long

<u>Gas</u>	<u>Temperature (° K)</u>	<u>Diffusion Coefficient (ft²/sec)</u>
Argon	295	1.16
Helium	295	2.68
	77	0.936
Air	295	1.55

Sample 2: Double-aluminized Mylar-Dexiglas, 70 layers/in., 36 in. long

<u>Gas</u>	<u>Temperature (° K)</u>	<u>Diffusion Coefficient (ft²/sec)</u>
Helium	295	0.966
	77	0.414

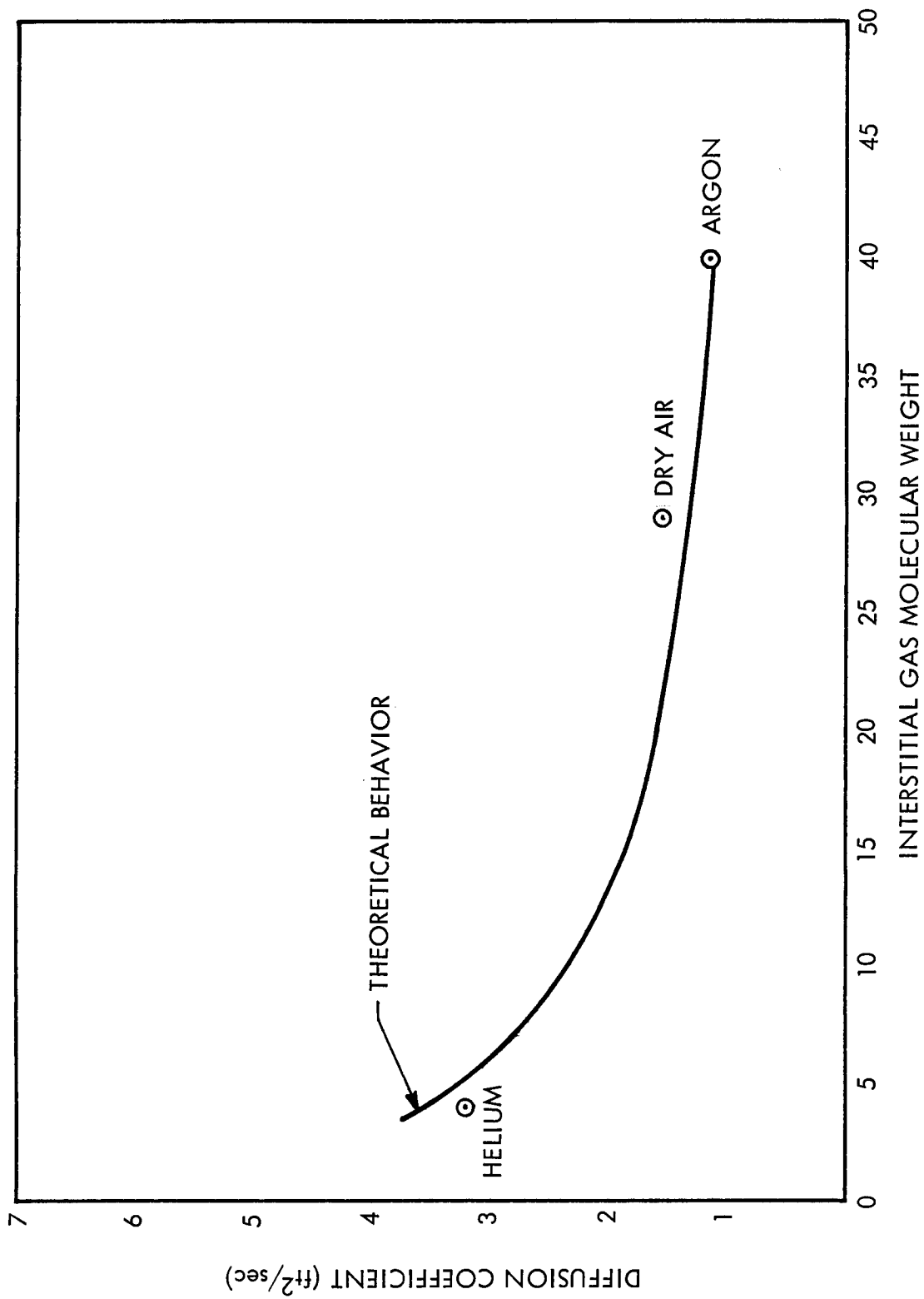


Fig. 4.3-15 Effect of Gas Molecular Weight on Diffusion Coefficient

4.3-33

Heat Flux of Multilayer Composites as a Function of Compressive Load

The type of material, cold-wall temperature, and number of layers for each material callout are tabulated below. The warm-side temperature for each sample is room temperature.

<u>Sample No.</u>	<u>T_{cold} (°R)</u>	<u>No. of Layers</u>	<u>Material</u>
1	140	60	Crinkled aluminized polyester film
2	140	60	Aluminized polyester film
		61	Fiberglass cloth
3	37	10	Aluminized polyester film
		11	Perforated fiberglass mat
4	140	20	Aluminized polyester film
		11	Fiberglass mesh
5	37	20	Soft aluminum
		21	Polyester fiber
6	37	10	Tempered aluminum
		11	Perforated fiberglass mat
7	37	10	Tempered aluminum
		10	Glass fiber paper (0.003 in.)
8	140	6	Aluminized polyester film
		7	CT-449 (11 percent support area, 0.080 in.)
9	37	10	Waffled aluminum
		11	Fiberglass mat
10	37	10	Waffled aluminum
		11	Three fiberglass cloth
11	37	10	Tempered aluminum
		11	CT-449 (11 percent support area, 0.020 in.)
12	37	10	Tempered aluminum
		11	CT-449 (0.020 in.)
13	37	10	Double aluminized polyester film both sides
		11	Nylon netting (0.007 in.)

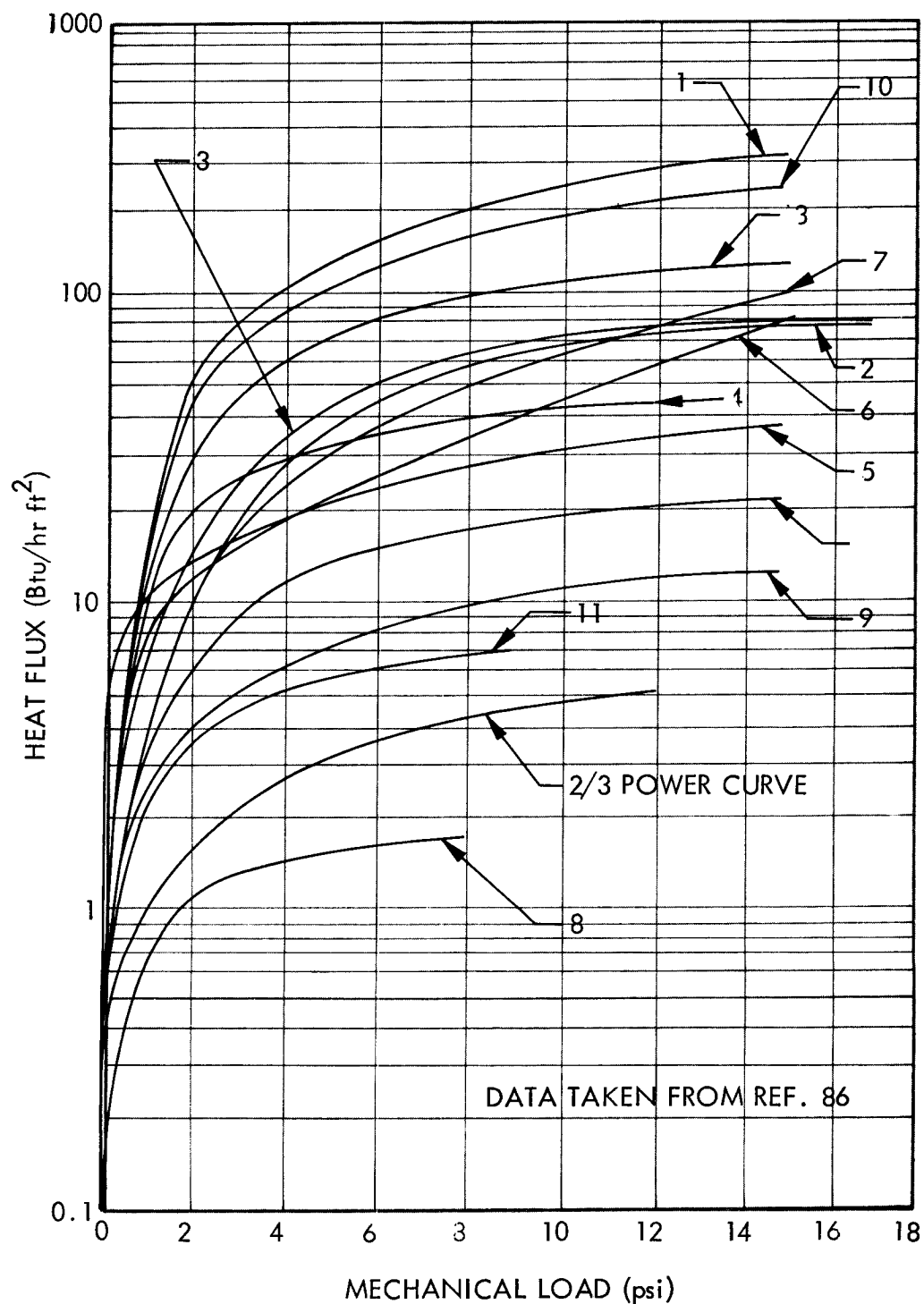


Fig. 4.3-16 Heat Flux of Multilayer Composites as a Function of Compressive Load

Heat Flux Ratio of Multilayer Composites as a Function of Compressive Load

Information about the following composites appears in the figure:

<u>Composite</u>	<u>Key</u>	<u>Reference</u>
1/4-mil aluminum foil and 2.8-mil Dexiglas paper spacers	FOIL + PAPER	87
1/4-mil crinkled Mylar, aluminized one side, and 8-mil fiberglass paper with 50 percent perforations	MYLAR + PAPER	88
1/4-mil crinkled Mylar, aluminized one side	CRINKLED MYLAR	89

Arrows indicate the trend of heat flux ratio as a function of an increasing or decreasing mechanical load.

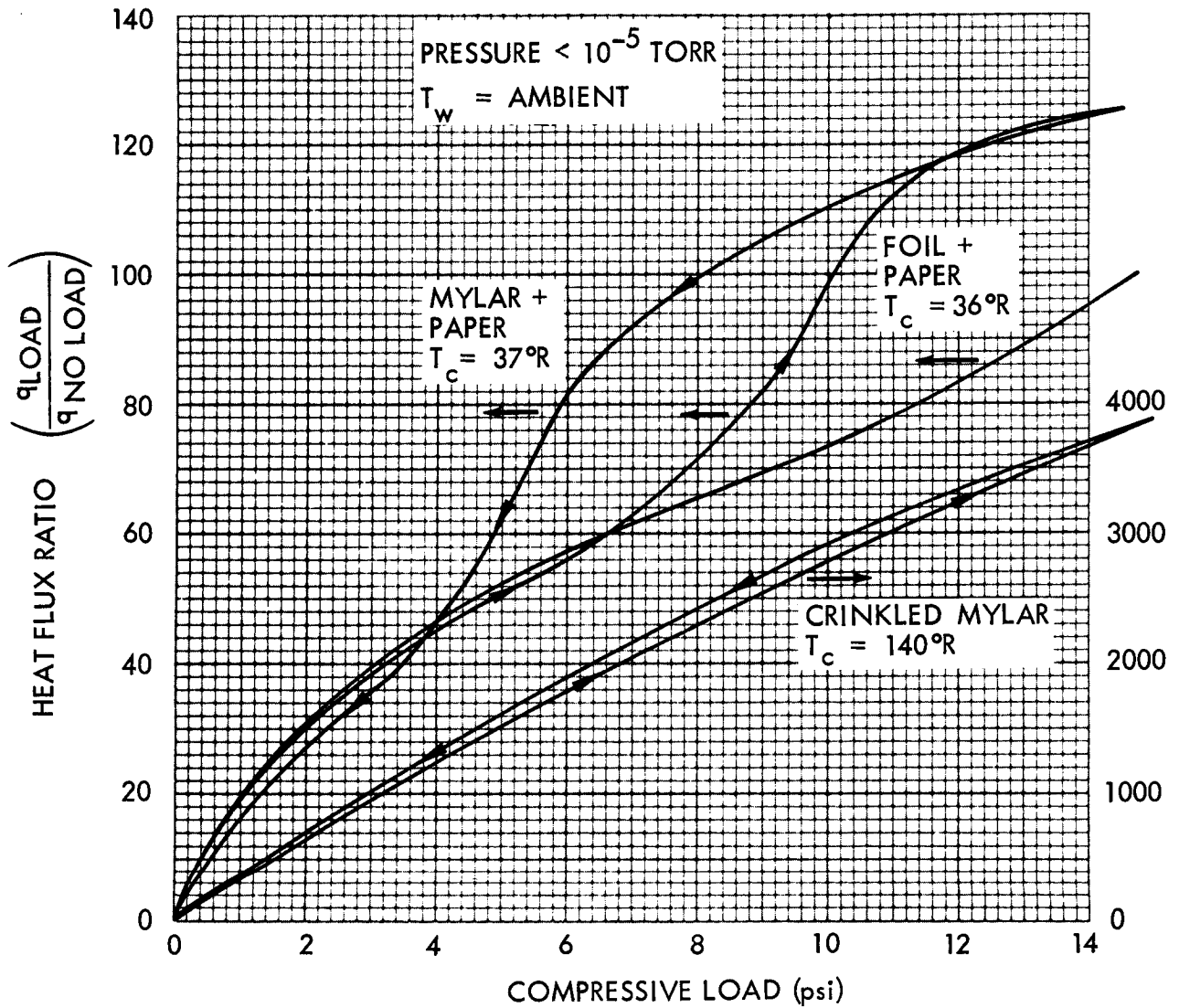


Fig. 4.3-17 Heat Flux Ratio of Multilayer Composites as a Function of Compressive Load

4.3-37

Specific Heat of Multilayer Composites as a Function of Temperature

Information about the following composites appears in the figure:

<u>Composite</u>	<u>Key</u>	<u>Reference</u>
Linde SI-62	FOIL + PAPER	90
1/4-mil Mylar, aluminized two sides, and 2.8-mil Dexiglas paper spacers	MYLAR + PAPER	69, 90
1/4-mil crinkled Mylar, aluminized one side	CRINKLED MYLAR	69

Specific heat of Mylar was available only at room temperature. The curve was extrapolated to a zero value at 0°R following the general shape of other polymer curves as explained in the text accompanying Fig. 4.2-3.

The specific heat of Dexiglas was calculated from Ref. 90 as explained in the text accompanying Fig. 4.2-3.

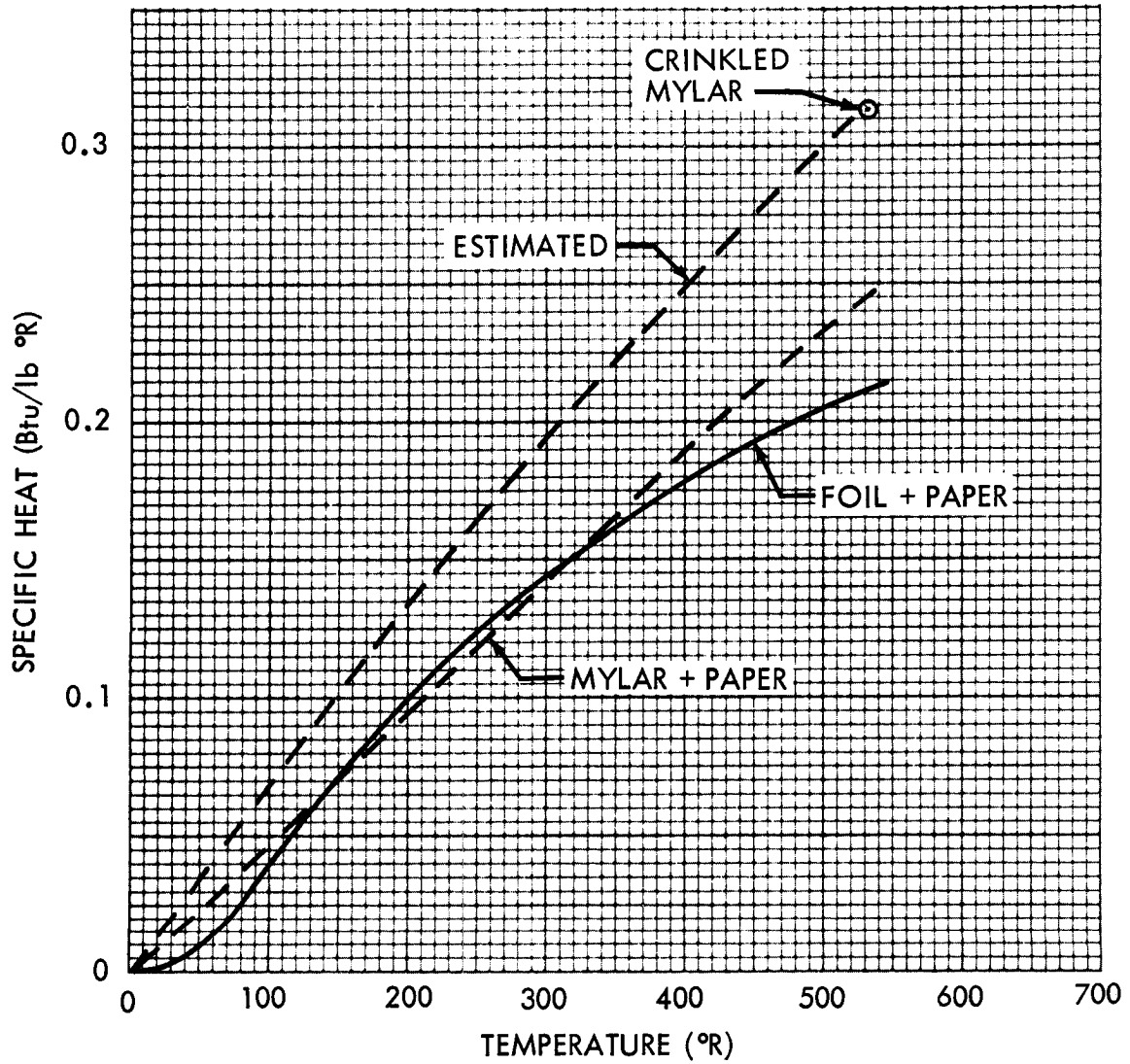


Fig. 4.3-18 Specific Heat of Multilayer Composites as a Function of Temperature

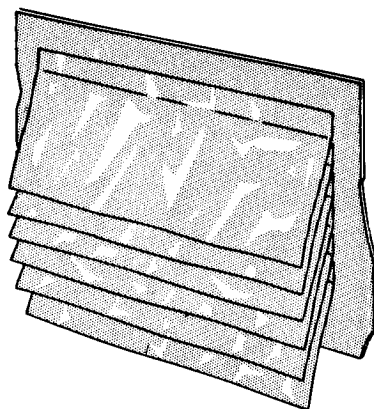
4.4 ATTACHMENT METHODS

In order for multilayer insulations to be installed on flight tanks for cryogenic propellants, methods must be devised for supporting the insulation in a flight environment. Two of the more promising methods tested to date are the shingle and button attachment methods. The shingle system requires adequate structural strength in the multilayers, such as crinkled aluminized Mylar, to allow attachment along one edge. The button system was devised to support the fragile Dexiglas paper spacer with radiation shields of either aluminized Mylar or aluminum foil.

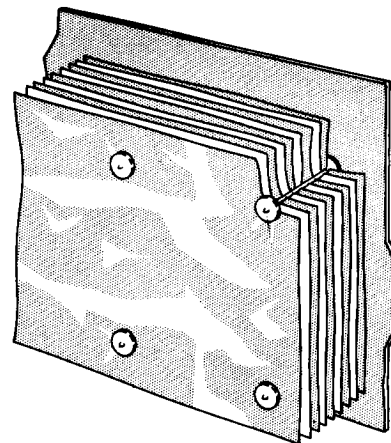
Both these attachment methods have been tested in acceleration environments to 20 g, in acoustic environments to 150 db, in simulated flight vibration environments, and in rapid-pressure-drop environments to 0.2 psi/sec maximum, using a 26-in. -diameter tank filled with liquid hydrogen. No structural damage or change in thermal performance was observed or measured.

The properties covered in this section are thermal conductivity as a function of shingle length, thermal conductivity as a function of warm-side temperature, and effect of leaking gas on thermal performance.

Appendix I describes an analytical method for calculating shingle thermal performance for different shingle lengths and boundary temperatures.



SHINGLE ATTACHMENT:
CRINKLED ALUMINIZED
MYLAR



BUTTON ATTACHMENT:
ALUMINIZED MYLAR AND
DEXIGLAS SPACERS

Effective Thermal Conductivity of Multilayer Shingle Insulation
as a Function of Shingle Length

Forty effective layers of 1/4-mil crinkled Mylar shingles, aluminized one side, were tested at a layer density of 40 layers/inch. This layer density is optimum for crinkled Mylar on the basis of its thermal-conductivity/density product. The data points shown were obtained on a cryostat test setup. The curves were calculated by the analytical method described in Appendix I. The infinite values for shingle length are experimentally determined thermal-conductivity values for an equivalent number of parallel shields.

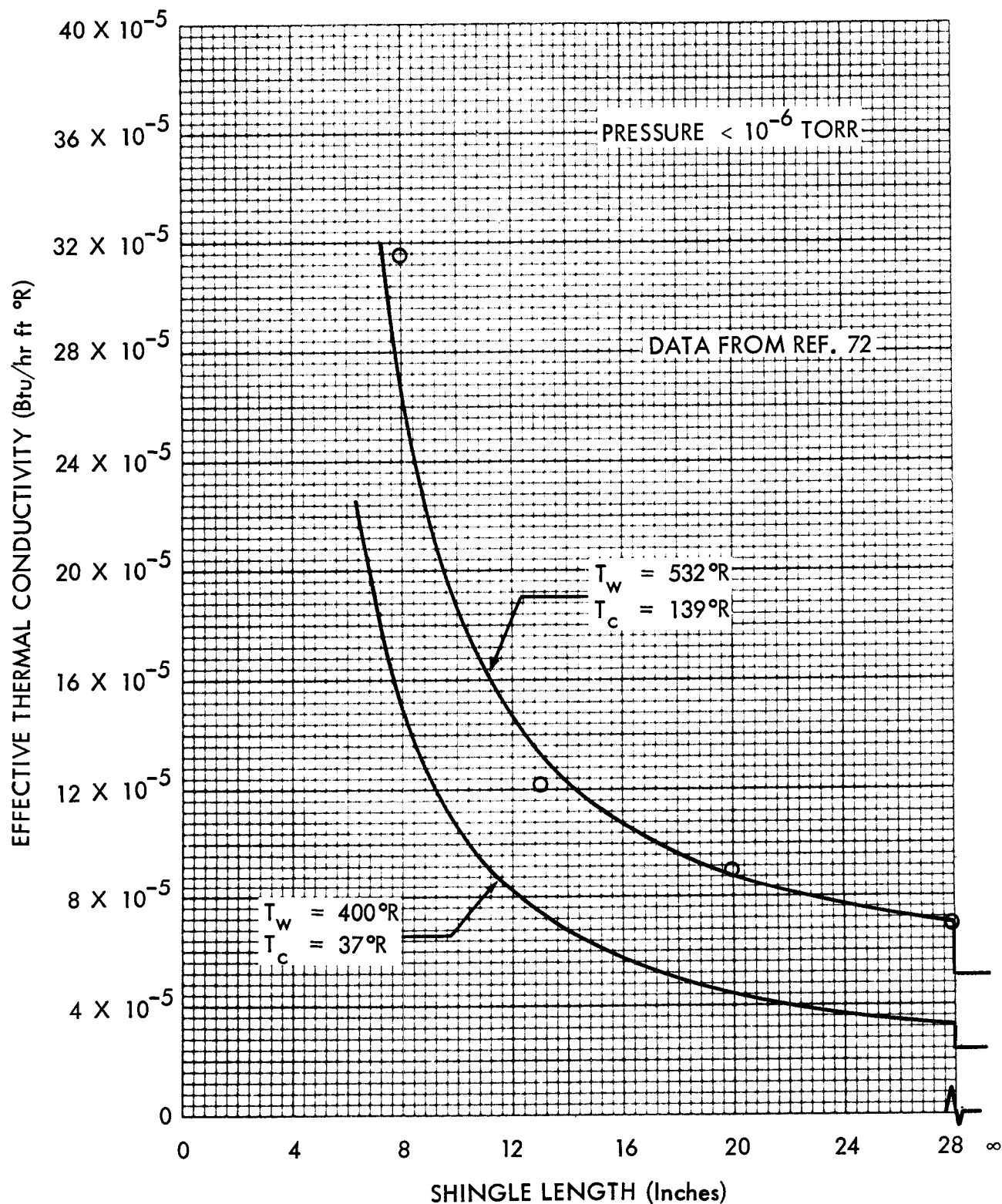


Fig. 4.4-1 Effective Thermal Conductivity of Multilayer Shingle Insulation as a Function of Shingle Length

Thermal Conductivity of Shingle Multilayer Insulation as a
Function of Warm-Side Temperature

Forty effective layers of 13-in. long, 1/4-mil crinkled Mylar shingles, aluminized one side, were tested at a layer density of 40 layers/inch. The 13-in. shingle length was dictated by the maximum size of cryostat available with cold-wall capability. The points represent experimental data, and the curve was calculated by the analytical method described in Appendix I.

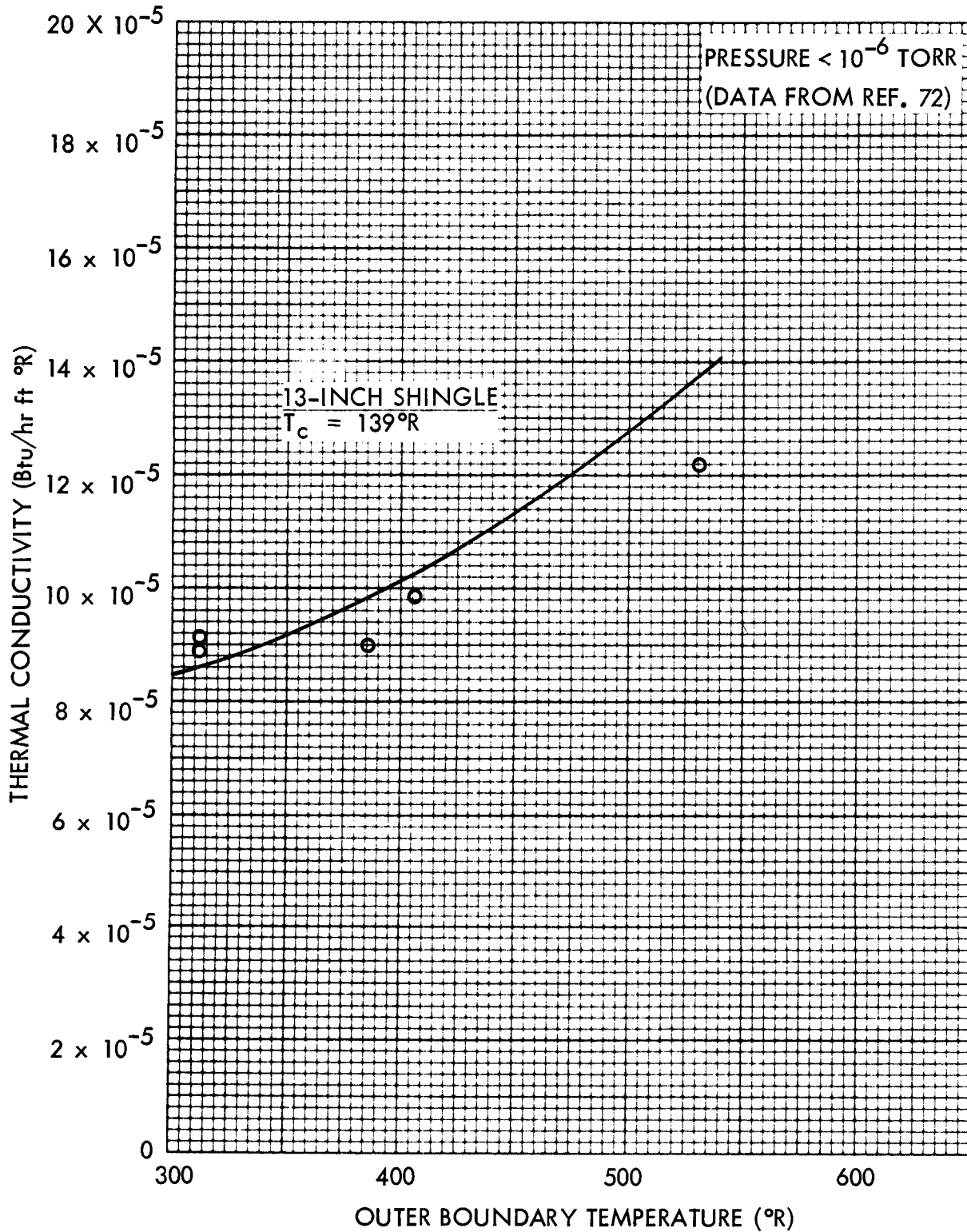


Fig. 4.4-2 Thermal Conductivity of Shingle Multilayer Insulation
as a Function of Warm-Side Temperature

Thermal Conductivity of Button Multilayer Insulation as a Function
of Outer Boundary Temperature

Information about the following insulation appears in the figure:

<u>Insulation</u>	<u>Buttons</u>	<u>Layers</u>	<u>Layers/Inch</u>	<u>Key</u>
1/4-mil Mylar, aluminized two sides, and 2.8-mil Dexiglas spacers	On 4-in. centers	60	68	○
1/4-mil Mylar, aluminized two sides, and 2.8-mil Dexiglas spacers	On 8-in. centers	40	120	△

Blankets of ten radiation shields with nine spacers were applied with a longitudinal butt joint. This butt joint, held together with Mylar/Dacron tabs between buttons, was rotated 90 deg for each successive blanket around the circumference.

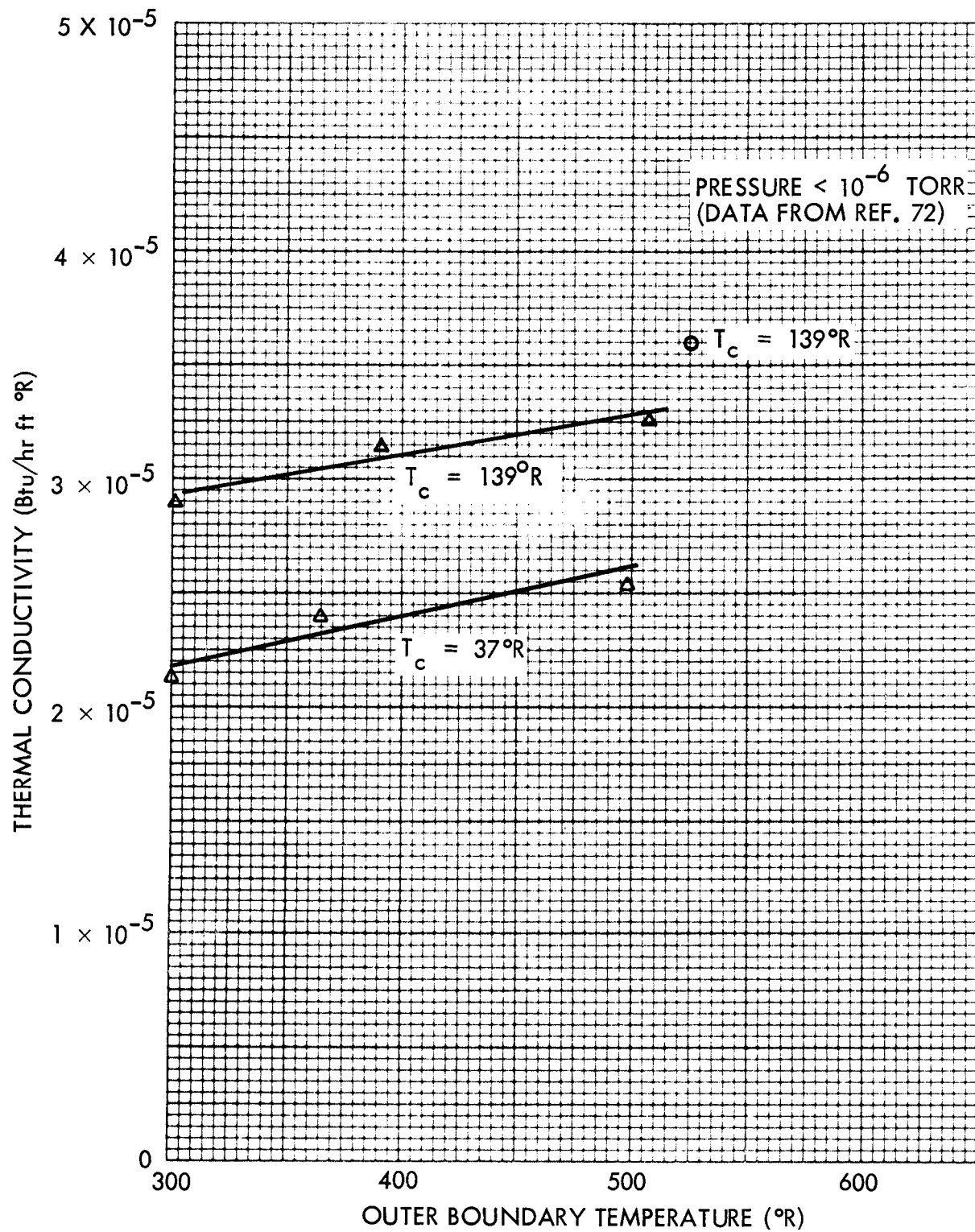


Fig. 4.4-3 Thermal Conductivity of Button Multilayer Insulation as a Function of Outer Boundary Temperature

Normalized Heat Flow Through Multilayer Systems as a Function
of Point-Source Leakage Rate

In a space environment, gas leaking from valves, welds, etc. can permeate the evacuated multilayers and degrade the equilibrium thermal performance. To determine the magnitude of this effect, tests were conducted with helium gas on 26-in.-diameter tanks with multilayer insulation.

Leakage at a constant rate was introduced at various points, and measurements were taken when the boiloff stabilized. Some venting probably occurred at the three support pins in the cylindrical section and at the fill and vent line, as well as at the vent paths shown in Fig. 4.4-5.

Information about the following insulation appears in the figure:

<u>Insulation</u>	<u>Total Layers</u>	<u>Layers per Blanket</u>	<u>Buttons</u>	<u>Shingle Length</u>	<u>Key</u>
Mylar, aluminized 2 sides, and Dexiglas paper spacers	70	10	On 4-in. centers	—	1
Mylar, aluminized 2 sides, and Dexiglas paper spacers	36	9	On 8-in. centers	—	2
Crinkled Mylar, aluminized one side	40	—	—	Approx. 3 & 4 26 in.	

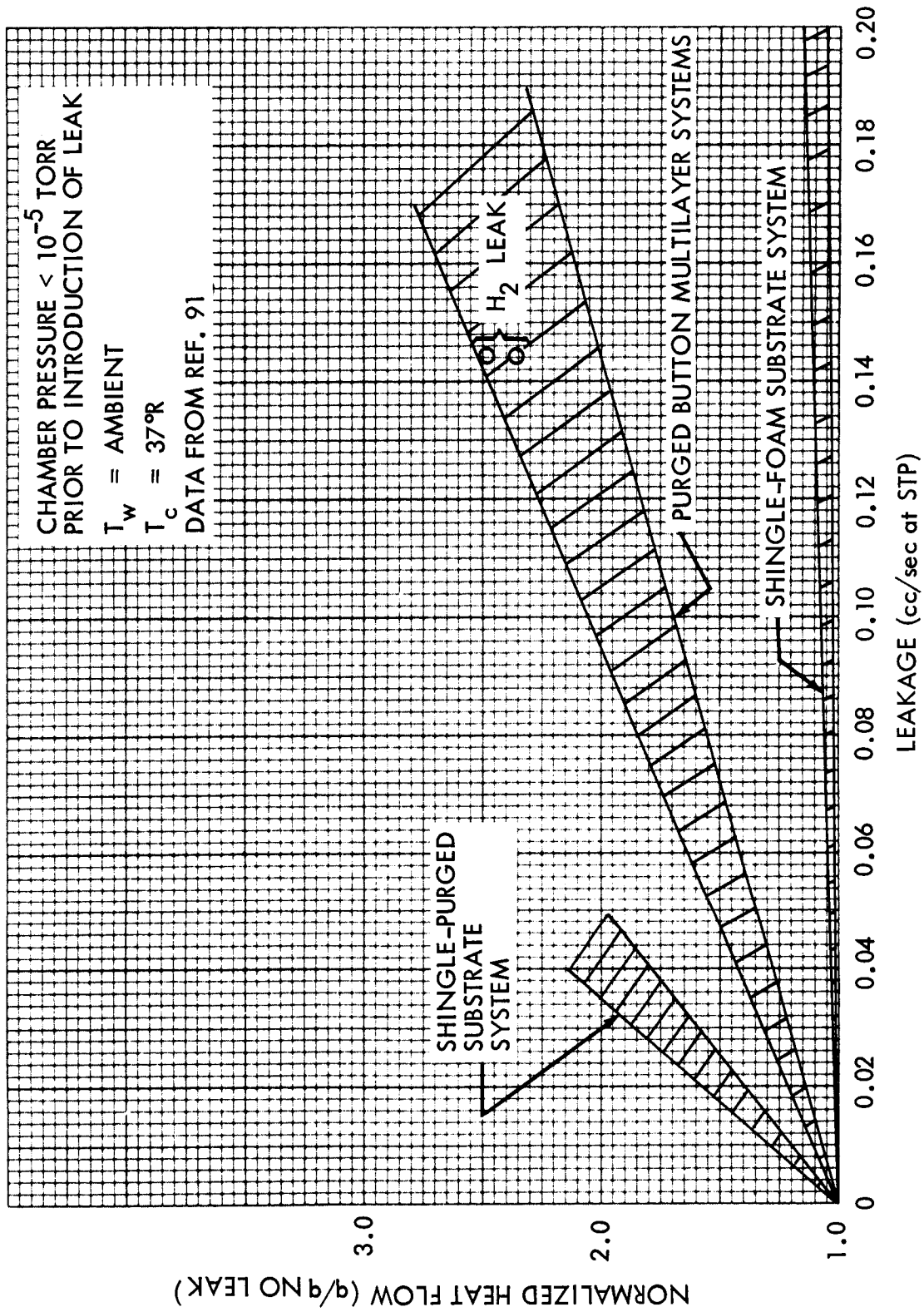


Fig. 4.4-4 Normalized Heat Flow Through Multilayer Systems as a Function of Point-Source Leakage Rate

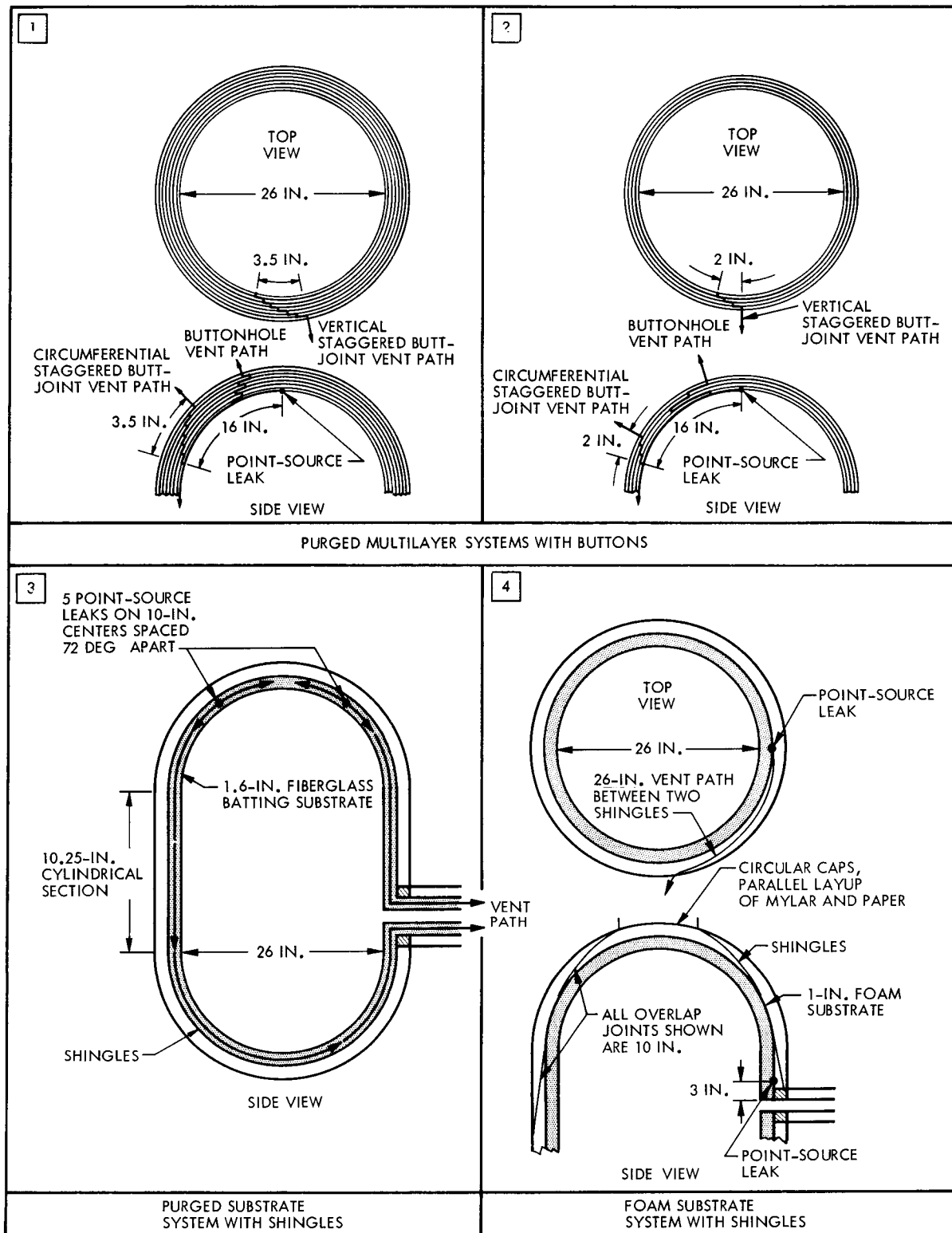


Fig. 4.4-5 Probable Vent Paths Through Multilayer Insulation for Point-Source Leakage Test

4.5 EXPERIMENTAL METHODS

Two methods of determining the effective thermal conductivities of cryogenic insulation systems over a wide range of variables have been utilized extensively within the cryogenics industry. One method utilizes a National Bureau of Standards (NBS) type cylindrical cryostat where the heat flow is radially inward. The other method utilizes a flat-plate calorimeter (FPC) where the insulation specimen is in the form of a disk and the heat flow is normal to the layers. Both methods are based on the calorimetric principle of determining heat energy transport through insulation specimens.

All heat energy entering the apparatus is intercepted by a fluid maintained at or near its normal boiling point such that the intercepted heat energy goes totally into boiling of the calorimeter fluid. In this manner, effective thermal conductivities of materials can be determined by metering the calorimeter fluid boiloff rate from the apparatus test section and by the knowledge of the material dimension and calorimetric fluid thermodynamic properties. Due to this calorimetric technique and the high resistance to heat flow in multilayer insulations, the temperature gradient maintained across the insulation specimen must necessarily be large (by several hundred degrees) in order to obtain sufficient cryogen boiloff to meter accurately. The thermal transport data which result from these test methods are effective thermal conductivities for the boundary conditions tested.

In order to give the thermal analyst a better appreciation of the limitations of existing thermal transport data a detailed description of present testing techniques is presented in this section. Although the testing techniques and test equipment described are those developed by LMSC, they are typical of those utilized throughout the industry.

Flat-Plate Calorimeter

The FPC as shown in Figures 4.5-1 and 4.5-2 was designed to measure the thermal conductivity of insulation systems for both the cryogenic and high-temperature regimes, and its more salient features can be summarized as follows:

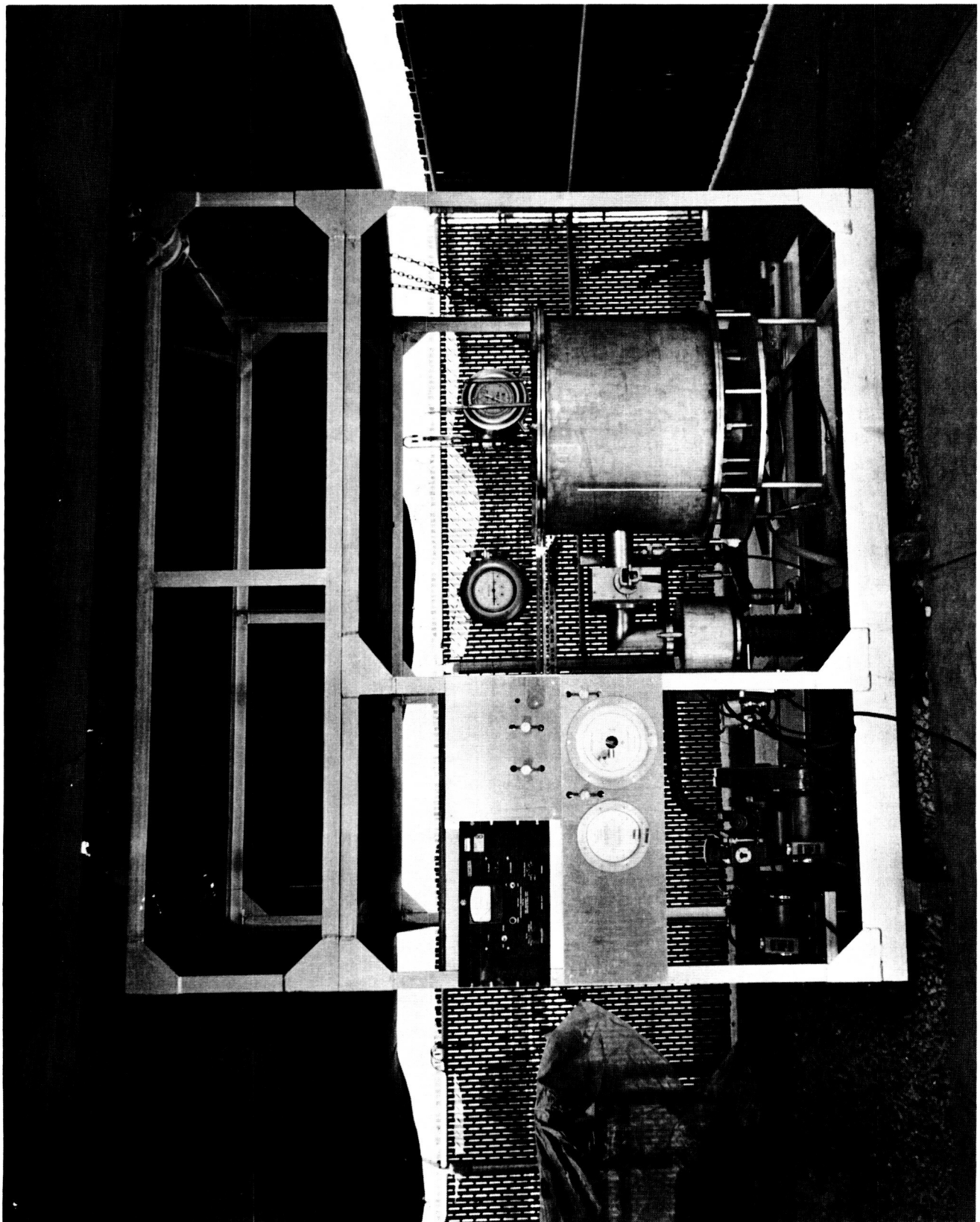
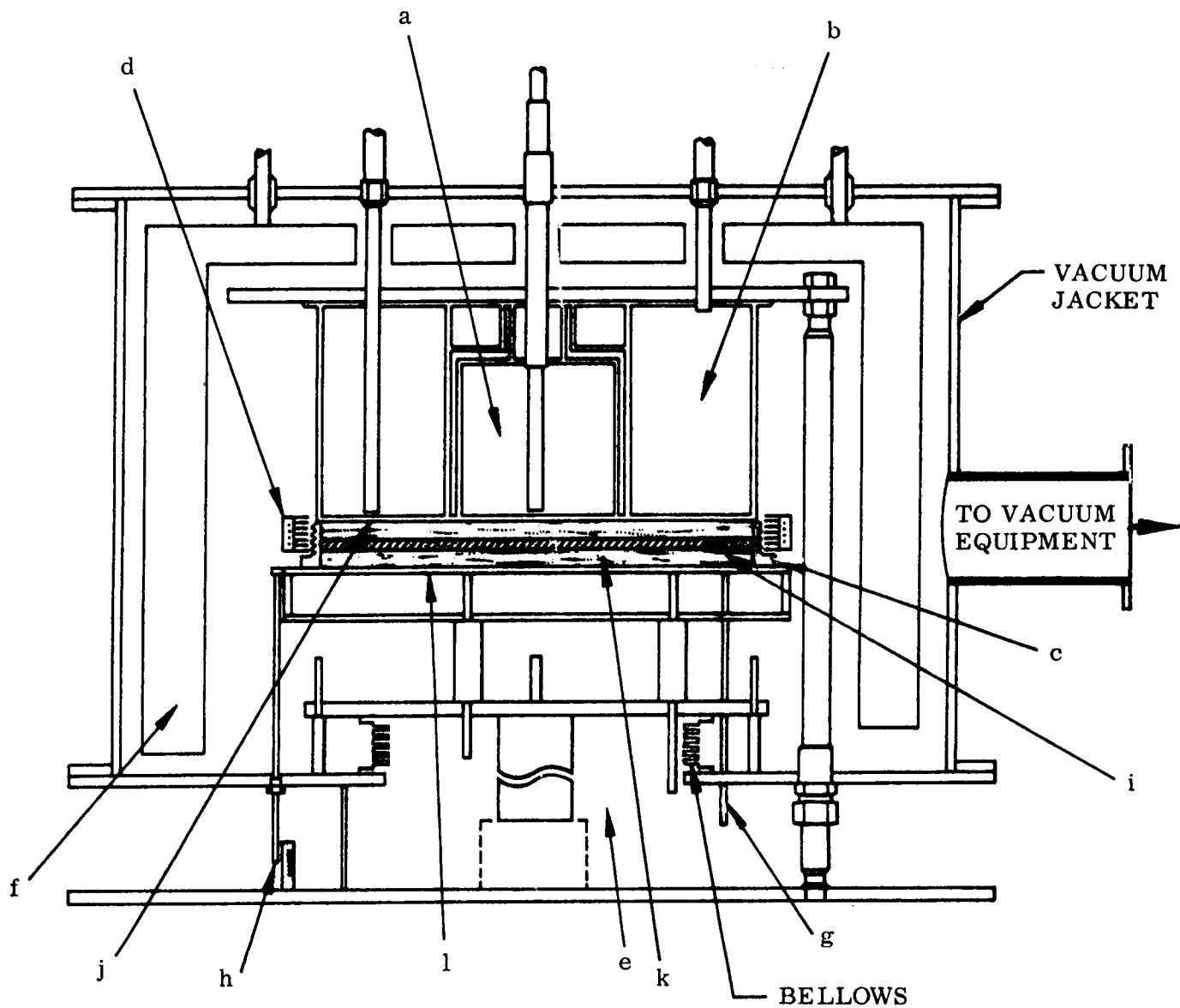


Fig. 4.5-1 Flat Plate Calorimeter

4.5-2



- | | |
|------------------------------|--------------------------------------|
| a. CALORIMETER RESERVOIR | g. INSTRUMENTATION PORTS |
| b. GUARD RESERVOIR | h. MICROMETER |
| c. ENCAPSULATING GAS BELLOWS | i. WARM TEMPERATURE BOUNDARY HEATERS |
| d. EDGE GUARD HEAT EXCHANGER | j. INSULATION SPECIMEN |
| e. LOAD CHAMBER | k. HEATER INSULATION |
| f. OUTER RESERVOIR | l. WATER COOLED SUPPORT RATE |

Fig. 4.5-2 Flat Plate Calorimeter Schematic Diagram

- Heat-sink temperature range is dependent on choice of calorimeter fluid, ranging from -424°F (liquid hydrogen) to 32°F (liquid butane).
- Source temperature can be varied from -320°F to 1500°F by utilizing a combination of cryogenic cooling and/or electrical heaters.
- The thermal conductivity range over which the FPC is applicable is 10^{-1} to 10^{-5} Btu/hr-ft $^{\circ}\text{R}$.
- Interstitial gas pressure of insulation specimen can be varied from 10^{-6} torr to 2000 torr.
- Insulation specimen can be subjected to mechanical pressures of up to 50 psi during the course of a test.

Shown in Fig. 4.5-2 is a working cross-sectional view of the FPC. In the center of the apparatus is located the calorimeter fluid reservoir. The test surface of the calorimeter reservoir has a 6-inch OD and provides a portion of the cold-temperature boundary of the insulation specimen.

The guard reservoir (b) encapsulates the calorimeter reservoir except at the cold-temperature boundary of the insulation specimen. With a 15.75-inch OD and a 6.25-inch ID, it is filled with the same liquid cryogen as the calorimeter reservoir and thus provides an adiabatic surface around the calorimeter reservoir. Besides serving to isolate the calorimeter reservoir, the guard reservoir provides a radial guard to the insulation specimen by extending the cold-temperature boundary.

A bellows (c) or edge-guard temperature boundary (d) can be used in conjunction with the FPC. The bellows can be filled with a residual gas at pressure from 10^{-6} to 2000 torr to study the effect of residual gas conduction on the performance of the insulation systems. The edge-guard temperature boundary is provided to determine the extent of two-dimensional heat transfer within insulation systems. Either the bellows or the edge-guard can be used, but not both at the same time.

A five-ton hydraulic actuated ram and a secondary vacuum chamber (e) are provided to position the insulation specimen with respect to the cold-temperature surface of the

calorimeter and guard reservoirs, and also to provide loads up to 50 psi on the insulation systems. The maximum travel of the hydraulic ram is 1.625 inches.

The outer reservoir (f) is provided to minimize the heat transfer to the guard reservoir when LH_2 is used as the calorimeter cryogen. The cryogen used in the outer reservoir is LN_2 .

Instrumentation feedthroughs (g) are provided to measure the temperature and pressure of the insulation. A micrometer (h) is provided to measure the relative location of the warm-temperature boundary to that of the cold-temperature boundary of the insulation specimen. This measurement is used to determine the thickness of the test specimen.

The warm-temperature boundary (i) of the insulation system can be supplied by a liquid heat exchanger and/or an electrical heater unit which contains a 6.00-inch diameter main heater and a 6.125-inch ID by 16-inch OD guard heater constructed of 1/4-inch thick copper plates. Heaters are fabricated from 1-mil stainless steel foil and are insulated from the copper surface plates with sheet mica.

The calorimeter system is enclosed in a welded stainless steel vacuum enclosure. Vacuum capabilities of 10^{-5} torr is provided by a 4-inch Consolidated Vacuum Corporation oil diffusion pump backed by a 15-cfm mechanical vacuum pump. When the calorimeter reservoir and guard reservoir are filled with cryogen fluids, the pressure in the test chamber of the FPC is reduced to less than 10^{-6} torr.

Analytical Analysis

The FPC is adequately guarded to measure one-dimensional heat transfer through insulation systems such as foams, powders, and reinforced foams and plastics, and to determine their conductivity. But when applying the same measuring technique to multilayer insulation systems which are highly anisotropic, one must use utmost

discretion in using the FPC. In order to form guidelines for the applicability of the FPC in measuring the thermal conductivity of anisotropic materials, a computer program (Ref. 115) was developed at LMSC to study the heat transfer in the test section of the FPC. The computer program was derived specifically to provide information as to the extent of heat leakage to the test section of the calorimeter through multilayer insulation from the guard section and the exposed edge of the insulation specimen. The program was developed to include the use of an intermediary insulation to separate the multilayer insulation from the exposed edge of the test section.

Typical results of the computer analysis showing the influence of sample thickness, edge environment temperature, and use of intermediary insulation at the outer radius of the multilayer insulation on the ratio of heat flux (Q_c/Q_{ID}) are presented in Figs. 4.5-3, 4.5-4, and 4.5-5. The heat flux ratio Q_c/Q_{ID} is defined as the ratio of actual heat flux to the calorimeter test sections (Q_c) to the heat flux for one-dimensional heat transfer (Q_{ID}). The temperature of the hot surface and cold surface of the insulation system analyzed was 70°F and -320°F, respectively. In Figure 4.5-3 is shown the effect on the ratio of heat flux Q_c/Q_{ID} when the insulation is exposed to a black body at 70°F and -320°F. For test specimens of multilayer insulation thicker than 0.10 inch and with $k_{\perp}^* = 10^{-5}$ Btu/hr-ft °R or less, the edge temperature of 70°F would increase the heat transfer into the test section and result in a high value of conductivity, whereas the edge temperature of -320°F decreases the heat transfer and would result in a low measurement of thermal conductivity.

In Figure 4.5-4 is plotted the ratio of heat fluxes (Q_c/Q_{ID}) versus edge temperature for an insulation with $k_{\perp} = 10^{-5}$ Btu/hr-ft °R and a thickness of 0.25 inch. For an edge temperature of -180°F, the ratio heat fluxes (Q_c/Q_{ID}) is approximately 1.0 for either of the two values of k_{\parallel}^{**} shown. By controlling the edge temperature of the insulation one could thus eliminate the anisotropic effect of the insulation. But to apply this technique the experimentalist must be able to make a good estimate of the thermal conductivities both parallel and perpendicular to the multilayers and predict the required edge temperature prior to test.

*Thermal conductivity of materiel normal to insulation.

**Thermal conductivity of materiel parallel to insulation.

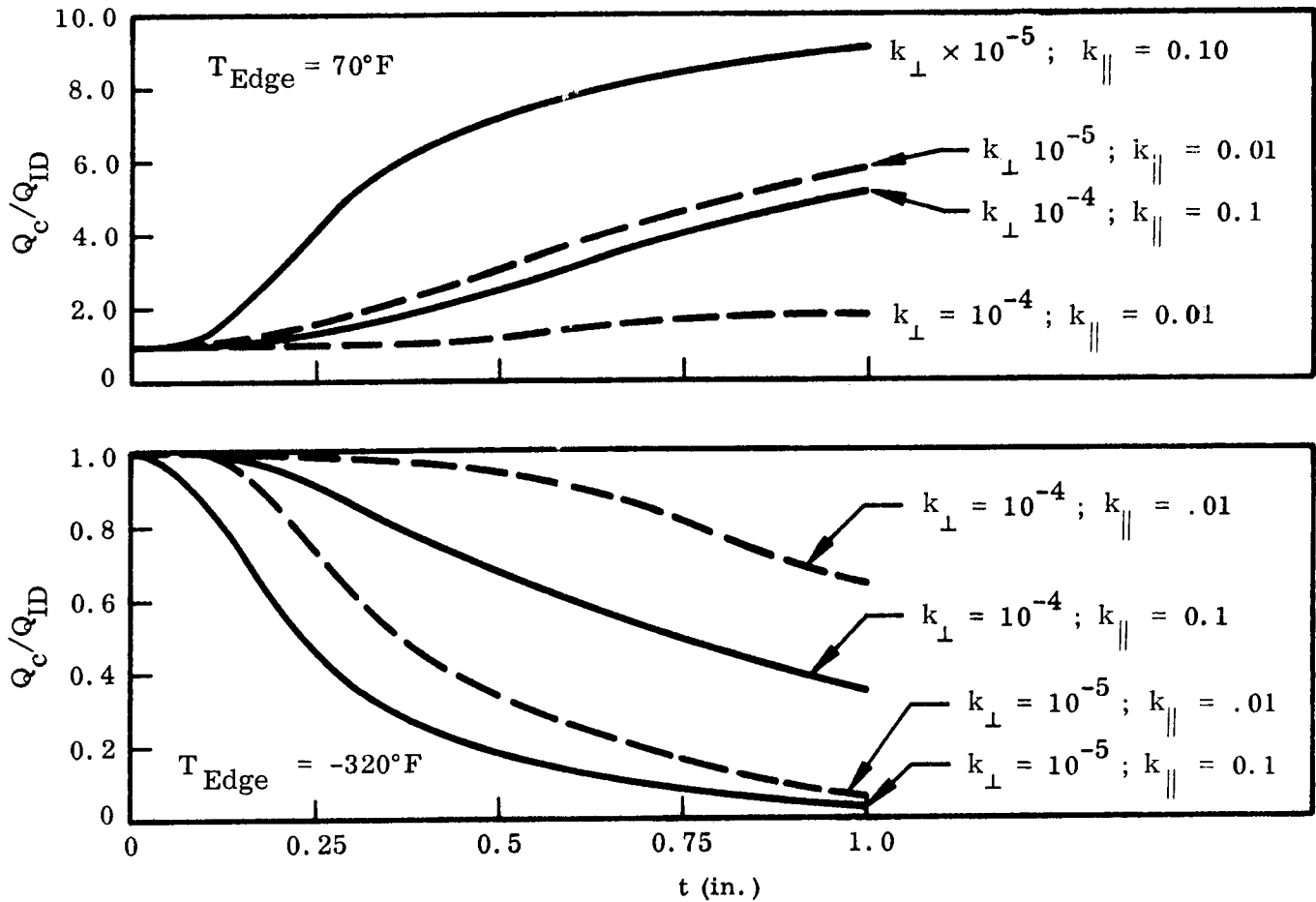


Fig. 4.5-3 Ratio of Heat Flux to Calorimeter to Heat Flux for One-Dimensional Case (Q_c/Q_{ID}) as a Function of Sample Thickness (t), Edge Temperature, and Thermal Conductivities (k_{\perp} and k_{\parallel}) in Btu/hr-ft $^{\circ}R$

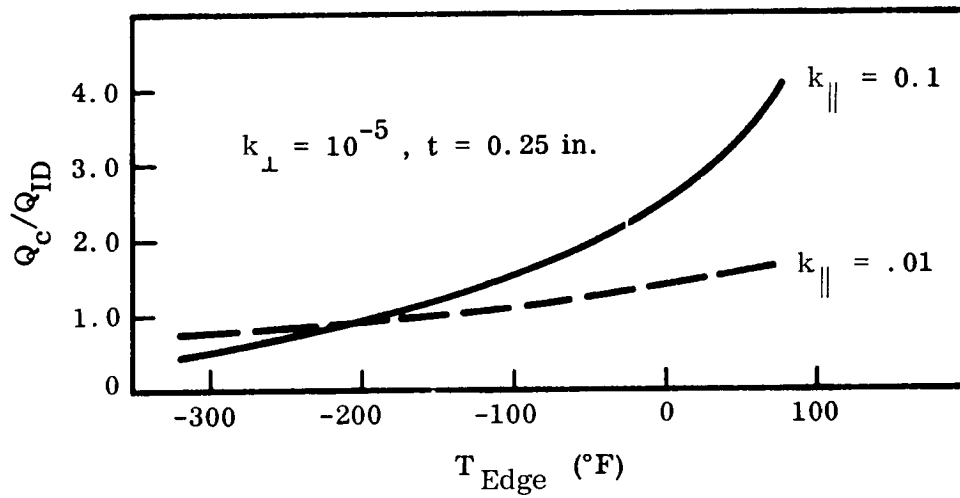


Fig. 4.5-4 Ratio of Heat Fluxes (Q_c/Q_{ID}) as a Function of Edge Temperature and Thermal Conductivities (k_{\perp} and $k_{||}$) in Btu/hr-ft $^{\circ}R$

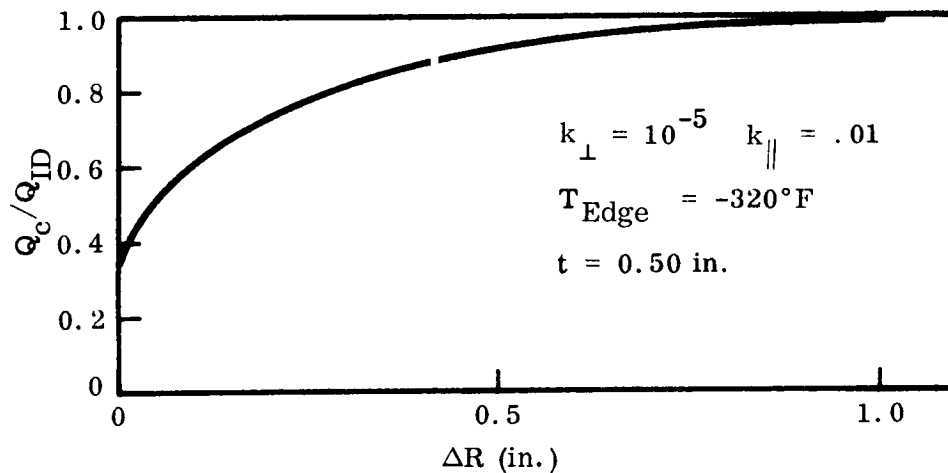


Fig. 4.5-5 Ratio of Heat Fluxes (Q_c/Q_{ID}) as a Function of Intermediary Insulation Width (ΔR) at Outer Radius

Another method of overcoming the two-dimensional heat transfer of anisotropic insulation systems is to introduce an isotropic intermediary insulation at the outer radius of the test specimen. The intermediary insulation serves to uncouple the anisotropic test specimen from the edge environment. As shown in Figure 4.5-5, the ratio of heat fluxes (Q_c/Q_{ID}) converges to unity as the width of intermediary insulation is increased. For an insulation system with $k_{\perp} = 10^{-5}$ and $k_{\parallel} = 10^{-2}$ Btu/hr-ft °R and an edge temperature of -320°F, an intermediary width of 0.75 inch is sufficient to eliminate the two-dimensional heat transfer effects ($Q_c/Q_{ID} \geq 0.99$). The thermal conductivity of the intermediary insulation was taken as 4×10^{-4} Btu/hr-ft °R.

Test Procedure and Results

Specimens are placed in the apparatus, and the thickness is set using a micrometer which measures the separation between guard reservoir and heater plate surfaces. The system is then evacuated to a pressure of 10^{-5} torr before the appropriate cryogen is transferred to the reservoir and before power is applied to the heaters. In some instances, power is applied to the heaters, in order to preheat the sample and aid in outgassing of the insulation system.

The maximum uncertainties assigned to the significant measurement and instrumentation errors are as follows:

- Measurement of insulation thickness, 4 percent
- Boiloff measurement, 3 percent
- Gas density, 2 percent
- Temperature difference across boundaries, 2 percent

The percentage errors due to temperature measurement increase as t and ΔT decrease; thus, when determining the thermal conductivity of multilayer insulation systems that are highly anisotropic and require samples of less than 0.1-inch thickness, these errors will be greatest. For isotropic materials the error due to thickness measurement is negligible for samples from 0.5 to 1.0 inch thick. The principal error in thermal conductivity, other than thickness and temperature measurement, lies in the measurement of boiloff flow rate and gas density. Both of these are attributed to the control of

the ullage pressure above the cryogen and amount to a maximum probable error of 5 percent. Thus, the probable error in thermal conductivities ranges from 5 percent for isotropic materials to a maximum of 10 percent for anisotropic materials such as multilayer insulations.

After attainment of steady-state temperature, both boiloff and temperatures are recorded for an 8-hr to 24-hr period. Thermal equilibrium is assumed when a variation in boiloff of not more than 2 percent is observed for at least 4 hours. Pressure in the vacuum chamber ranges from 1×10^{-6} to 5×10^{-7} torr when either LN_2 or LH_2 is used as the cryogen.

The thermal conductivity is calculated using the following formulae:

$$k_e = \frac{Q_c t}{A_c \Delta T} \quad \text{where } Q_c = \dot{V}_g \rho_g \ell_v \quad \text{and} \quad \rho_g = \frac{P_g}{RT_g}$$

where

K_e = Effective thermal conductivity (Btu/hr-ft °R)

Q_c = Calorimeter heat input (Btu/hr)

A_c = Calorimeter Test Section Area (0.204 ft²)

t = Thickness of sample (ft)

T = Temperature difference across t (°R)

\dot{V}_g = Volume flow rate of calorimeter gas (ft³/hr)

ρ_g = Density of gas

P_g = Gas pressure (lb/ft²)

T_g = Gas temperature (°R)

R_g = Gas constant (ft/°R)

ℓ_v = Latent heat of vaporization (Btu/lb)

Cryostats

Cryostats are similar in principle to the flat-plate calorimeter in that energy passing through the insulation system under investigation is manifested in the calorimeter fluid vapor efflux rate. Typical cryostats now being utilized at LMSC are shown in Fig. 4.5-6.

These cryostats have been modeled after those utilized by the Cryogenic Engineering Laboratory of the NBS. However, due to the highly anisotropic characteristics of multilayer insulations, as pointed out in a previous section, the guard sections on the LMSC cryostats are considerably longer than those which were utilized by the NBS at the time of construction. The final guard dimension was arrived by a combined experimental and analytical effort (Ref. 111). A cross-sectional schematic of the cryostats is presented in Fig. 4.5-7, while the entire system with support equipment is depicted in the schematic of Fig. 4.5-8. Cryostats have been designed with the following capabilities:

- Variation of the insulation outer-boundary temperature from -320°F to 212°F
- Variable insulation inner-boundary temperature (dependent on choice of calorimeter fluid) from -424°F to 32°F
- Insulation interstitial gas pressure range of 10^{-7} torr to 760 torr with variety of gases
- Measurement of thermal conductivity in the region of 0.1 to 10^{-5} Btu/hr-ft $^{\circ}\text{R}$

As indicated in Figures 4.5-6 and 4.5-7, the cryostats are cylindrical with two inter-connected guard sections and an annular test section. The test section volume is 0.12 ft^3 while the entire guard volume is 0.15 ft^3 . In order to minimize temperature gradients within the guard sections, there is a 1/4-inch diameter copper rod extending the length of the cryostat, as well as 3 similar copper rods equally spaced within each guard section. This is particularly necessary with such cryogen as liquid hydrogen where considerable stratification can occur. The upper guard is approximately four inches longer than the lower guard in order to accommodate changes in the cryogen level without appreciably affecting the test section. In investigating multilayer insulation with aluminum radiation shields it has been found necessary to use additional guards in the form of copper plates which are in intimate contact with the cryostat guard section and

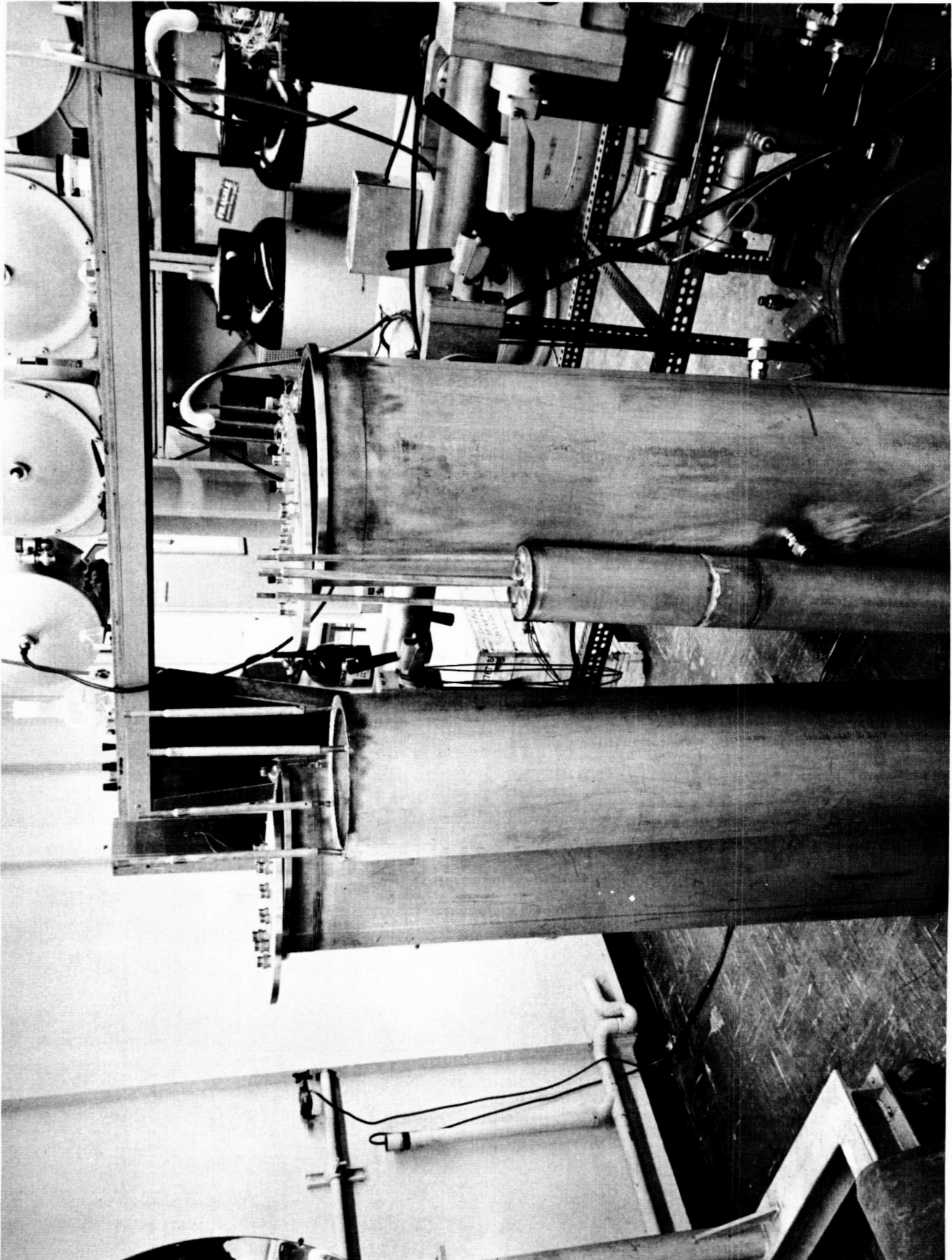


Fig. 4.5-6 Photograph of Cryostat Components (Including Outer Cold Wall and Calorimeter Section)

4.5-12

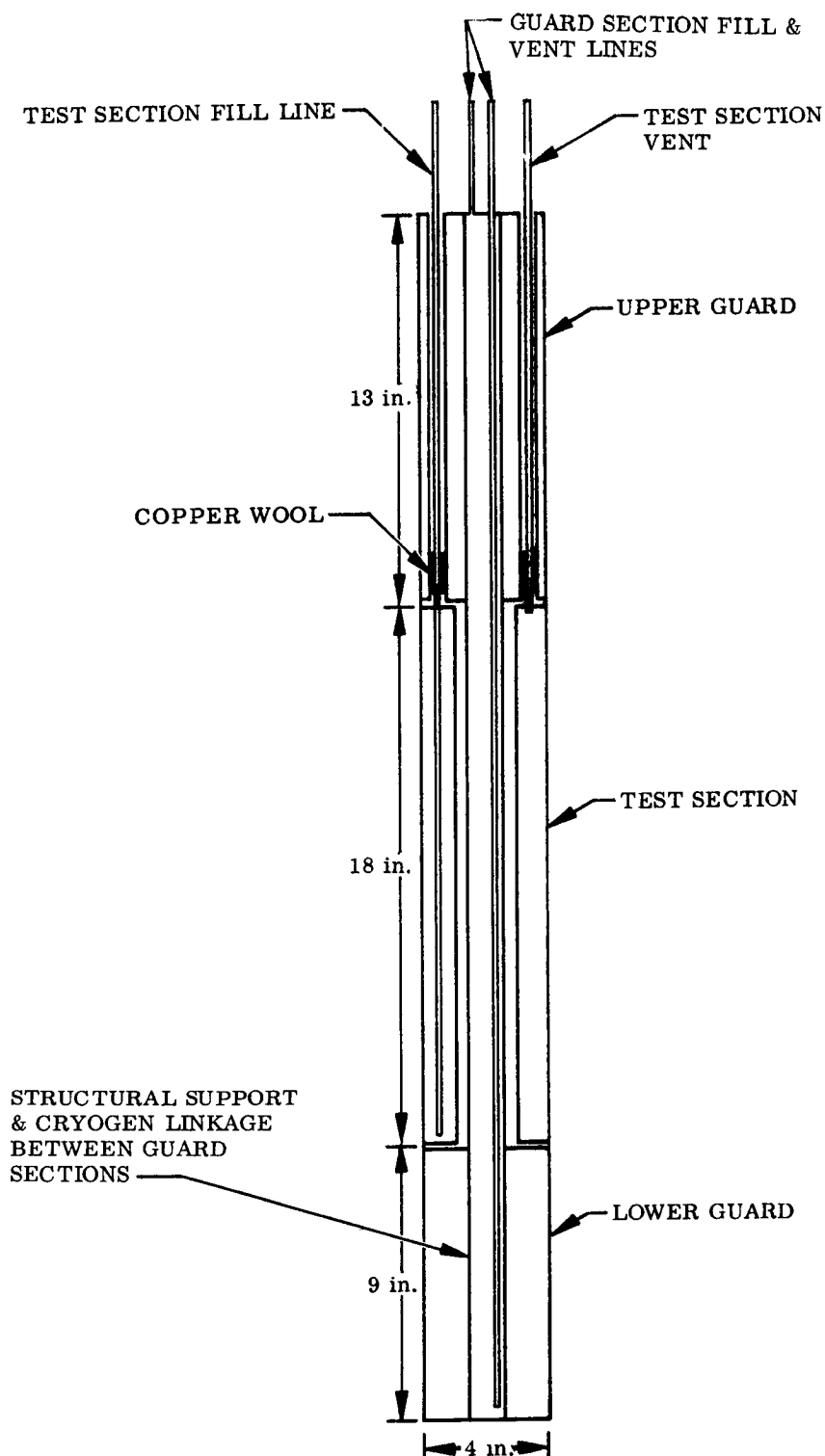


Fig. 4.5-7 Cryostat Cross-Section

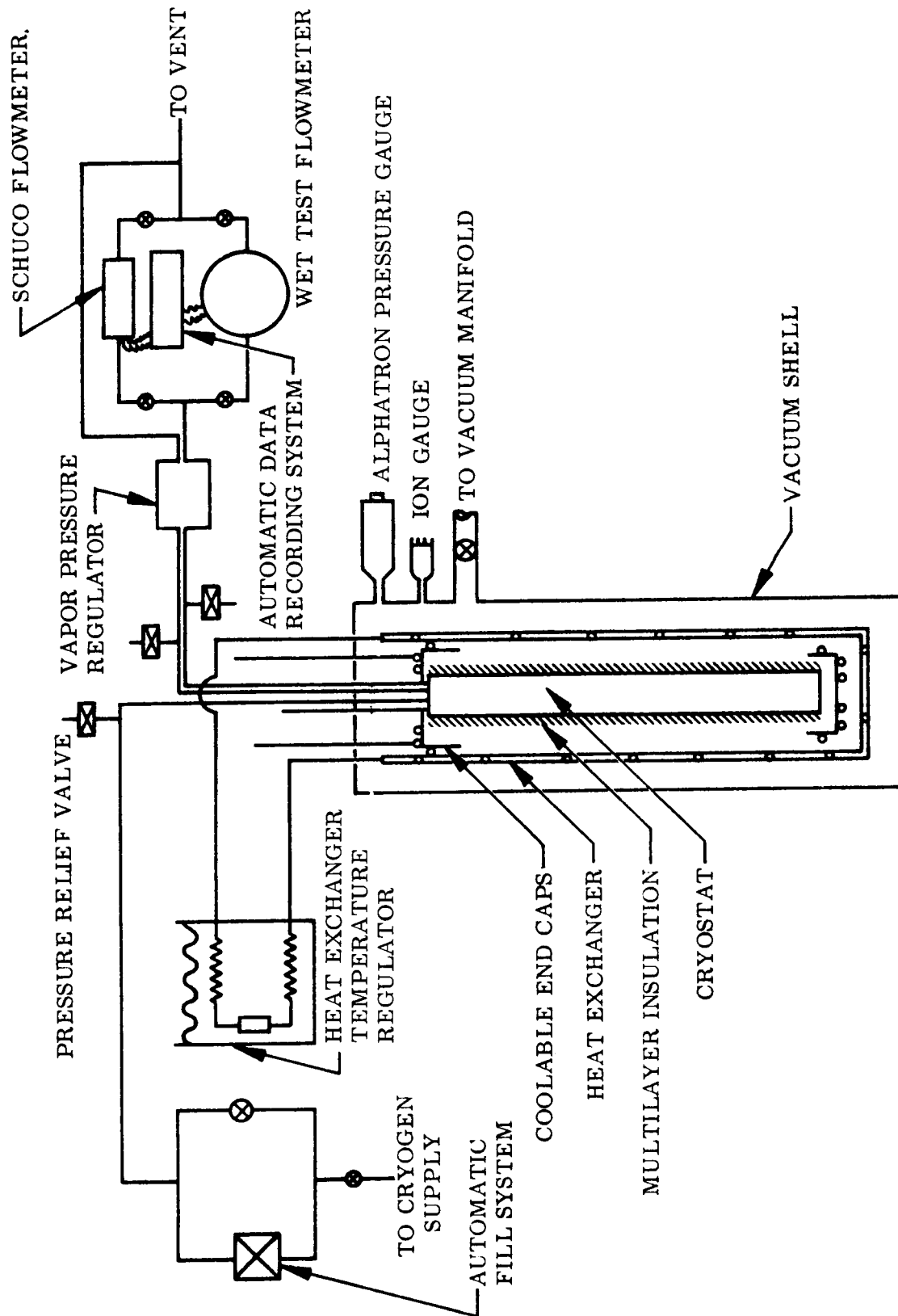


Fig. 4.5-8 Schematic of Cryostat and Associated Instrumentation

resting slightly above the insulation ends. In addition, the radiation shields are terminated approximately three inches from the insulation edge when using either aluminum or metalized Mylar. This greatly reduces the effects of anisotropics and ensures that the energy enters the test section in a direction normal to the insulation surface.

The 1/4-inch diameter 10-mil wall stainless tubing vent and fill lines of the test section reach the external warm environment through reentrant lines which extend the length of the upper guard section. In order to minimize energy entering the test section by radiation and conduction via the vent and fill lines, copper wool has been placed in these lines near the lower end of the guard section. Effluent cryogen vapors cool the copper wool and intercept the majority of energy which would normally enter the system.

While the inner-boundary temperature of the insulation is dictated by the choice of cryogen, the outer-boundary temperature is regulated by radiative energy transport between the outer insulation layer and the heat exchanger as indicated in Fig. 4.5-7. The heat exchanger has been designed such that it can be utilized with a single heat transfer medium such as water or liquid nitrogen or used with two heat transfer media such as acetone in the annular volume with cold nitrogen gas being circulated in the copper tubing. This flexibility allows a wide range of temperature on the outer boundary. From a practical standpoint, the boundary temperatures have been limited to -320°F to 212°F .

In order to ensure that changes in the equilibrium boiling points of the calorimeter fluid are small and will not introduce transients into the test data, control must be maintained over the calorimeter fluid vapor pressure. Fluctuations in barometric pressure can be sufficiently large to introduce transients into the system if the calorimeter fluid is vented directly to the atmosphere.

The overall accuracy of the thermal conductivity measurements with the cryostat is estimated to be ± 15 percent. In general, the sources of error are identical to those discussed for the FPC with the exception of the insulation specimen thickness. Due to the specimen configuration, it is somewhat difficult to obtain an absolute measurement of its thickness. In practice the circumference of the insulation specimen is normally taken at several locations and its measurements averaged. However, those familiar

with multilayer insulation will appreciate the difficulty in making such measurements without deforming the insulation specimen. It is estimated that the thickness measurement alone contributes a probable error of ± 10 percent to the thermal conductivity measurements. In addition, there is another probable source of error which is somewhat difficult to assess and will normally occur in specimen preparation. That is, during specimen preparation it has been found that maintaining a uniform tension on the composite materials is rather difficult. This can and usually does result in a non-uniform layer density throughout the insulation specimen. Although this condition would be expected to occur on insulated space vehicles, probably to a much greater extent, its exact effect on laboratory thermal conductivity measurements is not known.

In order to determine the effects of anisotropies on the proposed experiments and to form guidelines for test procedures and insulation sample preparation, an analytical thermal model was developed and solution effected with the aid of a computer program and experimental data. Reference 111 describes the thermal model that was devised for conducting the studies outlined above, and additionally describes the computer program that was used for its solution.

The solution obtained not only delineates the need for employing an isotropic intermediary, but also shows the optimum amount of intermediary insulator to utilize. In addition, the computer program results indicate that even if an optimum amount of intermediary is employed at such boundaries, insulation performance is still degraded by a factor of 2 to 2.5 for a significant distance about the disturbance. In terms of the cryostat depicted in Fig. 4.5-7, it has been found that when the insulation specimen is composed of alternate layers of 1/4-mil Mylar aluminized on both sides and a fiberglass paper spacer (Dexiglas), it is necessary to terminate the radiation shields approximately 3 in. from the end of the cryostat and the fiberglass paper spacer in order to ensure one-dimensional heat transfer within the test section. This has been verified experimentally by preparing an insulation specimen (thickness of 0.865 inch comprised of 45 layers of radiation shield and spacers) having the radiation shields terminated one-half inch from one end and three inches from the other. The ensuing tests of this insulation specimen resulted in the following:

Test Condition	Heat Rates into Test Section (Btu/hr)	Effective Conductivity (Btu/hr-ft °R)
No cold plates on either end	0.291	2.86×10^{-5}
Cold plates on 3-inch end	0.29	2.86×10^{-5}
Cold plates on both ends	0.21	2.06×10^{-5}

In a similar manner the anisotropies within the insulation system composed of 1/4-mil aluminum foil and fiberlass paper spacers were investigated. Anistropies within this insulation system are much higher than for the previously mentioned insulation due to the higher thermal conductivity of the aluminum. As a result it was found to be necessary not only to terminate the radiation shields three inches from either end, but also to use cold plates on either end. In an insulation specimen 0.865-inch thick and containing 65 layers, the following results were obtained with the aluminum foil terminated three inches from either end:

Test Condition	Heat Rates into Test Section (Btu/hr)	Effective Conductivity (Btu/hr-ft °R)
No cold plates	0.302	2.96×10^{-5}
Cold plates on both ends	0.236	2.32×10^{-5}

5. REFERENCES

1. Handbook of Chemistry and Physics, Chemical Rubber Publishing Company, 40th ed., 1958-1959
2. Ibid., pp. 616-617
3. Johnson, V. J., ed., A Compendium of the Properties of Materials at Low Temperature (Phase I), Part I, Properties of Fluids, WADD TR 60-56, Wright-Patterson AFB, Ohio, Oct 1960, seventh data sheet under 1.006
4. Ibid., fourth data sheet under 1.005
5. Handbook of Chemistry and Physics, pp. 612-613
6. Johnson, op. cit., eighth data sheet under 1.001
7. Roder, H. M. and Goodwin, R. D., Provisional Thermodynamic Functions for Para-Hydrogen, National Bureau of Standards Tech. Note 130, Dec 1961, pp. 80-81
8. Johnson, op. cit., third data sheet under 3.002
9. Ibid., fifth data sheet under 3.001
10. Ibid., first data sheet under 3.003
11. Ibid., 3.006
12. Ibid., fourth data sheet under 3.004
13. Ibid., second data sheet under 3.005
14. Barney, J. D. and Magee, P. M., Analytical and Preliminary Design Studies of Nuclear Rocket Propulsion Systems, Vol VI, Aerojet General Report No. 1999, Jun 1961, p. 20

15. Chelton, D. B. and Mann, D. B. , Cryogenic Data Book, NBS/CEL, UCRL 3421, 15 May 1956, p. 81
16. Johnson, op. cit. , third data sheet under 4.003
17. Ibid. , eighth data sheet under 4.004
18. Ibid. , fourth data sheet under 4.006
19. Ibid. , tenth data sheet under 4.005
20. Ibid. , fourth data sheet under 10.003
21. Ibid. , fourth data sheet under 10.006
22. Ibid. , fourth data sheet under 10.001
23. Ibid. , second data sheet under 10.006
24. Ibid. , sixth data sheet under 10.004
25. Ibid. , sixth data sheet under 10.002
26. Cryogenic Materials Data Handbook, A. F. Materials Laboratory, Research & Technology Division, ML-TDR-64-280, Aug 1964, C.7. T
27. Pennock, A. P. , Insulation Material Properties, Lockheed Missiles & Space Company Informal Report, 14 Jun 1963, p. 192
28. Scott, R. B. , Cryogenic Engineering, D. Van Nostrand Co. , Inc. , 1962, Table 10.6
29. Pennock, op. cit. , p. 174
30. Cryogenic Materials Data Handbook, B.5. T
31. Ibid. , B.7. T
32. Ibid. , A.4. T
33. Ibid. , A.15. T
34. Pennock, op. cit. , p. 184
35. Steels for Low Temperature Applications, USS Catalog, p. 35

36. Goldsmith, A. , et al. , Handbook of Thermophysical Properties of Solid Materials, Vol. 2, The MacMillan Co. , 1961, p. 821
37. Ibid. , p. 161
38. Johnson, op. cit. , Part 4, p. 89
39. Pennock, op. cit. , p. 191
40. Timmerhaus, K. D. , ed. , Advances in Cryogenic Engineering, Vol. 8, New York, Plenum Press, Inc. , 1962, p. 275
41. Johnson, op. cit. , Part 4, p. 82
42. Ibid. , p. 57
43. Scott, op. cit. , Table 10.4
44. Timmerhaus, op. cit. , Vol. 8, 1962, p. 271
45. "Titanium," Design News, 29 Sep 1961, pp. 69, 81
46. Goldsmith, et al. , op. cit. , Vol. 2, p. 189
47. Ibid. , Vol. 1, p. 659
48. Ibid. , Vol. 2, p. 761
49. Ibid. , p. 823
50. Ibid. , p. 199
51. Ibid. , p. 207
52. Ibid. , Vol. 1, p. 665
53. Scott, op. cit. , p. 347
54. Campbell, M. D. , "Thermal Expansion Characteristics of Some Plastic Materials and Composites from Room Temperature to -253° C" (paper presented at Cryogenic Engineering Conference, Philadelphia, Aug 1964)
55. Hertz, J. and Haskins, J. E. , "Thermal Conductivity of Reinforced Plastics at Cryogenic Temperatures" (paper presented at Cryogenic Engineering Conference, Philadelphia, Aug 1964)

56. Campbell, M. D., Hertz, J., O'Barr, G. L., and Haskins, J. F., "Thermophysical Properties of Plastic Materials and Composites to Liquid Hydrogen Temperature (- 423° F)," Wright-Patterson AFB, Report ML-TDR-64-33 PT, 1965
57. Unpublished experimental data from Lockheed Multilayer-Insulated 26-in. Tank Tests
58. Timmerhaus, op. cit., Vol. 7, 1961, p. 357
59. Ibid., Vol. 5, p. 174
60. Thermophysical Properties of Thermal Insulating Materials, Wright-Patterson AFB, Report ML-TDR-64-5, Apr 1964, p. 153
61. Johnson, op. cit., Part 2, second data sheet under 4.402
62. Scott, op. cit., p. 331
63. Caren, R. P., et al., "Low-Temperature Tensile, Thermal Contraction and Gaseous Hydrogen Permeability Data on Hydrogen Vapor Barrier Materials" (paper presented at Cryogenic Engineering Conference, Philadelphia, Aug 1964)
64. Scott, op. cit., p. 333
65. Johnson, op. cit., Part 4, 13.501
66. Thermophysical Properties of Thermal Insulating Materials, p. 221
67. Allied Chemical Products Data Sheet A-1-660
68. E. I. du Pont de Nemours & Co., Film Dept., Bulletin H-1, "H Film" Wilmington, Delaware, n.d.
69. -----, Bulletin M-2A, "Mylar"
70. Thermophysical Properties of Thermal Insulating Materials, p. 154
71. Johnson, op. cit., Part 4, 13.132
72. Lockheed Missiles & Space Co., unpublished data, Thermophysics Laboratory, 1964-65

73. Stabler, R. E., E. I. du Pont de Nemours & Co., Wilmington, Delaware, private communication, 5 Mar 1965
74. Goldsmith, op. cit., Vol. 4, p. 537
75. Goldsmith, op. cit., Vol. 1, p. 39
76. Arthur D. Little, Inc., Report 65958-00-02, 29 May 1964, p. V-5
77. -----, Report 65958-00-03, Aug 1964, p. III-12
78. Lockheed Missiles & Space Co., Research Brief, Low Temperature Emittance Determination, TP-1455, 1965, p. 9
79. Arthur D. Little, Inc., Report 65958-00-02, 29 May 1964, p. II-13
80. Wang, D. I., "Multiple Layer Insulations," Aerodynamically Heated Structures, ed., P. E. Glaser, Prentice-Hall, Inc., 1962, p. 45
81. Arthur D. Little, Inc., Report 65008-00-02, Apr 1963, p. 76
82. Wang, D. I., Linde Co., Division of Union Carbide, Tonawanda, N. Y., private communication, 22 Mar 1965
83. Thermophysical Properties of Thermal Insulating Materials, p. 150
84. Arthur D. Little, Inc., Report 65008-00-03, Jul 1963, p. 36
85. Lockheed-California Co., Progress Report II; Storage of Cryogenic Fluids for Long Duration Spacecraft Missions, by J. E. Boberg, Report 17410, 25 Mar 1964, p. 21
86. Arthur D. Little, Inc., Report 65958-00-03, Aug 1964, p. II-7
87. Linde Co., Division of Union Carbide, Linde Co. Superinsulation Applied to Space Vehicles, by C. R. Lindquist, 1 Dec 1962
88. Arthur D. Little, Inc., Report 65008-00-01, Jan 1963, p. 25
89. Ibid., p. 20
90. Thermophysical Properties of Thermal Insulating Materials, p. 153

91. Lockheed Missiles & Space Co., data from Independent Development Program and Contract NAS 3-4199, Development of Thermal Protection System for a Cryogenic Spacecraft Module (in preparation)
92. Vol. V of this report, "Analytical and Experimental Studies of Purge Gas Flow Through Multilayer Insulation," Aug 1965
93. Scott, op. cit., pp. 272, 277, 291, 304, 314
94. Linde Co., Table, "Physical Property Equivalents of Some Cryogenic Fluids"
95. Air Products and Chemicals, Inc., Table, "Low Temperature Physical Properties of Gases," 1962
96. Hu, J. H., White, D., and Johnston, H. L., "Condensed Gas Calorimetry. V. Heat Capacities, Latent Heats and Entropies of Fluorine from 13 to 85° K; Heats of Transition, Fusion, Vaporization and Vapor Pressures of the Liquid," J. Am. Chem. Soc., Vol. 75, 1953, p. 5642
97. General Dynamics/Astronautics, Liquid Hydrogen Technology, R. T. Parmley, GD/Astronautics Report AE 62-0774, Sep 1962, p. 247
98. International Critical Tables, Vol. 1, McGraw-Hill Book Co., Inc., 1926, p. 104
99. Simons, J. H., Fluorine Chemistry, Vol. I, Academic Press, Inc., New York, N.Y., 1950, p. 316
100. International Critical Tables, Vol. 1, McGraw-Hill Book Co., Inc., 1926, p. 102
101. Johnson, op. cit., 3.008
102. Johnson, op. cit., 4.008
103. Johnson, op. cit., 10.008
104. Johnson, op. cit., Part 4
105. Ibid, Part 2
106. Cunningham, G. R., Funai, A., and Lindahn, A., "Elevated Temperature Multiple Layer Insulation Study," Interim Technical Report, Contract NAS2-2441, LMSC 4-05-66-4, Nov 1966

107. "Advanced Studies on Multilayer Insulation Systems," Arthur A. Little, Inc., Final Report on Contract NAS3-6283, NASA CR-54929, June 1, 1966
108. Super-Temp Corporation, Cryogenic Division, Communique, October, 1966
109. Cody, J. C. and Hyde, E. H., "Thermal Problems Associated with the Development of a Flight Configured Cryogenic Insulation System," Conference Proceedings from Long-Term Cryo-Propellant Storage in Space, Marshall Space Flight Center, Huntsville, Alabama, Oct 1966
110. Burge, G. W., "System Effects on Propellant Storability and Vehicle Performance," Douglas Aircraft Co., DAC-59314, Final Technical Report AFRPL TR-66-258, Oct 1966
111. Gilcrest, A. S. and Fick, J. L., "Thermal Problems Related to the Utilization of Highly Anisotropic Multilayer Insulation Systems," presented at AIAA Annual Meeting, New York, Jan 1964
112. "Basic Investigations of Multilayer Insulation Systems," Arthur D. Little, Inc., Final Report on Contract NAS3-4181, NASA CR-54191, Oct 30, 1964
113. "Performance of Multilayer Insulation Systems for the 300° to 800° K Temperature Range," Materials Report No. 1, NAS2-2441, LMSC 4-05-65-9, Aug 1965
114. Coston, R. M., "Study on High-Performance Insulation Thermal Design Criteria," Vol. I, Final Report, Contract NAS8-20353, Jun 1967
115. Cunningham, G. R. and Zierman, C. A., "Measurement of Thermal Conductivity of Highly Anisotropic Insulations Using a Flat Plate Apparatus," presented at 5th Conference on Thermal Conductivity, Denver, Colorado, Oct 1965

4.4 Attachment Methods

4.5 Test Methods

For all data presented herein, sources in the published literature are provided. The data presented comprise all those available to the author, including a considerable amount of data derived from the Lockheed Independent Development Program for Cryogenics. Other experimental data on multilayer systems have been published by several space-vehicle contractors. Since these investigations were company-funded, the results are considered proprietary and are not included in this report.

All data were graphed in English units. Where available, the equations describing the curves are presented in the text. Explanatory text is presented on a lefthand page, with the related figure(s) on the righthand facing page.

The back of each page was left blank to facilitate the updating procedure as new data become available; each individual set of text and figure can be replaced without disturbing or reprinting any of the remaining sets. So that the graphs would be easier to read, the grids were lightened to provide greater contrast with the curves.

Recently, considerable interest has developed in the shingle multilayer insulation system. The effective thermal conductivity of this insulation has been measured at Lockheed and was correlated using an analytical technique. The recommended technique is described in Appendix I. The correlation of the measured and theoretical data is presented in Figs. 4.4-1 and 4.4-2 for selected boundary temperatures. The relations provided in Appendix I are recommended for use where the conductivities for other boundary temperatures are required.

A tabulation of conversion factors for changing from English units to metric units is provided in Appendix II.

Appendix II CONVERSION FACTORS

DENSITY

$$1 \text{ lb/cu. ft} = 0.016018 \text{ gm/cc}$$

$$1 \text{ lb/cu. ft} = 0.016019 \text{ gm/ml}$$

GAS CONSTANT

The following tabulation gives the values of R for temperatures in degrees Rankine:

<u>Density</u>	<u>Pressure</u>			
	<u>atm</u>	<u>kg/cm²</u>	<u>mm Hg</u>	<u>psi</u>
gm/cc	22.6126	23.3639	1,7185.6	332.316
lb/ft ³	0.362216	0.374252	275.284	5.32313

HEAT UNITS

$$1 \text{ Btu} = 251.98 \text{ cal}$$

$$1 \text{ Btu/hr} = 0.2930 \text{ w}$$

$$1 \text{ Btu/lb} = 0.5556 \text{ cal/gm}$$

$$1 \text{ Btu/lb } ^\circ\text{R} = 1 \text{ cal/gm } ^\circ\text{K}$$

$$1 \text{ Btu/hr ft } ^\circ\text{R} = 4.134 \times 10^{-3} \text{ cal/cm sec } ^\circ\text{K}$$

$$1 \text{ Btu/hr ft } ^\circ\text{R} = 17.30 \text{ mw/cm } ^\circ\text{K}$$

LENGTH

$$1 \text{ A} = 3.281 \times 10^{-10} \text{ ft}$$

$$1 \text{ mil} = 10^{-3} \text{ in.}$$

$$1 \text{ cm} = 0.3937 \text{ in.}$$

$$1 \text{ m} = 3.281 \text{ ft}$$

PRESSURE

$$1 \text{ mm Hg} = 1 \text{ torr}$$

$$1 \text{ psia} = 51.714 \text{ torr}$$

$$1 \text{ psia} = 0.06804 \text{ atm}$$

$$1 \text{ psia} = 0.07031 \text{ kg/cm}^2$$

$$1 \text{ atm} = 760 \text{ torr}$$

TEMPERATURE

$$1 \text{ }^{\circ}\text{R} = 0.5556 \text{ }^{\circ}\text{K}$$

VISCOSITY

$$1 \text{ lb/ft sec} = 14.882 \text{ poise}$$

VOLUME

$$1 \text{ ft}^3 = 2.8317 \times 10^4 \text{ cc}$$

$$1 \text{ ft}^3 = 2.8316 \times 10^4 \text{ ml}$$

WEIGHT

$$1 \text{ lb} = 453.67 \text{ gm}$$